UNIVERSITI TEKNOLOGI MARA

ACCURATE PREDICTION OF THE FREQUENCY RESPONSE FUNCTIONS OF TOBACCO COMPOSITE PANELS USING EXPERIMENTAL MODAL ANALYSIS AND MODEL UPDATING

NURUL FATIN HAMIZAH BINTI AH SIAK @ MOHD HELMI

MSc

July 2026

UNIVERSITI TEKNOLOGI MARA

ACCURATE PREDICTION OF THE FREQUENCY RESPONSE FUNCTIONS OF TOBACCO COMPOSITE PANELS USING EXPERIMENTAL MODAL ANALYSIS AND MODEL UPDATING

NURUL FATIN HAMIZAH BINTI AH SIAK @ MOHD HELMI

Thesis submitted in fulfilment
of the requirements for the degree of
Master of Science
(Mechanical Engineering)

Faculty of Mechanical Engineering

July 2026

CONFIRMATION BY PANEL OF EXAMINERS

I certify that a Panel of Examiners has met on 26 May 2026 to conduct the final examination of Nurul Fatin Hamizah Binti Ah Siak @ Mohd Helmi on her Masters of Science thesis entitled "Accurate Prediction of the Frequency Response Functions of Tobacco Composite Panels Using Experimental Modal Analysis and Model Updating" in accordance with Universiti Teknologi MARA Act 1976 (Akta 173). The Panel of Examiner recommends that the student be awarded the relevant degree. The Panel of Examiners was as follows:

Baljit Singh A/L Bhatal Singh, PhD
Associate Professor
Faculty of Mechanical Engineering
Universiti Teknologi MARA
(Chairman)

Valliyappan David Natarajan, PhD
Associate Professor
Faculty of Mechanical Engineering
Universiti Teknologi MARA
(Internal Examiner)

Mohammad Yazdi Harmin, PhD
Associate Professor
Faculty of Engineering
Universiti Putra Malaysia
(External Examiner)

PROFESSOR DR HJH ZURAEDA BINTI IBRAHIM
Dean
Institute of Postgraduates Studies
Universiti Teknologi MARA
Date: 29 July 2026

AUTHOR'S DECLARATION

I declare that the work in this thesis was carried out in accordance with the regulations of Universiti Teknologi MARA. It is original and is the results of my own work, unless otherwise indicated or acknowledged as referenced work. This thesis has not been submitted to any other academic institution or non-academic institution for any degree or qualification.

I, hereby, acknowledge that I have been supplied with the Academic Rules and Regulations for Post Graduate, Universiti Teknologi MARA, regulating the conduct of my study and research.

Name of Student	:	Nurul Fatin Hamizah binti Ah Siak @ Mohd Helmi
Student ID. No.	:	2024686126
Programme	:	Master of Science (Mechanical Engineering)
Faculty	:	Mechanical Engineering
Thesis Title	:	Accurate Prediction of the Frequency Response Functions of Tobacco Composite Panels using Experimental Modal Analysis and Model Updating
Signature of Student	:	…………………………………………..
Date	:	July 2026

ABSTRACT

Accurate vibration prediction of a Tobacco Composite Panel (TCP) using finite element (FE) analysis requires a physically accurate representation of both stiffness and damping. While stiffness governs natural frequency locations, Frequency Response Function (FRF) resonance peak amplitude and bandwidth are predominantly controlled by modal damping, and aligning resonance frequencies alone does not ensure accurate FRF prediction. Conventional FE model updating approaches largely focus on stiffness correction and introduce damping through proportional assumptions or nominal modal values, which frequently produces acceptable frequency agreement but persistent errors in FRF peak magnitude and bandwidth. This limitation is particularly pronounced in bio-based composites such as TCP, where damping is inherently high, variable between modes and specimens, and cannot be adequately represented by classical low-damping assumptions. The primary novelty of this study is the development of a staged FE model updating methodology that explicitly decouples stiffness updating from modal damping calibration, providing a physically traceable and reproducible framework for improving FRF prediction accuracy in composite structures with significant damping variability. The framework is developed and validated through experimental modal analysis (EMA) of tobacco composite strip specimens under approximate free-free boundary conditions, supported by quasi-static tensile testing for stiffness comparison and verified using steel dog-bone specimens as a controlled reference. Numerical models are constructed in PATRAN and solved using MSC NASTRAN for modal and FRF analyses, with model updating implemented in FEMTools. The updating sequence comprises four traceable stages, namely an initial FE model, a tensile-test-based stiffness model, a modal-updating-based stiffness model, and a final damping-updated model. In the stiffness stage, elastic parameters are updated to reduce natural frequency error to below 0.52% and improve mode shape correlation using the Modal Assurance Criterion. In the damping stage, EMA-derived modal damping ratios are systematically assigned and selectively refined mode by mode to improve FRF peak amplitude and bandwidth while preserving the aligned resonance locations. Applying this methodology, the final updated TCP FE model achieves Signature Assurance Criterion values of 0.88 to 0.90, representing a substantial improvement from the baseline value of 0.27 and confirming strong global FRF agreement. The proposed methodology resolves the stiffness-damping coupling ambiguity that undermines conventional updating approaches, and establishes a technically defensible route for FRF-based FE model updating of bio-based composite structures where damping variability is a defining characteristic.

ACKNOWLEDGEMENT

First and foremost, I would like to express my sincere gratitude to Allah SWT for granting me the strength, patience, and perseverance to complete this Master's research. This journey has been both challenging and rewarding, and I am thankful for every lesson, opportunity, and guidance that made this work possible.

I would like to convey my deepest appreciation to my main supervisor, Dr. Muhamad Norhisham bin Abdul Rani from Structural Dynamics Analysis and Validation (SDAV), Universiti Teknologi MARA (UiTM) Shah Alam, for his continuous guidance, constructive feedback, and consistent encouragement throughout this study. I am also sincerely grateful to my co-supervisors, Assoc. Prof. Ir. Dr. Mohd Azmi bin Yunus from SDAV, UiTM Shah Alam, and Assoc. Prof. Dr. Andreas Kyprianou from the University of Cyprus, for their valuable advice, insightful suggestions, and support that strengthened the quality and direction of this study. Many challenging problems were clarified during informal discussions over coffee, moments that I truly appreciated and will always remember with gratitude. Special thanks are also extended to Eddy Dascotte, General Manager of Dynamic Design Solutions (DDS), for his guidance and continuous assistance in using FEMTools, which greatly supported the FE model updating work in this study.

I would also like to extend my appreciation to the members and colleagues of SDAV for their cooperation, helpful discussions, and support throughout my study. Their assistance and encouragement contributed to a positive research environment and made the research process more meaningful.

My deepest gratitude goes to my family for their unwavering love and support. I would like to honour the memory of my late father, Mohd Helmi Abdullah @ Ah Siak bin Embing, whose values and prayers continue to inspire me. I am profoundly thankful to my mother, Shaharina Othman, for her endless sacrifices, encouragement, and constant belief in me. Special thanks are also extended to my siblings for their support and understanding throughout my academic journey.

Finally, I would like to express my sincere appreciation to my husband, Nahit Bey bin Aminuddin, for his patience, motivation, and continuous support during the completion of this thesis. I am also grateful to my parents-in-law, Dr. Aminuddin bin Mohammed and , for their kindness, prayers, and encouragement. To everyone who contributed directly or indirectly to this work, thank you for being part of this journey and for helping me reach this milestone.

TABLE OF CONTENTS

LIST OF TABLES

LIST OF FIGURES

LIST OF PLATES

LIST OF SYMBOLS

Symbol	
c_n	Modal damping coefficient for mode (n)
E	Young's modulus (isotropic)
E_1	Young's modulus in material direction 1 (x-direction)
E_2	Young's modulus in material direction 2 (y-direction)
$f(t)$	Applied force (time domain)
F	Excitation amplitude (frequency domain)
$H(\omega)$	Frequency response function (FRF) matrix
$H_a(\omega)$	Accelerance FRF (acceleration/force)
$H_{jk}(\omega)$	FRF between response DOF (j) and input DOF (k)
$H_v(\omega)$	Mobility FRF (velocity/force)
$H_x(\omega)$	Receptance FRF (displacement/force)
i	Imaginary unit, $\sqrt{-1}$
m_n	Modal mass for mode (n)
N	Number of modes used in modal summation
t	Time
$x(t)$	Displacement response (time domain)
$\dot{x}(t)$	Velocity response (time domain)
$\ddot{x}(t)$	Acceleration response (time domain)

X	Steady-state response amplitude (frequency domain)
α	Mass-proportional Rayleigh damping coefficient
β	Stiffness-proportional Rayleigh damping coefficient
ν	Poisson’s ratio (isotropic)
ν_{12}	Poisson’s ratio (orthotropic, x and y-direction)
ω	Angular frequency
ω_n	Natural angular frequency for mode (n)
ϕ_{jn}	Mode shape component at response DOF (j) for mode (n)
ϕ_{kn}	Mode shape component at input DOF (k) for mode (n)
ρ	Density
ζ_n	Modal damping ratio for mode (n)

LIST OF ABBREVIATIONS

Abbreviations

DOF	Degree of Freedom
EMA	Experimental Modal Analysis
FE	Finite Element
FRF	Frequency Response Function
MAC	Modal Assurance Criterion
SAC	Signature Assurance Criterion
TCP	Tobacco Composite Panel

LIST OF NOMENCLATURE

Nomenclatures

C	**Damping matrix**
K	**Stiffness matrix**
M	Mass matrix

CHAPTER 1
INTRODUCTION

1.1 Introduction

Vibration performance is a critical design consideration in engineering systems because excessive or uncontrolled vibration can reduce structural reliability, shorten service life, and compromise system accuracy under operating conditions (Chu et al., 2024; Dharmajan & AlHamaydeh, 2025; Zmarzły et al., 2025). Engineers aim to predict dynamic behaviour at the design stage so that vibration-related problems can be identified and addressed before fabrication commences (Sudin et al., 2025; Yaacob et al., 2025). FE analysis is widely employed for this purpose because it enables efficient numerical prediction of modal behaviour and vibration response, allowing designers to evaluate structural performance before physical testing is conducted (Charoensuk & Sethaput, 2023; Mohd Kahar et al., 2024). The accuracy of FE predictions is directly dependent on how well the model replicates the actual structure in terms of geometry, material properties, and damping behaviour (Ereiz et al., 2022; Y. Lee et al., 2023). This need for reliable and validated vibration prediction forms the general context of the present study.

Composite structures are increasingly being used in engineering applications and the vibration behaviour of these structures frequently needs to be modelled carefully as the mechanical response of the structure depends on the constituent distribution and the fabrication effects (Kalusuraman et al., 2023; Michal et al., 2024; Nori et al., 1996). Composite systems can exhibit variability in stiffness and energy dissipation even when geometry is controlled (Cai et al., 2022). This variability becomes more relevant when composites are produced using processes that may introduce non-uniformity in fibre–matrix distribution. Such behaviour can lead to differences in measured FRFs between nominally similar specimens (Mesogitis et al., 2014; Sanei & Fertig, 2015; Waterbury & Drzal, 1989). This study focuses on a TCP system where non-uniform fibre-matrix distribution makes vibration prediction more challenging than for conventional isotropic materials. The dynamic properties of TCP are influenced by heterogeneous microstructure, which can introduce scatter in both effective stiffness and modal damping between specimens.

Existing modelling practice often treats stiffness representation more reliably than damping representation, which creates a common gap in FRF prediction (Moens & Vandepitte, 2005; Navarro-Quiles et al., 2022). Stiffness governs resonance locations through natural frequencies and mode shapes, while damping governs resonance peak amplitude and bandwidth in FRFs (P. Kumar et al., 2023). In many FE applications, stiffness properties can be assigned using available material data, but damping is often introduced using simplified assumptions because it is difficult to characterise directly. When damping assumptions are not representative, FE predictions may reproduce resonance locations but still fail to match FRF peak behaviour (Arora et al., 2009a; J. Huang et al., 2022). This persistent mismatch in FRF peak behaviour motivates a modelling approach that explicitly refines damping representation through systematic updating.

Common experimental approaches such as the tensile testing provide useful information on stiffness but not directly on damping as required for the prediction of vibration. Tensile testing is also destructive, which limits its usefulness when specimens must be preserved for dynamic testing. Even when tensile-derived stiffness is assigned into FE analysis, FRF agreement can remain poor because resonance peak behaviour is strongly affected by damping (Bhattacharjee & Roy, 2020; Butaud et al., 2013; Ebrahimi & Ahari, 2024). This limitation demonstrates that improving stiffness input alone is not sufficient when the objective is accurate FRF peak matching. A dynamic-based route is therefore required to refine damping representation using experimentally measured evidence.

EMA provides a non-destructive method to measure FRFs and to extract modal parameters, including modal damping ratios, which can be used directly as reference targets for FE model improvement (F.-L. Huang et al., 2007; Ramli et al., 2017; Yilmaz et al., 2023). The measured FRFs provide the experimental baseline required to evaluate FE predictions under controlled conditions. When EMA is used as the reference, FEMU can be carried out systematically to improve agreement with measured resonance behaviour (Hassan & Ramle, 2018; Ramli et al., 2017). In this study, the modelling process begins with reducing stiffness-related mismatch so that resonance locations are aligned, and subsequently applies systematic modal damping updating so that FRF peak behaviour approaches the measured response. This combined approach supports the formulation of a staged damping updating scheme for TCP, with the aim of achieving a final updated FE model with demonstrably low error when compared with EMA measurements.

1.2 Background of the Study

Structural dynamics analysis evaluates how a structure responds when subjected to time-varying loads, which can excite vibrations that impact performance and safety (Dharmajan & AlHamaydeh, 2025; C. Wang et al., 2022). Excessive vibration can contribute to fatigue, decreased reliability and can contribute to premature failure if not properly managed (Kamei & Khan, 2021). The primary purpose of structural dynamics analysis is to ensure that vibration responses remain within acceptable limits under operating conditions, thereby supporting safe and reliable structural performance throughout the intended service life. This analysis informs design decisions concerning stiffness, mass distribution, and damping, which collectively determine the dynamic response of a structure. Structural dynamics methods are applied widely in aerospace, automotive, and mechanical engineering applications where accurate dynamic prediction is essential for design verification and performance assurance (Dharmajan & AlHamaydeh, 2025).

Over the past decades, different analytical, numerical, and experimental methods were developed to study the vibration behaviour of engineering structures (Fahlovi et al., 2024; Wilk-Jakubowski et al., 2025; Yarar et al., 2023). These approaches are used extensively in industries like aerospace, automotive and mechanical engineering, where dynamic prediction of the accurate data is essential for design and verification (Aggarwal, 2010; Tang, 2025). Among the available techniques, FE analysis and EMA are commonly used since they offer complementary numerical and experimental descriptions of the structural dynamics. FE analysis provides the possibility of predictions of modal behaviour and response trends before testing is carried out and EMA provides measured vibration evidence that directly reflects the physical structure under the chosen test conditions (Banwell et al., 2012; Gabbert et al., 1995; Mohd Kahar et al., 2024).

However, FE analysis inherently relies on idealised geometry, simplified material models, and assumed boundary conditions that cannot always fully represent real-world structural behaviour (Langer et al., 2021; Mobarhan Zad et al., 2026). As a result, FE analysis is widely used to approximate the dynamic behaviour for complex structures but may suffer from certain inaccuracy by some assumptions, such as idealised supports and simplified damping models (Barazzutti et al., 2024; Ereiz et al., 2022). This limitation is especially important in composite materials, for which heterogeneous microstructure, when combined with fibre-matrix interaction, may introduce complicated damping behaviour.

TCPs, which are produced through fibre-based manufacturing processes, can exhibit non-uniform fibre–matrix distribution and material variability (Ardani et al., 2026). Such variability influences both effective stiffness and damping behaviour under dynamic loading. Although quasi-static tensile testing is often used to determine Young's modulus for FE modelling, tensile response may not fully represent global vibration stiffness, particularly when localised deformation or material heterogeneity is present (Alkhatib, 2023). Furthermore, tensile testing does not provide direct information regarding modal damping behaviour, which is essential for accurate FRF peak prediction.

EMA provides a global dynamic characterisation route by extracting natural frequencies, mode shapes, and modal damping ratios from measured FRFs, Through correlation measures such as natural frequency error, mode shape consistency, and FRF agreement, discrepancies between FE predictions and EMA results can be assessed and reduced. In practice, resonance locations are typically aligned through stiffness-related updating, while FRF peak amplitude and bandwidth require careful refinement of damping representation (Banwell et al., 2012; Hassan & Ramle, 2018). For highly damped composite structures such as TCP, inadequate damping modelling can result in persistent resonance peak mismatch even when frequencies are well aligned.

Therefore, although FE and EMA are commonly used together for vibration analysis, a structured methodology for systematically refining damping representation in TCP remains insufficiently established. This limitation directly motivates the problem addressed in the following section.

1.3 Problem Statement

Despite the availability of tensile testing and EMA for characterising TCP, the primary modelling challenge is not stiffness representation alone but the accurate incorporation of damping within the FE framework. Highly damped composite specimens produce FRFs whose peak amplitude and bandwidth are sensitive to boundary condition implementation, suspension configuration, and damping extraction procedures (Schneider et al., 2018; Treviso et al., 2015), and if these factors are not carefully controlled, the reliability of the identified damping parameters can be compromised.

When damping is poorly represented in the FE model, FRF peak mismatch persists even after resonance frequencies and mode shapes have been successfully aligned through stiffness-related updating (Barazzutti et al., 2024). Direct assignment of experimentally obtained EMA damping ratios into an FE model does not always guarantee accurate reproduction of FRF peak characteristics, particularly for composite materials with variable energy dissipation behaviour such as TCP (Murčinková, Adamčík, et al., 2022). This limitation undermines predictive confidence and restricts the reliability of FE-based vibration assessment for TCP structural applications.

The central problem addressed in this study is the absence of a systematic and experimentally validated modal damping updating scheme for TCP. Existing modelling practice does not offer a structured framework that explicitly separates stiffness-related updating from damping-related calibration in the FE modelling of composite structures (Arora et al., 2009b; Berriet & Link, 1994; Ereiz et al., 2022; Okolie et al., 2025). Without such a dedicated scheme, FE models of TCP remain vulnerable to FRF peak mismatch and unreliable dynamic prediction even when conventional stiffness characterisation methods have been properly employed. The gap is methodological in nature, as no traceable and validated sequence has been established that links stiffness alignment to subsequent damping refinement and confirms improvement at each stage against measured FRF evidence for TCP. This unresolved gap forms the motivation for the formulation, implementation, and evaluation stages defined in this study.

Plate 1.1 Tobacco Composite Panel (TCP) Showing Fibre–Matrix Distribution

1.4 Research Objectives

This study aims to develop and validate a staged FE model updating approach that improves agreement between FE predictions and EMA results for TCP by explicitly addressing both material stiffness inaccuracies and modal damping modelling limitations. The specific research objectives of this study are presented below.

a) To develop a systematic staged methodology that explicitly decouples stiffness-related parameter updating from modal damping calibration for TCP, using EMA measurements as the experimental reference.

b) To implement the staged updating sequence by first reducing natural frequency error to below 1% through stiffness calibration, and subsequently improving FRF peak amplitude and bandwidth through modal damping calibration.

c) To validate the developed framework by comparing updated FE predictions with EMA results using natural frequency error, MAC, and SAC metrics, and evaluating progressive improvements in resonance alignment and FRF peak correlation across all updating stages.

1.5 Research Questions

This study is guided by the following research questions, which are derived directly from the research objectives.

a) What systematic staged methodology can explicitly decouple stiffness-related parameter updating from modal damping calibration for TCP, using EMA measurements as the experimental reference for both stages?

b) How does the staged updating sequence reduce natural frequency error to below 1% through stiffness calibration, and to what extent does subsequent modal damping calibration improve FRF peak amplitude and bandwidth agreement with EMA?

c) What level of progressive improvement in natural frequency error, MAC, and SAC is achieved by the developed framework when updated FE predictions are compared with EMA results across all updating stages?

1.6 Scope and Limitations of the Study

The scope of this study is defined according to the three research objectives, and the associated limitations are stated to clarify the boundaries of the work.

RO1: To develop a systematic staged methodology that explicitly decouples stiffness-related parameter updating from modal damping calibration for TCP, using EMA measurements as the experimental reference.

- The study focuses on vibration-based correlation between FE predictions and EMA outputs, specifically natural frequencies, mode shapes, and FRFs, for the tobacco composite strip and the steel dog-bone specimen.
- The FE models are prepared using PATRAN for pre-processing and analysed using MSC NASTRAN as the solver, with MAT8 orthotropic shell elements assigned for the tobacco composite strip and MAT1 isotropic solid elements for the steel dog-bone specimen.

- EMA measurements are conducted under approximate free-free boundary conditions using soft suspension to reduce support influence on the measured response.
- The correlation is evaluated using consistent metrics including natural frequency error, MAC, and SAC to ensure repeatable and traceable interpretation of discrepancies between FE predictions and EMA results.
- An initial uniform modal damping ratio of 0.01 is applied to all modes in the baseline FE model as a simplifying assumption to provide a consistent starting point for FRF generation before any damping updating is applied.

Limitation: The correlation quality depends on EMA data quality and the adequacy of the FE model assumptions. The orthotropic material model for TCP considers only the primary in-plane elastic moduli and Poisson's ratio as updating parameters, which represents a simplification of the generally anisotropic nature of the material.

RO2: To implement the staged updating sequence by first reducing natural frequency error to below 1% through stiffness calibration, and subsequently improving FRF peak amplitude and bandwidth through modal damping calibration.

- The updating process targets stiffness-related elastic moduli in the first stage and modal damping ratios in the second stage, so that both modal parameters and FRF resonance peak behaviour are improved in a traceable and ordered sequence.
- FEMU is carried out using FEMTools, where EMA-extracted natural frequencies and mode shapes serve as updating targets in the stiffness calibration stage, and FRF peak characteristics serve as the basis for evaluating improvement during modal damping calibration.
- The updating strategy is implemented in stages so that stiffness-related discrepancies are fully addressed before damping representation is refined for FRF peak matching.
- The analysis is restricted to the first two bending modes within the tested frequency range, as these modes are consistently and reliably identified from EMA across all specimens.

Limitation: The updated parameters represent an effective dynamic model within the tested frequency band and setup, and they may not uniquely represent all underlying microstructural variability of TCP. Modal damping updating is applied on a mode-by-mode basis and does not extend to frequency-dependent or full damping matrix updating.

RO3: To validate the developed framework by comparing updated FE predictions with EMA results using natural frequency error, MAC, and SAC metrics, and evaluating progressive improvements in resonance alignment and FRF peak correlation across all updating stages.

- Validation is conducted by comparing the updated FE model with EMA using the same correlation metrics applied consistently across all model stages, from the initial FE model through to the final updated FE model, so that improvement is measured in a directly comparable manner.
- The validation focuses on demonstrating quantitative improvement in modal parameter agreement and reproduction of FRF resonance peak behaviour, with SAC used as the primary indicator of FRF correlation quality across all updating stages.

Limitation: The validation is limited to the tested TCP specimen configuration and measurement strategy. Results may vary if TCP fabrication quality, fibre distribution, or test setup produce different variability patterns in other specimen batches.

1.7 Significance of Study

This study is important because it enhances the robustness of the vibration-based modelling for TCP by defining a traceable workflow between initial FE predictions and EMA results. Reliable dynamic modelling is required where vibration response has an impact on performance, durability and safe operation of engineering components. A clear FE-EMA correlation process assists engineers in interpreting the discrepancy between the predicted and measured behaviour based on uniform indicators such as natural frequency, mode shape agreement and FRFs. By targeting TCP, this work promotes a better understanding of bio-based composites dynamics in which material variability can have a strong influence on the vibration response. This contribution is important when TCP is considered for functional engineering applications that require reliable vibration prediction.

This study is also significant as it opens a practical way to enhance the accuracy of FE prediction by considering the stiffness and damping as separate but related modelling requirements. Many vibration studies are able to achieve acceptable natural frequency alignment by stiffness adjustment, however FRF peak behaviour may be mismatched when damping is calculated based on simplified assumptions. In the present study, the mismatch related to stiffness is reduced by correlation and forming modal-updating-based FE model first and damping representation is refined by modal damping updating to obtain the updated FE model. This order is better for traceability since damping refinement is only done once stiffness alignment is achieved, which means that peak mismatches will not be corrected using stiffness changes which are not physically meaningful. As a result, the updated FE model gives a more realistic model of TCP response in the frequency band selected.

This study also has an academic and practical contribution as it offers a structured methodology combining EMA practice, FE analysis, correlation metrics and FEMU in a single coherent workflow. The workflow is used to illustrate the work flow on how experimental FRFs and modal parameters can serve as references in assessing modelling assumptions and for systematically improving FE predictions. The results provide support for future work on TCP by providing a repeatable procedure for getting stiffness and damping inputs to better represent the measured dynamic response. In industrial terms, the more reliable the dynamic model is the better the design decisions can be made safely and cost effectively when the vibration performance is considered a design constraint. Therefore, the value of this study is to both researchers and practitioners by focusing on the issue of FE-EMA consistency and damping representation.

1.8 Thesis Outline

This thesis is organised into 5 chapters that introduce a systematic methodology for correlating the FE predictions to the EMA results and improving the damping representation for TCP. The chapters follow a logical progression with the motivation and problem definition followed by the method development, implementation, and final validation. The structure is in place to ensure a level of experimental evidence from EMA is always used as the reference to evaluate the accuracy of the FE models. This arrangement ensures that the research objectives are covered in a definite order, from the formulation of the problem to its verification.

Chapter 1 presents the introduction of the study which includes background information, the problem statement, research objectives, research questions, scope, limitations, and the importance of the study. This chapter puts the need for a systematic FE--EMA correlation approach for TCP in the context of the technical gap of accurate damping representation. It describes how the study will be evaluated with a comparison of base line predictions of the FE with the results of EMA, model updating and validation. This chapter establishes the context of the study and is setting the direction for the methodology of the entire study.

Chapter 2 presents a review of the literature to support the theory and techniques that will be required for this study. The characteristics of TCP, the fundamentals of vibration, EMA and FRF based modal identification, FE modelling for dynamic prediction and FEMU approaches are discussed in this chapter. The literature review supports the selection of the indicators of correlation and the necessity of a structured scheme of update where damping has a significant effect on the FRF resonance behaviour. The chapter ends with a summary which relates the research gap to the goals outlined in Chapter 1.

Chapter 3 provides details of the research methodology, describing the workflow that connects the initial FE predictions, EMA testing, correlation and FEMU. The chapter explains the way EMA is carried out as a non-destructive reference for dynamic behaviour of TCP, and how tensile testing is a comparative way as a route after EMA. It also describes the staged process of updating, in which resonance alignment is updated first and secondly damping updating to improve FRF peak behaviour is done. This chapter is to ensure the procedural traceability from the raw measures to the updated model results for evaluation.

Chapter 4 presents the results and discussion including the comparison of FE predictions and EMA results before and after updating. The chapter reports on the baseline mismatch patterns and how the updating process reduces the discrepancies in the modal parameters and FRF resonance peak behaviour. A comparative analysis of the tensile-based stiffness with respect to the stiffness and damping parameters found by FE updating is also presented with reference to the EMA as the experimental base. This chapter is to validate the methodology developed to determine the improvement of the agreement with the experimental reference.

Chapter 5 concludes the thesis by summing up the key findings and drawing some overall conclusions in line with the research objectives. The chapter focuses on the success of the proposed workflow of correlation and updating to improve the representation of TCP damping in FE prediction. It also offers suggestions for future work, on the possibility of extending to other TCP geometries, to wider frequency ranges or to other damping formulations. The thesis concludes with a focus and emphasis on the technical contributions and practical implications of the study.

CHAPTER 2
LITERATURE REVIEW

2.1 Introduction

Accurate dynamic characterisation is a necessary requirement to composite and engineering materials subjected to vibration loading since the vibration response depends on modal parameters and FRFs which need to be identified and interpreted reliably (Gibson, 2000; J. Kumar et al., 2025). Natural frequencies and mode shapes are related to stiffness-mass behaviour of a structure whereas damping controls FRF resonance peak amplitude and bandwidth (Ren & Cao, 2021). These peak characteristics are often the reason for mismatch between predicted and measured response even at similar resonance frequencies. For composite materials, dynamic characterisation is more difficult due to the heterogeneity of the material and sensitivity to boundary conditions, which may affect the measured FRFs as well as the FE predictions (Ballard & Whitcomb, 2019; Raza et al., 2025). Such difficulties require well-organized experimental-numerical working procedures where discrepancies are not only observed but also diagnosed in order to understand whether stiffness or damping modelling is the predominant cause of error.

This chapter takes a review of the literature for the methodology of the present study, which is concerned with the FE-EMA correlation and the systematic improvement of the FE predictions for TCP by identifying the material property and damping modelling inaccuracies. The review draws from journals, conference proceedings, technical reports, and theses to establish current practices in vibration testing, FE dynamic prediction, correlation metrics, and model updating. The discussion highlights how FRF-based evidence from EMA can serve as the experimental reference for evaluating FE accuracy. The chapter also explains how the literature supports updating decisions that are guided by measurable mismatch patterns rather than arbitrary tuning.

The chapter further explains why resonance frequency agreement and FRF peak agreement are commonly treated as two different accuracy requirements in vibration modelling. Resonance frequencies are mainly influenced by stiffness and mass, which are reflected through natural frequencies and mode shapes. In contrast, FRF peak height and FRF bandwidth are strongly affected by damping representation, which is often simplified in baseline FE models. For this reason, many studies first reduce stiffness-related mismatch and then focus on damping refinement to improve FRF peak behaviour once natural frequencies are already aligned. This logic matches the updating flow adopted in this thesis and supports the emphasis on modal damping updating for TCP.

To ensure a structured discussion that matches the objectives of this study, the literature review is organised into the following subtopics:

2.2 Dynamic Characterisation of Materials and Structures
2.3 EMA Techniques for Vibration Analysis
2.4 Tensile Testing for Material Property Evaluation
2.5 FE Modelling and FE Model Updating Methods
2.6 Model Correlation Techniques and Research Gap
2.7 Concluding Remarks

In the final part of this chapter, the key research gaps related to FE–EMA discrepancy interpretation and damping representation for TCP are identified. The discussion emphasises the need for a systematic methodology that links correlation outcomes to targeted updates of material properties and damping parameters. Based on these gaps, the motivation for the workflow adopted in this study is established, where FE predictions are validated directly against EMA results before and after updating. This conclusion section connects the reviewed literature to the method development and validation presented in Chapter 3.

2.2 Dynamic Characterisation of Materials and Structures

Dynamic characterisation evaluates structural behaviour under time-varying or harmonic excitation and therefore provides the basis for interpreting vibration response in service. The dynamic response is governed by mass, stiffness, and damping, which collectively determine natural frequencies, mode shapes, and FRFs that describe the vibration signature of a structure (Mugabo et al., 2019; Packard, 1997). For TCP, dynamic characterisation is essential because heterogeneous microstructure and non-uniform fibre–matrix distribution can produce variability in effective stiffness and damping (Okolie et al., 2023b). This variability can influence resonance location and resonance peak behaviour even when geometry is kept constant.

TCP belongs to the category of plant fibre composites, in which energy dissipation behaviour is governed by viscoelastic effects at the fibre-matrix interface, moisture sensitivity, and non-uniform fibre distribution introduced during fabrication (Liu et al., 2021; Ma et al., 2021). These characteristics produce damping levels that are substantially higher and more variable between specimens than those typically observed in synthetic fibre composites or metallic structure (Haris et al., 2022) s. The non-uniform tobacco fibre distribution within the matrix cannot be fully controlled during production, which leads to specimen-to-specimen variability in both effective stiffness and modal damping ratios, making TCP a challenging yet relevant case study for FRF-based FE model updating (Ardani et al., 2026). Polymeric composite materials of this type also exhibit frequency-dependent damping behaviour that is not easily captured using proportional damping assumptions, because the energy dissipation mechanisms at the fibre-matrix interface are sensitive to the amplitude and frequency of dynamic loading (Murčinková, Postawa, et al., 2022). This material behaviour distinguishes TCP clearly from conventional isotropic materials and underscores the need for a dedicated damping updating scheme.

Steel, by contrast, is a well-characterised isotropic material that exhibits predictable and repeatable dynamic behaviour with low and consistent modal damping ratios across specimens (P. Kumar et al., 2023). The elastic modulus and Poisson's ratio of structural steel are well established, and its isotropic symmetry means that a single set of elastic constants is sufficient to define stiffness behaviour in FE modelling without requiring extensive calibration. The inclusion of the steel dog-bone specimen in this study therefore serves a deliberate verification purpose within the FE-EMA correlation and updating framework: it allows the EMA procedure, FE modelling workflow, and updating strategy to be evaluated using a material for which the dynamic behaviour is predictable and repeatable, before the same procedures are applied to the more variable TCP specimens (Michal et al., 2024). The contrast between the polymeric composite TCP and the isotropic steel also provides a controlled comparison that highlights how strongly material damping variability influences the difficulty of FRF peak matching, since steel specimens require comparatively less damping refinement than TCP to achieve acceptable FRF correlation. This deliberate pairing of specimens therefore strengthens the overall validation of the proposed methodology.

Dynamic properties obtained under vibration conditions can be more representative for vibration prediction than quasi-static properties because oscillatory motion activates additional dissipation mechanisms. Under dynamic excitation, viscoelastic effects, interface friction, and micro-slip mechanisms can contribute to energy loss that is not captured clearly in static loading (DICKENS, 2000; Yaacob et al., 2025). This difference affects the apparent stiffness–damping combination that governs the measured FRF. Consequently, stiffness values derived from static testing may not represent the effective global stiffness controlling vibration response. This limitation motivates the use of vibration-based characterisation when FRF peak agreement is required (Ammar et al., 2022; Y. Wang et al., 2022).

Unreliable dynamic characterisation can reduce confidence in FE-based vibration prediction because it can lead to incorrect resonance identification and unrealistic FRF resonance peak behaviour. This risk is more critical in lightweight TCP structures because damping strongly controls resonance peak bandwidth and amplitude (Murčinková, Adamčík, et al., 2022; Okolie et al., 2023a). When damping is not represented appropriately, a model may align resonance locations but still fail to reproduce peak sharpness and decay behaviour. Therefore, a structured theoretical framework is required to interpret discrepancies between FE predictions and EMA results in a traceable way. This framework supports a staged approach where stiffness-related mismatch is addressed first, followed by damping-related refinement.

Section 2.2 summarises the core structural dynamics relationships needed to interpret FE predictions and EMA results for TCP, with emphasis on how stiffness and damping influence FRF behaviour. The section starts with the governing equation of motion and introduces the undamped form used for modal prediction. It then presents the eigenvalue formulation used to obtain natural frequencies and mode shapes for correlation. Next, damping is introduced through modal damping ratio and practical damping models used in FE analysis. The FRF formulation is then presented in matrix and modal forms to relate resonance location and peak behaviour to stiffness and damping. Finally, a generic updating objective function is introduced to link correlation and updating within a systematic workflow.

2.2.1 Governing Equation of Motion for Structural Dynamics

The vibration response of a structure is governed by the equation of motion that relates inertia, damping, and stiffness to the applied excitation (Du et al., 2025). The general forced vibration relationship in matrix form is written as

$$M\ddot{x}(t) + C\dot{x}(t) + Kx(t) = f(t) \tag{2.1}$$

where M, C, and K are the mass, damping, and stiffness matrices, $x(t)$ is the displacement vector, and $f(t)$ is the applied force vector. This formulation is fundamental because it defines the physical sources of response and clarifies the separate roles of stiffness and damping. It is also consistent with FE prediction because M and K are derived from geometry and material properties while C represents the damping model (Friswell et al., 1998; Ko & Boo, 2022; Zeng et al., 2025). For TCP, Equation (2.1) is especially relevant because matching FRF peak behaviour requires a damping representation that is physically consistent.

The undamped free vibration form is used when the objective is limited to predicting natural frequencies and mode shapes without considering damping effects (You et al., 2022). By setting $f(t) = 0$ and neglecting damping, the governing relationship reduces to

$$M\ddot{x}(t) + Kx(t) = 0 \tag{2.2}$$

which isolates stiffness–mass behaviour. This form supports early-stage correlation because resonance locations are governed mainly by stiffness and mass. It also prevents damping-related mismatch from being compensated incorrectly through stiffness changes. For that reason, Equation (2.2) provides a structured starting point for evaluating stiffness modelling accuracy before damping refinement.

2.2.2 Natural Frequencies and Mode Shapes

Natural frequencies and mode shapes are obtained by solving the eigenvalue formulation derived from the undamped equation of motion. Assuming harmonic motion $x(t) = \phi e^{i\omega t}$, substitution into Equation (2.2) yields

$$(K - \omega^2 M)\phi = 0 \quad (2.3)$$

which relates stiffness, mass, and the mode shape vector ϕ. The condition for non-trivial solutions is expressed by the characteristic equation

$$\det(K - \omega^2 M) = 0 \quad (2.4)$$

which produces the set of natural frequencies $\omega_n$and corresponding mode shapes ϕ_n. These parameters are central to FE–EMA comparison because they define resonance locations and deformation patterns that are directly observable in EMA. For TCP, frequency mismatch is typically interpreted as stiffness-related modelling inaccuracy before damping effects are evaluated.

Mode shapes are expressed in normalised form in numerical analysis to support consistent interpretation and stable comparison across modes. A common choice is mass normalisation, written as

$$\phi_r{}^T M \phi_s = 0, \qquad r \neq s \quad (2.6a)$$

and

$$\phi_r{}^T K \phi_s = 0, \qquad r \neq s \quad (2.6b)$$

and these properties support modal superposition and mode tracking during correlation. In EMA, experimental mode shapes may have different scaling, so correlation focuses on relative shape agreement rather than absolute magnitude (Kranjc et al., 2013). This approach maintains meaningful comparison even when different test setups affect response amplitude scaling.

2.2.3 Damping Representation and Modal Damping Ratio

Damping must be represented explicitly when the objective is to reproduce FRF resonance peak behaviour rather than resonance location alone (Gazdagh & Vehovszky, 2021). In Equation (2.1), damping appears through $C\dot{x}(t)$, which governs energy dissipation and influences peak bandwidth and decay behaviour. A practical descriptor used in vibration analysis is the modal damping ratio ζ_n, defined in an equivalent single-mode form as

$$\zeta_n = \frac{c_n}{2m_n\omega_n} \tag{2.7}$$

where c_n is the modal damping coefficient, m_n is the modal mass, and ω_n is the natural circular frequency. This relationship indicates that once ω_n and the effective modal inertia are established, the damping term becomes the key contributor to resonance peak bandwidth and amplitude. For TCP, modal damping is a critical modelling component because damping levels can be higher and more variable than in metallic structures.

Practical damping modelling in FE analysis often uses simplified assumptions to represent energy dissipation within the available solver framework (Zareian & Medina, 2010). A widely used proportional form is Rayleigh damping, expressed as

$$C = \alpha M + \beta K \tag{2.8}$$

where α and β are coefficients selected to match target damping ratios at selected modes. This form is convenient because it depends only on mass and stiffness matrices that are already available in the model. However, Rayleigh damping may be limited when damping varies strongly across modes, as may occur in composite materials (Murčinková, Postawa, et al., 2022). Therefore, mode-dependent damping representation becomes important when the goal is to match FRF resonance peak behaviour accurately.

2.2.4 FRF Formulation in the Frequency Domain

FRF provides a frequency-domain relationship between force input and response output and therefore forms the main bridge between EMA measurements and FE predictions (Lázaro et al., 2010; U. Lee & Shin, 2002). For harmonic excitation $\mathrm{f}(t) = \mathrm{F}e^{i\omega t}$ and steady-state response $\mathrm{x}(t) = \mathrm{X}e^{i\omega t}$, substitution into Equation (2.1) yields

$$(-\omega^2 M + i\omega C + K)X = F \quad (2.9)$$

which represents dynamic equilibrium in the frequency domain. Rearranging Equation (2.9) gives the frequency response matrix

$$H(\omega) = \frac{X}{F} = (K + i\omega C - \omega^2 M)^{-1} \quad (2.10)$$

showing that resonance location is governed mainly by stiffness and mass, while peak sharpness is influenced by damping through the $i\omega$C term. This separation supports staged correlation strategy because stiffness changes mainly shift resonance positions, while damping changes affect peak width and amplitude. For TCP, this relationship explains why damping refinement is required after resonance alignment is achieved.

FRFs can be expressed in different response forms depending on whether displacement, velocity, or acceleration is used as the output quantity (Xu & Lu, 2021). If receptance $H_x(\omega)$ is defined as displacement over force, the mobility relationship is

$$H_v(\omega) = i\omega H_x(\omega) \quad (2.11a)$$

and the accelerance relationship is

$$H_a(\omega) = (i\omega)^2 H_x(\omega) = -\omega^2 H_x(\omega) \quad (2.11b)$$

which are direct frequency-domain differentiation relationships. This distinction matters because impact testing commonly measures force input and acceleration output, meaning experimental FRFs often correspond to accelerance. Consistent FRF definition avoids mismatched comparisons when FE predictions are validated against EMA. This consistency becomes especially important when damping is updated using resonance peak behaviour as a target.

2.2.5 Modal Form of FRF and Link to Modal Parameters

The modal form of FRF provides an explicit connection between modal parameters and the resonance peak behaviour observed in measured FRFs (Zrayka & Mucchi, 2019). Under modal superposition, the receptance FRF between a response DOF j and input DOF k is written as

$$H_{jk}(\omega) = \sum_{n=1}^{N} \frac{\phi_{jn}\phi_{kn}}{{\omega_n}^2 - \omega^2 + i2\zeta_n\omega_n\omega} \tag{2.12}$$

where ϕ_{jn} and ϕ_{kn} are mode shape components and ζ_n is the modal damping ratio. This formulation shows that ω_n controls resonance location while ζ_n controls bandwidth and peak amplitude. It also clarifies why stiffness updates mainly align resonance positions, while damping updates are required to reproduce peak sharpness once resonance location is corrected. For TCP, Equation (2.12) provides a direct theoretical basis for prioritising damping updating when FRF peak matching is required.

Modal parameter extraction is possible because measured FRFs contain resonance information in both magnitude and phase across frequency (Topaloglu & Karadag, 2022). In EMA, identification procedures estimate ω_n, ϕ_n, and ζ_n by fitting FRFs within the frequency band of interest. Damping estimation is typically more sensitive than frequency estimation because damping depends on peak bandwidth and peak shape rather than resonance location alone. For TCP, higher damping and potential close mode spacing can reduce peak sharpness, which increases uncertainty if FRF quality is not controlled. Therefore, consistent test setup and processing are essential when EMA results are used as the updating reference for damping refinement.

2.2.6 Relevance to FE–EMA Correlation and Updating

The formulations in Section 2.2 provide a structured basis for interpreting discrepancies between FE predictions and EMA results in a staged and traceable workflow. Frequency mismatch is primarily linked to stiffness–mass modelling through Equations (2.2) until (2.4), while peak width and amplitude mismatch are linked to damping modelling through Equations (2.7), (2.10), and (2.12). This separation supports an ordered procedure in which resonance locations are aligned first through stiffness-related correction, and resonance peak behaviour is then refined through damping-related correction. Such staging reduces ambiguity because each correction step targets a different physical cause of mismatch. This approach aligns with the objective of developing a damping updating scheme that improves FRF peak agreement for TCP.

Model updating can be represented as an optimisation process that minimises the residual between predicted and measured dynamic quantities. A generic objective function is written as

$$J(p) = \|y_{EMA} - y_{FE}(\mathrm{p})\|^2 \tag{2.13}$$

where p is the update parameter vector and ymay include modal parameters and/or FRF data. This formulation supports systematic updating because it links modelling parameters to measurable response quantities. Within this framework, stiffness-related parameters influence K and therefore resonance location, while damping-related parameters influence C or ζ_n and therefore resonance peak behaviour. In this study, EMA provides the baseline reference and the updated FE model is validated by improvement in modal agreement and FRF peak characteristics. Therefore, Section 2.2 justifies treating damping as a central update target when accurate vibration prediction is required for TCP.

2.3 EMA Techniques for Vibration Analysis

2.3.1 Overview of EMA Workflow

EMA is used in this study to obtain experimental FRFs and modal parameters that represent the specimen dynamic behaviour and serve as the reference for FE correlation and subsequent updating. The workflow begins by selecting a suspension and test configuration that approximates free-free behaviour so that support influence on the measured response is minimised (Bondsman & Peplow, 2025; Sharma, 2019). After the test condition is defined, the excitation method is selected to provide sufficient input energy within the frequency range of interest (Gülbahçe & Çelik, 2022; Varahram et al., 2019). The response measurement strategy is then established by specifying sensor type, sensor orientation, and measurement points so that the dominant vibration behaviour is captured consistently across repeated tests (Kuś et al., 2025; Pei et al., 2025). Next, acquisition settings such as sampling rate, frequency resolution, and averaging are selected to ensure stable FRF estimation (Żółtowski & Napieraj, 2017). Finally, the measured signals are processed to compute FRFs and extract natural frequencies, mode shapes, and modal damping ratios that are later used for FE–EMA correlation and for developing the updated FE model through stiffness alignment followed by damping refinement (Abdullah et al., 2017; Huňady et al., 2021; Pradhan & Modak, 2018).

EMA planning is essential because reliable correlation and updating require modal parameters that are consistent, repeatable, and based on high-quality FRFs (Tamizifar et al., 2022). A measurement layout is defined first so that the selected points can describe the targeted mode shapes within the chosen frequency band (X. Jiang & Jiang, 2020; Nimityongskul & Kammer, 2009; Sun et al., 2025). The excitation location is then selected to ensure adequate response for the expected modes while avoiding nodal regions that weaken the measured signal (Khoo et al., 2020). Sensor orientation and mounting are controlled to capture the intended motion direction while limiting mass-loading influence on the measured response (McClintock et al., 2024). Repeatability is strengthened by applying consistent impact procedure and averaging so that random noise is reduced and FRF stability is improved (Żółtowski & Napieraj, 2017). These planning steps ensure that the extracted modal parameters and FRFs provide a dependable experimental basis for stiffness-related correlation and for damping updating focused on FRF peak behaviour.

2.3.2 Boundary Conditions and Suspension

Boundary conditions must be controlled because they directly influence measured modal parameters and FRFs, which later become the reference for FE correlation and updating (Sharma, 2019). Free-free condition is commonly targeted so that the measured response represents the inherent dynamics of the specimen rather than restraint effects from a fixture (D. Jiang et al., 2024). In practice, free-free condition is approximated using soft suspension so that the support stiffness remains small compared to the specimen stiffness within the frequency range of interest (Tamizifar et al., 2022). Suspension locations are then selected to minimise interference with dominant deformation regions of the targeted modes so that mode shapes and resonance behaviour remain representative (Sayahkarajy, 2018). Suspension compliance is also selected to avoid introducing support resonances that could distort FRF peaks and bias damping estimation (Sekulic & Dedović, 2011). These boundary control steps improve confidence that the measured FRFs reflect specimen behaviour and can be used reliably in the subsequent updating stages.

Suspension design must also prevent support-induced artefacts because composite strips can be sensitive to local constraint effects that reduce repeatability. Soft suspension can introduce low-frequency rigid-body modes, so the suspension is configured such that rigid-body motion remains below the analysis band and does not overlap with structural modes of interest (Freddi et al., 2025; Kowalski, 2025). The specimen is suspended in a stable configuration to minimise rocking and to maintain consistent impact response across repeated measurements. Contact conditions are kept constant throughout testing because changing contact can introduce nonlinearity and reduce coherence, which weakens the reliability of extracted damping (Dharmajan & AlHamaydeh, 2025; Xie & Hua, 2024). FRF consistency across repeated impacts is therefore used as a practical indicator that support influence remains minimal (Brown et al., 2025; Sevkat et al., 2010). With these controls, the extracted modal parameters, including damping, are more suitable for developing and validating the proposed damping updating scheme.

2.3.3 Excitation and Response Measurement

Excitation must be selected carefully because FRF estimation requires a measurable input force with adequate bandwidth across the frequency range of interest (Altun et al., 2023; Schoukens et al., 2004). Impact excitation is suitable for EMA because it provides broadband input content that supports FRF estimation over a wide frequency band (Lim et al., 2018). The location of impact is chosen so that the targeted modes are excited and the nodal regions are avoided that cause low response amplitude and less observability of modes (Loi et al., 2022). Hammer tip selection is adjusted in order to tailor the input force spectrum to deliver enough energy in the frequency band of analysis without suffering double hits (Zahari & Sani, 2017). Impact consistency is maintained in terms of repeatable hit direction and duration of contact so that averaging will improve FRF stability (Kwon & Lin, 2004). These practices yield input-output data which are reliable for the extraction of the resonance location as well as the damping-related peak behaviour.

Response measurement also needs to be set up carefully since accurate modal parameters require response signals which represent specimen motion without excessive measurement distortion. Accelerometers are used because they provide direct response measurement within the frequency range of interest, and their output is suitable for acceleration FRF estimation (Pimenov et al., 2022). Three monoaxial accelerometers (MMF KS91C) are employed with consistent sensor orientation so that response direction remains comparable across measurements (Yu et al., 2023). Sensor mounting is controlled to reduce mass loading and local stiffening effects, which is especially important for lightweight composite strips (Janeliukstis & Mironovs, 2021; Lu et al., 2021). Cable routing and attachment are managed to minimise cable-induced stiffness and to reduce electrical and handling noise (Pang et al., 2024; Sanjeevi & Vashista, 2023). With these controls, the measured response supports stable FRFs and consistent extraction of mode shapes for FE correlation.

2.3.4 FRF Estimation and Data Quality

FRF quality must be ensured because modal parameter extraction depends on stable and repeatable input–output measurements. FRFs are computed from the measured force and acceleration signals using standard estimators implemented in the acquisition and analysis software (Zhu et al., 2020). The coherence function is evaluated to confirm that the measured response is linearly related to the measured input over frequency and that noise contamination is limited (Ciura et al., 2023). Windowing is applied to reduce leakage effects associated with impact testing, while averaging is applied to reduce random noise and improve repeatability (Jwo et al., 2019). Trigger settings are regulated to ensure that the impact events are captured consistently and there is less variation in the force input from run to run (Yazdi et al., 2024). These steps aid reliable FRF characteristics which are appropriate for correlation and further staged updating.

Signal processing settings need to be carefully chosen due to the frequency resolution and noise level, which has an influence on the resonance definition in the measured FRFs (Allemang et al., 2022; Ichiki & Tadokoro, 2013). Frequency resolution is chosen to ensure that the peaks of resonances may be distinguished clearly and separated from the neighbouring modes, which enhances stability in the frequency and damping estimation (Deng et al., 2024). The number of averages is selected to enhance signal-to-noise ratio without making testing time practical and ensuring consistent quality of impact (Brown et al., 2025). Repeatability is measured by comparing trends in FRF magnitude and phase with repeated impacts done under the same set up. Any abnormal coherence drops are investigated as they may represent poor sensor attachment, non-linear contact behaviour or lack of excitation energy (Modak, 2023). By solving these problems at an early stage, the extracted modal data set is more defensible for the update of that, which aims at both resonance alignment and damping behaviour.

2.3.5 Modal Parameter Extraction

Modal parameter extraction is required because FE correlation and updating rely on modal parameters obtained from experimental FRFs. Natural frequencies are identified from resonance locations in the measured FRFs, and mode shapes are obtained by combining FRFs measured at multiple response points to form relative deformation patterns (Azhar et al., 2023). Damping ratios are estimated using identification procedures that interpret resonance peak bandwidth and peak shape, which makes damping more sensitive to measurement quality than frequency (González et al., 2012; Ni et al., 2023). Frequency resolution and signal-to-noise ratio are therefore controlled to ensure that damping estimates remain stable and repeatable (Sinha et al., 2024). The extracted modal parameters and FRFs are then used as the experimental reference for evaluating FE predictions. This linkage is essential in this study because EMA results provide the baseline for validating stiffness and damping modelling.

Identification strategy must be selected appropriately because composite specimens can exhibit higher damping and closely spaced modes that complicate extraction. Peak Picking is used as an initial method when modes are well separated and FRF quality is high, because resonance locations can be identified directly with minimal model assumptions (Treviso et al., 2015). Curve fitting methods, including PolyMAX, are used when modes overlap or when more robust damping estimation is required based on both magnitude and phase behaviour (Peeters et al., 2004). Mode selection is restricted to modes with repeatable FRF peaks and stable phase trends so that the updating targets are not biased by non-repeatable measurements. Damping results are interpreted cautiously because damping is sensitive to boundary condition consistency and processing choices (Brandt et al., 2017; Mares et al., 2006). With these controls, the experimental modal dataset supports staged updating, where resonance alignment is addressed before damping refinement is evaluated.

2.3.6 EMA System Used in This Study

The measurement system must be stated because acquisition hardware and analysis software define the environment in which FRFs and modal parameters are generated. Simcenter SCADAS is used to acquire force and acceleration signals and to compute FRFs within the selected frequency bands. Simcenter Testlab is used to perform FRF processing and modal parameter extraction using tools such as Peak Picking and PolyMAX curve fitting (Kharchenko et al., 2023). An impact hammer (PCB 086C02) is used as an excitation source to provide a broadband force input and monoaxial accelerometers (MMF KS91C) are used as response sensors. Acquisition settings are applied in a consistent manner so that variations in the results come from specimen behaviour and set-up variation rather than the software defaults that are present. This consistency contributes to the reliable use of the results of EMA for the baseline correlation and update.

Platform consistency is important since variations in the estimation's and processing settings can cause FRF magnitude, coherence and damping estimates to vary (Úradníček et al., 2025). Using a single acquisition and processing environment helps to minimise the possibility of mismatches due to software specific default parameters. Data management within the same system also improves traceability from raw time signals to processed FRFs and extracted modal parameters. Repeatability checks are strengthened when consistent templates are used for acquisition and processing across all setups and specimens. This traceability becomes important when the study aims to justify damping updating decisions based on measured FRF peak behaviour. With these controls in place, the EMA dataset remains defensible as the experimental reference for evaluating FE modelling and the proposed damping updating scheme.

2.4 Tensile Testing for Material Property Evaluation

2.4.1 Purpose of Tensile Testing in This Study

Tensile testing is included in this study as a quasi-static and destructive approach for estimating Young's modulus from a controlled uniaxial loading condition. The tensile result provides a conventional stiffness value that is widely reported for materials and is commonly used in engineering design (Yildiz, 2025). In this thesis, tensile testing is not treated as the baseline reference for dynamic validation because the primary reference is the EMA-derived FRFs and modal parameters. Instead tensile testing is placed in the position of providing a comparison stiffness route that can be evaluated against dynamic-based identification. This positioning contributes to the focus of the study on improving FE agreement with EMA before improving the representation of damping. The tensile modulus is thus a benchmark that emphasises possible differences between representation of static and dynamic stiffness.

Tensile testing is also included because it offers a clear and repeatable procedure that can be applied consistently across multiple specimens. The method produces stress–strain curves that allow direct extraction of modulus from the linear region under quasi-static loading (Giani & Locarno, 2025). This output is useful for discussing the extent to which local material response can represent global vibration response for TCP-derived strips. The destructive nature of tensile testing motivates performing EMA first in the overall methodology so that the specimen dynamics are captured before failure. The tensile results are later used to support comparison discussions rather than to define the updating reference. Through this role, tensile testing contributes to a more balanced evaluation of stiffness identification approaches in the thesis.

2.4.2 Tensile Response and Stress–Strain Fundamentals

Tensile testing characterises material response by relating applied force to deformation through engineering stress and engineering strain definitions. Engineering stress is calculated using the applied force divided by the initial cross-sectional area,

$$\sigma = \frac{F}{A_0} \tag{2.14}$$

and engineering strain is calculated using elongation divided by the initial gauge length,

$$\varepsilon = \frac{\Delta L}{L_0} \tag{2.15}$$

where F is the force, A_0 is the initial area, ΔL is elongation, and L_0 is the gauge length. These definitions provide a consistent basis for producing stress–strain curves from measured load–displacement data. The stress–strain curve is then interpreted to identify the region suitable for modulus estimation. This foundation is needed because the extraction of the modulus is sensitive to the inputs of the geometry as well as the interpretation region used (Goharian, 2017).

The stress–strain curve is typically interpreted by separating an initial linear elastic segment from later non-linear response. The linear segment is associated with elastic deformation where strain increases proportionally with stress, while non-linear behaviour may indicate damage initiation, viscoelastic effects, or progressive microstructural changes in composites. This distinction matters because Young's modulus is defined in the linear region, and using data beyond the linear region can bias the estimated slope (Mat Samudin et al., 2025). The earliest portion of the curve may also be influenced by grip seating and alignment, which can reduce apparent linearity even before true material non-linearity occurs (Jeannin et al., 2024). For that reason, the stress–strain fundamentals are directly linked to the need for a consistent modulus extraction procedure. This consistency becomes important when tensile-derived stiffness is later compared with stiffness implied by EMA-based updating.

2.4.3 Young's Modulus Determination from Tensile Data

Young's modulus is obtained from tensile testing by measuring the slope of the stress–strain curve within the linear elastic region. The modulus is defined as

$$E = \frac{d\sigma}{d\varepsilon} \tag{2.16}$$

and is usually estimated using linear regression over a selected strain interval. A defined interval is necessary because the curve can exhibit small deviations from ideal linearity due to experimental effects and composite material variability. Using regression rather than two-point slope reduces sensitivity to random noise in the measured force and displacement signals (International, 2008). The resulting modulus value provides a stiffness parameter that can be used for comparison with stiffness parameters obtained through vibration-based correlation and updating. This step therefore establishes how tensile testing contributes to stiffness evaluation in the thesis.

A consistent modulus extraction procedure is required because the chosen fitting range influences the slope and therefore the reported modulus (International, 2008). The initial portion of the curve may include seating effects where the specimen and grips settle into a stable load path, which can underpredict modulus if included in the fit. For composites, early micro-damage can also reduce the slope, which can cause modulus to depend on the strain interval even within a visually "linear" region (Kostic et al., 2022). For this reason, the same fitting approach should be applied to all specimens to ensure comparability across repeats. Reporting should also include repeated tests so that scatter can be evaluated and unrealistic outliers can be identified. This procedure ensures that tensile-derived modulus values are defensible as comparison data in later discussions.

2.4.4 Specimen Preparation and Test Standard Considerations

Specimen preparation affects tensile response because geometry and surface condition influence stress distribution and repeatability. In this study, strip specimens are prepared from TCP and are intended to develop strain primarily within a defined gauge region. Dimensional measurement is important because thickness and width determine the initial area used in Equation (2.14), and small errors directly influence stress and modulus. Edge quality is controlled because rough edges can introduce stress concentration and promote early failure outside the intended gauge behaviour. Gauge length definition is also maintained consistently because it appears explicitly in Equation (2.15) through L_0. These controls assure that measured contrasts of stress extension response will not be governed by stuff that were avoided off-important geometric inconsistencies.

Test practice is also driven by standard considerations given that tensile modulus requires uniform gripping, alignment and loading definition. Standards for tensile testing of composites can be referred to in order to justify the specimen handling, gauge definition and reporting conventions without reproducing the complete standard procedure (Fazlali et al., 2025). Alignment is emphasised as eccentrical loading will introduce bending strain resulting in the stress-strain curve becoming less representative of pure uniaxial (Flauder et al., 2025). Gripping method is used to hold the specimen in a stable manner by minimising local crushing and slip close to the grips (Polilov et al., 2021). Preparation consistency is particularly important for TCP derived strips as there is already microstructural variability which already contributes to scatter. With these considerations, you can see that the tensile dataset is more defensible for comparison to the results of dynamic-based identification.

2.4.5 Test Setup and Instrumentation

Test setup has an effect on modulus estimation since quality of stress-strain curve depends on the quality of force measurement and quality of strain measurement. A universal tensile testing machine puts load through controlled crosshead movement and measures the force by load cell, and displacement and strain will be measured through the machine system or external measurement devices. The measured force and displacement signals are transformed to engineering stress and strain by Equations (2.14) and (2.15) which are based on the specimen geometry and gauge length. The crosshead speed or strain rate is controlled in order to maintain quasi-static conditions so as to minimise the rate-dependent effects in polymer-based composites (Ma et al., 2021). Grips are chosen to achieve a good level of clamping with minimum damage near the ends due to the fact that grip damage can distort the early linear response. These set up decisions provide support for generating stable stress-strain data for modulus extraction:

Instrumentation choices have also an effect of uncertainty since strain estimation can vary depending on crosshead displacement or local strain measurement. Crosshead displacement usually contains machine compliance and grip deformation which will overestimate the strain and underpredict the modulus if not corrected for (Kostic et al., 2022). Local strain measurement methods are able to reduce this issue but need careful attachment, calibration and consistent gauge placement (Song et al., 2023). Data acquisition settings must also have enough resolution so that the small changes of strains in the linear region can be recorded correctly (Kostic et al., 2022). Repeat tests are important because the instrumentation related scatter can be detected by making consistency cheques. By control of setup and instrumentation the tensile results are more meaningful when compared to the stiffness levels implied by EMA-based FE updating.

2.4.6 Common Error Sources and Uncertainty in Composite Tensile Tests

Tensile testing of composite strips can produce scatter because composite deformation is influenced by heterogeneous microstructure and local damage mechanisms. Local variations in fibre distribution and resin content can cause strain localisation even under nominally uniaxial loading. This localisation can lead to early deviation from ideal linearity and can affect the slope used for modulus estimation. Micro-damage such as matrix cracking or fibre–matrix debonding may also initiate before visible failure and can reduce stiffness progressively within the gauge region (Livingston & Koohbor, 2022). Grip pressure can introduce local crushing and initiate damage near the ends, which can influence measured response even if failure occurs elsewhere (Fazlali et al., 2023). These behaviours explain why tensile modulus of composite strips can vary more than metallic specimens under similar testing practice.

Measurement-related uncertainty also affects modulus because Young's modulus is highly sensitive to strain estimation accuracy. Specimen slippage in the grips introduces apparent extension that is not true gauge strain, which can reduce the computed modulus. Misalignment introduces bending strain, which produces a non-uniform strain field and biases the stress–strain slope (Flauder et al., 2025; Kostic et al., 2022). Crosshead displacement includes machine compliance, while local strain devices introduce their own attachment and calibration sensitivity (Kostic et al., 2022). These sources of uncertainty can be reduced through consistent gripping, careful alignment, and a consistent strain measurement approach across specimens. Even with controls, some uncertainty remains due to intrinsic composite variability, which supports the thesis decision to treat tensile modulus as a comparison route. This context is important when later interpreting differences between tensile-derived modulus and stiffness implied by EMA-based updating.

2.4.7 Relevance of Tensile-Based Modulus to Dynamic Prediction

Tensile-based Young's modulus is relevant to dynamic modelling because stiffness influences FE natural frequencies and resonance locations in FRFs through the stiffness matrix. If modulus is underestimated, predicted natural frequencies shift lower and FRF resonance peaks shift accordingly, while overestimation shifts resonance locations higher (Onyibo et al., 2025). These sensitivity effects make modulus selection important when the objective is to reproduce EMA-measured resonance behaviour with FE predictions. Tensile testing provides a stiffness value derived from quasi-static loading, which is often adopted as an initial stiffness input in modelling practice. However, the suitability of this value must be assessed against vibration-based measurements when the goal is accurate dynamic prediction. This need motivates comparison between tensile-derived stiffness and stiffness implied by EMA-based correlation (Zhao et al., 2023).

Tensile-derived modulus may differ from effective dynamic stiffness because tensile testing reflects local quasi-static behaviour while vibration response reflects global deformation with frequency-dependent dissipation. For TCP-derived strips, this difference can remain even when tensile tests are carefully performed because damping mechanisms and microstructural variability influence FRF peak behaviour beyond stiffness alone (Haris et al., 2022). The thesis therefore uses EMA as the baseline reference because EMA provides FRFs and modal parameters that directly represent measured vibration behaviour. Subsequent sections and chapters compare FE predictions with EMA results to identify stiffness-related discrepancies first and then refine damping representation through updating (Zhao et al., 2023). Tensile results are then used to support evaluation of whether a quasi-static modulus provides adequate agreement compared with parameters obtained through EMA-based updating.

2.5 FE Modelling and FE Model Updating Methods

2.5.1 FE Modelling for Dynamic Prediction

FE modelling is used in this study to predict modal parameters and FRFs so that numerical results can be compared directly with EMA as the baseline experimental reference. The FE model represents specimen geometry, mass distribution, and material properties so that stiffness and inertia are captured within a numerical framework. Geometry and element formulation are selected to represent the expected deformation characteristics of the TCP-derived strip and the TCP component being modelled. Material properties are assigned based on available information so that an initial dynamic prediction can be produced before any correlation or updating is performed. The model is then analysed to obtain predicted modal parameters and FRFs within the frequency range relevant to the experiment. These baseline predictions provide the starting point for identifying discrepancies relative to EMA results (Ereiz et al., 2022).

Mesh convergence is performed because discretisation quality can influence predicted natural frequencies and FRFs even when material properties are correct (Aleyaasin, 2025). The convergence process begins with an initial mesh and repeats the analysis using progressively finer meshes to observe changes in predicted natural frequencies. When the frequency shifts reduce and stabilise with refinement, the mesh is considered adequate for modal prediction in the modes of interest. FRF sensitivity to discretisation is also considered because local stiffness distribution and numerical damping effects can influence resonance amplitudes and bandwidth trends (Aleyaasin, 2025). A converged mesh reduces the likelihood that model updating compensates for numerical error rather than correcting physical parameter mismatch (Ereiz et al., 2022). This control improves confidence that subsequent updating reflects material property and damping representation rather than modelling artefacts.

2.5.2 Modal and FRF Analysis in FE

Modal analysis is performed because the stiffness–mass relationship described in the governing structural dynamics equation (2.2) can be solved to obtain natural frequencies and mode shapes for correlation with EMA. In FE analysis, this is implemented as an eigenvalue solution in which the model matrices generated from geometry, material properties, and discretisation produce the predicted modal set within the frequency range of interest (Mahat et al., 2024). The predicted modes are then organised and paired consistently so that comparisons with experimentally extracted modes can be made without ambiguity. Mode shape scaling and coordinate consistency are handled carefully because correlation relies on relative deformation patterns rather than absolute amplitude. This modal dataset is used to identify whether mismatch is primarily stiffness-driven before damping refinement is considered. The outcome supports the staged workflow where resonance alignment is addressed first prior to damping updating.

FRF analysis is performed because FRFs provide a direct frequency-domain representation that can be compared with EMA FRFs under matching input–output

DOFs. The FE FRF calculation is based on the same governing dynamics relationship with damping representation (2.1), where damping influences resonance peak amplitude and bandwidth in addition to stiffness-driven resonance locations (J. Li et al., 2024). Input and response DOFs are defined to match the EMA excitation and accelerometer locations so that the comparison reflects the same physical points on the specimen. The frequency sweep is then performed over the analysis band so that resonance peak locations and peak shapes can be compared consistently. This approach allows stiffness-related mismatch to be distinguished from damping-related mismatch using the same FRF dataset. The FRF results therefore complement modal analysis by providing damping-sensitive evidence required for the second stage of the updating strategy (Mahat et al., 2024).

2.5.3 FE Model Correlation and Sources of Discrepancy

FE-to-EMA discrepancies occur because modelling assumptions and experimental conditions cannot be made perfectly identical, especially for composite specimens with variable microstructure. Boundary condition mismatch can shift natural frequencies and distort mode shapes if test constraints differ from those assumed in the model. Geometry idealisation can also introduce error when real specimens contain thickness variation, edge imperfections, or manufacturing-induced asymmetry. Material variability can lead to specimen-to-specimen differences in stiffness and damping that cannot be represented by a single property set without updating. Numerical factors such as element choice and mesh quality can further influence predicted modal parameters and FRFs. For these reasons, correlation is performed first to identify mismatch patterns before parameter updating is attempted (Ereiz et al., 2022).

Correlation metrics are applied because they provide objective measures for assessing agreement between FE predictions and EMA results across multiple modes and frequency ranges. Natural frequency error indicates whether the model is globally too stiff or too flexible for the modes of interest. Mode shape comparison is used in spatial validation to verify whether the predicted and the measured deformation patterns match in a consistent combination of modes. FRF comparison goes beyond correlation of modal parameters, in that it will consider the resonance peak location, amplitude, and bandwidth trends over the frequency band (Manring et al., 2022). These measures are interpreted in conjunction with each other in a way that allows the mismatch due to stiffness and mismatch due to damping to be separated in a structured way. This separation is in support of the thesis workflow in which resonance alignment is dealt with first before damping updating is evaluated (D. Lee, 2023). The correlation baseline produced is used as a reference to measure the improvement after each updating stage (Ereiz et al., 2022).

2.5.4 FE Model Updating Procedure

FEMU is applied because it offers a well-structured approach for minimising deviations between the FE model predictions and the EMA results with the adjustments of some model parameters. Updating is often expressed as an optimisation problem where an objective function that is based on response error is minimised subject to practical constraints (Ereiz et al., 2022). The choice of parameters is driven by sensitivity, in the sense that if a parameter changes there must be a corresponding change in the target responses (Lenticchia et al., 2025). In the first stage of updating, stiffness related parameters are taken as priority due to their direct effect on natural frequencies and locations of resonance. This stage has the stiffness-controlled portion of the response come to a great extent so that the resonance structure is consistent with EMA before attempting to refine the damping. The staged approach is favourable in your study objective to formulate damping updating scheme after stiffness related agreement is made.

An iterative updating workflow is used because they involve changing one of the parameters alters the FEA solution and the correlation has to be re-evaluated after each update. The process is initiated by picking target responses from EMA, e.g. natural frequencies, mode shape and FRF features, and computing the respective FE responses. Parameters are updated to decrease mismatch; however, the values of parameters are kept physically reasonable using bounds or constraints. Following every iteration, measure of correlation is re-calculated to assess the improvement, as well as whether the convergence has been reached. When resonance alignment is satisfactory, the focus of the updating is changed to whose parameters related with damping in order to make the FRF peak amplitude and bandwidth behaviour closer matched (Panda & Modak, 2023). The iterative loop continues until further changes in parameters don't result in significant improvement, which means the form of model and its parameters are at a practical best fit. This structure helps to emphasise the thesis on damping representation as the last stage of refinement.

2.5.5 Tools Used for FE Analysis and Model Updating in This Study

Software tools are stated since they identify the modelling, solution and updating environment to establish the results and traceability from model building to updated predictions. PATRAN is used for FE pre-processing such as the definition of the geometry representation, properties, mesh and analysis case set up. MSC NASTRAN is applied as a solver for modal analysis and FRF analysis to generate FE predictions in required frequency ranges. FEMTools is adopted as the updating platform for doing parameter updating using comparing FE responses with EMA targets under a uniform correlation framework. This toolchain enables a well-structured workflow mechanism in which stiffness related mismatch can be treated first and damping refinement is done as a subsequent updating phase. The consistent environment helps to reinforce the defensibility on the basis of improvements in correlation with corrected stiffness and damping representation instead of inconsistent modelling procedures.

2.6 Model Correlation Techniques and Research Gap

2.6.1 Purpose of Model Correlation

Model correlation is performed to quantify the agreement between FE predictions and EMA results, enabling an objective evaluation of improvements made through model updating. This correlation step is critical because visual comparisons alone can mask systematic mismatch, especially when several modes exist within a narrow frequency band (Will & Zhu, 2024). In this study, EMA is treated as the experimental baseline because it provides FRFs and modal parameters that directly reflect the measured dynamic behaviour of the specimen. FE outputs are compared against this baseline using consistent metrics, allowing for transparent tracking of the changes introduced by updating. Correlation also helps to distinguish whether the mismatch is primarily stiffness-related, mass-related, boundary-condition-related, or damping-related. This distinction is important because the proposed workflow first aligns resonance behaviour (natural frequencies and mode shapes) before focusing on damping refinement.

Correlation is essential because different response types reveal distinct aspects of the structure's dynamic behaviour, which support the staged updating strategy. Natural frequencies provide indicators of stiffness–mass behaviour and are useful for checking resonance alignment prior to assessing damping. Mode shapes verify whether FE and EMA describe the same deformation patterns, helping to prevent incorrect mode pairing that could mislead the updating process. FRFs provide additional information on resonance peak amplitude and bandwidth, which are directly influenced by damping representation. Using all of these response types together reduces the risk of concluding that the model is accurate based on only one indicator. The combined correlation process, therefore, supports a structured approach to refining damping representation, which is a key objective of this study’s methodology.

2.6.2 Natural Frequency Error

Natural frequency error is used to quantify how well the FE model reproduces the measured resonance frequency positions because natural frequencies are governed mainly by stiffness and mass (Ribeiro et al., 2022; Tian et al., 2024). The error is expressed as the percentage difference between FE and EMA natural frequencies for each paired mode. A small frequency error indicates that the FE stiffness–mass balance is close to the experimental condition for the selected mode set. A consistent positive bias across modes suggests that the FE model is too stiff, while a consistent negative bias suggests that the model is too flexible. This interpretation supports the first part of the workflow, where stiffness-related parameters are refined to align the FE natural frequencies with EMA before damping updating is evaluated. Frequency error is therefore used as an early indicator to confirm that stiffness alignment is adequate prior to focusing on FRF peak behaviour.

Natural frequency error must be evaluated using reliable mode pairing so that the compared frequencies represent the same physical deformation behaviour. Modes are first selected from EMA based on clear peaks, stable identification, and repeatable extraction within the frequency band of interest. FE modes are then paired to the same set so that comparisons remain consistent across the initial FE, tensile-test-based FE model, and modal-updating-based FE model stages. When modes are close in frequency, additional checks such as MAC are used to reduce the risk of mode switching, which can distort the frequency error trend. This pairing discipline ensures that any reduction in frequency error reflects genuine improvement of model stiffness–mass representation rather than changes in mode selection. As a result, natural frequency error provides a consistent basis for tracking stiffness-related updating performance before damping refinement is carried out to form the updated FE model.

2.6.3 Mode Shape Correlation Using MAC

MAC is applied because it provides an objective measure of similarity between FE and EMA mode shapes based on a normalised correlation index. A MAC value closer to 1 is a strong amount of similarity in terms of deformation pattern and vice versa. This is a significant metric to note because modes may have similar natural frequencies, but be different spatial deformation patterns. MAC therefore supports reliable pairing of FE and EMA modes so that subsequent comparison of frequencies and FRFs remains physically meaningful (Shao et al., 2022). In this study, MAC is used together with natural frequency error to confirm that stiffness alignment does not compromise deformation consistency. This combination supports a staged workflow in which stiffness alignment is confirmed on both frequency and shape before damping is refined.

MAC evaluation depends on consistent DOF mapping between the EMA measurement grid and the corresponding FE response coordinates. The response locations used in EMA are mapped to FE nodes or DOFs so that mode shapes are compared at equivalent spatial points. Coordinate direction consistency is maintained so that the comparison reflects the same physical response components, rather than mixed directions. Because MAC is normalised, it is not affected by scale differences between experimental and numerical mode shapes, which makes it suitable for cross-domain comparison. However, MAC can be influenced by limited measurement points, so it should be interpreted together with frequency and FRF evidence when spatial resolution is restricted (Castro et al., 2022). With these controls, MAC provides a defensible basis for judging whether updating improves agreement in both deformation pattern and resonance behaviour.

2.6.4 FRF Correlation and Agreement Assessment

FRF correlation is used in this study because FRFs provide direct evidence of damping-sensitive response behaviour that cannot be evaluated using natural frequencies and mode shapes alone. An FRF shows the resonance frequency, peak amplitude, bandwidth, and phase evolution across the frequency band, which allows stiffness-related mismatch to be separated from damping-related mismatch. In this context, stiffness and mass mainly govern resonance frequency, while damping mainly governs peak bandwidth and peak amplitude (J. Li et al., 2024). This separation is consistent with the correlation logic of this thesis, where resonance frequency agreement is confirmed first before damping agreement is assessed using FRF peak behaviour. For TCP, FRF-based assessment is especially important because damping effects are more pronounced and strongly shape the measured response.

FRF agreement is assessed systematically because an FRF contains many frequency lines and multiple resonances that may overlap within the frequency band of interest. The assessment begins by checking whether the FE prediction captures the EMA resonance frequency for the targeted modes, because resonance frequency mismatch indicates a stiffness–mass imbalance. The assessment then focuses on peak amplitude and bandwidth trends around each resonance, because these features reflect the adequacy of damping representation once resonance frequency is close. Phase behaviour around resonance is also checked because a consistent phase change supports correct dynamic representation and reliable mode pairing. When mismatch is concentrated near the resonance peaks through peaks that are too sharp or too broad, damping modelling is treated as the dominant contributor (Arora et al., 2023). When mismatch persists across a wider portion of the band beyond the peaks, modelling assumptions related to stiffness distribution, mass distribution, or boundary condition idealisation are treated as the likely contributors.

A quantitative FRF correlation metric is included to support consistent comparison when visual overlays become insufficient for judging agreement across specimens and model stages. In this study, the Signature Assurance Criterion (SAC) is used to measure the similarity between the complex-valued FE FRF and the measured FRF over the selected set of frequency lines. The SAC formulation used in this study is given in Equation 2.16:

$$\mathrm{SAC} = \frac{\left| \sum_{k=1}^{N_f} H_A(f_k)^* H_X(f_k) \right|^2}{\left(\sum_{k=1}^{N_f} H_A(f_k)^* H_A(f_k)\right)\left(\sum_{k=1}^{N_f} H_X(f_k)^* H_X(f_k)\right)} \tag{2.16}$$

where $H_A(f_k)$is the analytical FRF value from FE at frequency f_k, $H_X(f_k)$is the measured FRF value from EMA at frequency f_k, $(.)^*$ denotes complex conjugate, and $N_f$is the number of frequency lines used in the comparison. The SAC value increases as the predicted FRF approaches the measured FRF in both magnitude and phase over the evaluated frequency region. In this thesis, SAC is interpreted together with peak-based observation so that numerical correlation and physical interpretation remain aligned when evaluating damping-related FRF agreement.

2.6.5 Research Gap and Motivation for This Study

A research gap exists as many dynamic correlation studies are aimed at an enhanced frequency agreement, while fewer studies are given a structured scheme in which modal damping of bio-based composite panels can be updated and validated by FRF evidence (Zhao et al., 2023). For TCP, damping behaviour is important and impacted by microstructural variability which can limit the prediction accuracy of FRF even when matching of the resonance locations is achieved (Liu et al., 2021). In practice damping is often dealt with by simplified assumptions, or so-called general damping values without a systematic updating procedure based upon experimentally measured FRF peak behaviour. This limitation decreases the confidence in the use of the FE models for vibration analysis of TCP structures, where damping is the controlling factor in terms of resonance peak amplitude and bandwidth. Therefore, a technique explicitly decoupling the stiffness alignment and the damping refinement and testing both stages against EMA is required. This provides motivation for the work in this study, which is to formulate and evaluate a modal damping updating scheme for TCP.

Previous studies on plant fibre composites have reported that damping behaviour is sensitive to fibre content, fibre orientation, and fibre-matrix adhesion, with modal damping ratios substantially higher than those observed in metallic structures (Liu et al., 2021). Liu et al. (Liu et al., 2021) reviewed the damping mechanisms of plant fibre composites and identified that viscoelastic behaviour at the fibre-matrix interface, combined with moisture-related microstructural changes, produces elevated and variable damping characteristics that are difficult to represent using simplified proportional damping models. Haris et al. (Haris et al., 2022) investigated the dynamic mechanical properties of natural fibre reinforced hybrid polymer composites and demonstrated that damping is strongly influenced by fibre type, fibre-matrix adhesion quality, and testing frequency, further confirming that damping in plant fibre composites cannot be treated as a single constant value across modes. Ardani et al. (Ardani et al., 2026) characterised bio-composite panels produced from tobacco-derived fibres and reported that non-uniform fibre-matrix distribution influences the material properties in ways that are relevant to both static and dynamic performance, reflecting the broader variability that affects FRF peak behaviour in TCP. These studies collectively confirm that TCP represents a material system in which damping variability is the dominant challenge for accurate FRF-based FE prediction, and that the selection of TCP as the primary specimen in this study is well justified by its relevance to the research gap identified above.

The motivation of this study is to develop a correlation and updating methodology to improve the FE agreement with EMA in a traceable and defensible manner. The approach uses correlation metrics to secure resonance alignment and correct mode pairing before attempting damping refinement, which prevents damping updates from compensating for stiffness mismatch. After resonance alignment is achieved, damping updating is evaluated using FRF peak behaviour so that damping parameters reflect measured bandwidth characteristics. This staged validation supports the research objectives by linking the formulated damping updating scheme to measurable improvement in updated FE predictions relative to EMA. The outcome is a clearer basis for representing damping in TCP using updated FE models that reproduce experimentally observed FRF behaviour.

2.7 Concluding Remarks

This chapter reviewed the theoretical and methodological foundations relevant to modelling and updating the dynamic behaviour of TCP. The discussion first established core structural dynamics concepts, including the relationship between mass, stiffness, and damping in governing vibration response, and how these properties are reflected through modal parameters and FRFs. The chapter then reviewed EMA practice as a non-destructive approach for obtaining FRFs and extracting natural frequencies, mode shapes, and modal damping that serve as the experimental reference for correlation and updating. Next, tensile testing was discussed as a conventional destructive method for estimating Young's modulus, together with practical limitations that can influence modulus repeatability for composite strips. The chapter also summarised FE modelling approaches for predicting modal parameters and FRFs, and highlighted how modelling assumptions can lead to mismatch when compared with EMA results. Finally, the chapter presented correlation measures for evaluating agreement between FE and EMA and identified the need for a structured updating workflow that separates resonance alignment from damping refinement.

Overall, the reviewed literature consistently indicates that accurate vibration prediction for TCP requires not only appropriate stiffness representation but also a defensible damping representation capable of reproducing FRF resonance peak behaviour. The literature also suggests that damping for composite panels is often treated using simplified assumptions, which motivates the development of a systematic damping updating scheme validated using EMA as the baseline reference. Therefore, this chapter establishes the technical foundation for Chapter 3, which details the experimental procedures, FE modelling, correlation strategy, and the staged updating methodology used to formulate and evaluate the proposed modal damping updating scheme for TCP.

CHAPTER 3
RESEARCH METHODOLOGY

3.1 Introduction

This chapter presents the research methodology adopted to achieve the objectives of this study by improving agreement between FE predictions and EMA results for the tobacco composite strip and the steel dog-bone specimen through systematic correlation and damping updating. The methodology integrates experimental testing, numerical modelling, correlation analysis, and FEMU so that modelling mismatch can be identified and corrected with clear traceability. EMA provides the reference FRFs and modal parameters required for correlation and updating, while the FE work begins with development of the initial FE model to generate baseline predictions (K. Li et al., 2022). Tensile testing is included as a destructive comparison route for Young's modulus after EMA is completed. The overall workflow of the proposed methodology is presented in Section 3.2.

The methodology is structured into the following key sections:
3.2 Research Design and Approach
3.3 Specimen Description
3.4 Experimental Modal Analysis (EMA)
3.5 FE Modelling (Initial FE Model and Mesh Convergence)
3.6 Overview of Tensile Testing
3.7 FE–EMA Correlation
3.8 FE Model Updating Strategy
3.9 Validation of Updated FE Model
3.10 Concluding Remarks

The FE updating sequence in this study is organised into the initial FE model, the tensile-test-based FE model, the modal-updating-based FE model, and the final updated FE model. The tensile-test-based FE model is developed using Young's modulus obtained from tensile testing as a comparative stiffness input. The modal-updating-based FE model is obtained by updating stiffness-related parameters using

EMA modal targets to improve natural frequency agreement and MAC. Modal damping updating is then applied to improve FRF peak behaviour so that the final updated FE model achieves very low error when compared with EMA. The procedures described in this chapter prepare the required outputs for the results and discussion presented in Chapter 4.

3.2 Research Design and Approach

This study adopts a sequential experimental-numerical approach that integrates testing, modelling, correlation, and FE updating for two specimen types, namely the tobacco composite strip and the steel dog-bone specimen. The approach is organised so that experimental measurements provide the reference FRFs and modal parameters required as targets for correlation and updating. Numerical prediction begins with the initial FE model to establish baseline differences between FE and EMA results. Correlation is then used to quantify mismatch consistently so that the next FE models are developed based on observed evidence. The overall workflow of the proposed methodology is summarised in Figure 3.1.

Specimen preparation and definition of measurement points are carried out to ensure consistent data collection and consistent FE modelling for both specimens. Specimen dimensions and mass-related information are recorded so that the FE models represent the same physical specimens used in EMA and tensile testing. Measurement points are defined to support reliable FRF measurement and mode shape construction during EMA. The same reference labelling is maintained throughout the study so that all datasets remain traceable across stages. This preparation step ensures both specimens proceed into the experimental procedures with clear and consistent definitions.

EMA is conducted for both specimens under approximate free-free boundary conditions to obtain experimental FRFs and modal parameters with minimal support influence. The test is repeated and checked to ensure the measured FRFs have acceptable quality before modal parameters are extracted. The best suspension setup is selected so that the measured response is stable within the frequency range of interest. FRFs are then processed to extract natural frequencies, mode shapes, and modal damping ratios as the experimental reference dataset. This dataset is used directly for FE-EMA correlation and for guiding subsequent FE model development and updating.

Quasi-static tensile testing is performed for both specimens to obtain Young's modulus as a comparative stiffness reference after EMA testing is completed. The tensile-derived modulus is treated as a material input that can be assigned into FE to form the tensile-test-based FE model. This model provides a stiffness comparison route that is independent from modal targets and supports interpretation of stiffness representation. The tensile results are used to complement the EMA-based updating route rather than to replace EMA as the primary dynamic reference. This step strengthens comparative assessment between static stiffness input and dynamic response matching.

Baseline FE modelling and analysis are performed to generate numerical predictions for both specimens using the initial FE model. The initial FE model is developed based on measured geometry and baseline material assumptions so that the starting point is clearly defined before updating. Modal and FRF analyses are carried out using consistent excitation and response definitions so that predicted responses can be compared directly with EMA results. The initial FE predictions are then correlated with EMA to quantify baseline mismatch using consistent metrics. This baseline correlation provides the reference point for all subsequent improvements.

FE-EMA correlation is performed to quantify agreement using natural frequency error, MAC, and FRF comparison so that mismatch can be interpreted in both modal and frequency-domain forms. Natural frequency and MAC are used to support mode pairing and stiffness-related assessment. FRF comparison is used to assess resonance peak behaviour and bandwidth, which are sensitive to damping representation. The correlation trends are then used to justify the development of the tensile-test-based FE model and the modal-updating-based FE model. This correlation stage therefore links measured evidence to the choice of FE updating path.

FE updating is organised into a clear sequence of FE models so that each step has a defined purpose and output. The tensile-test-based FE model is obtained by assigning tensile-derived Young's modulus as the baseline stiffness input. The modal-updating-based FE model is then obtained by updating stiffness-related parameters using EMA modal targets to improve natural frequency agreement and MAC. Modal damping updating is subsequently performed to improve FRF peak amplitude and bandwidth agreement with EMA so that the final updated FE model achieves very low error. The sequence and decision loops that connect these stages are shown in Figure 3.1.

The decision blocks in Figure 3.1 represent quality or acceptance checks at each stage of the workflow, and the iteration paths associated with each decision block are described here to clarify the corrective actions required when the acceptance criterion is not satisfied. In the EMA data quality check, if the measured FRFs exhibit poor coherence, inconsistent resonance peaks, or unstable modal parameter extraction, the test is repeated with improved setup consistency, including re-seating of accelerometers, re-checking of suspension configuration, and re-performing impact averaging until acceptable FRF quality is confirmed. In the initial FE-EMA correlation check, if the baseline mismatch pattern is found to be inconsistent or ambiguous, the FE model geometry and material inputs are reviewed and corrected before proceeding to the updating stages. In the modal-updating-based FE-EMA correlation check, if the natural frequency error does not reduce to below 1% after the updating iteration, the updating parameter selection and bounds are reviewed in FEMTools and the iteration is repeated with adjusted parameter constraints until the target error is achieved. In the modal damping updating check, if the SAC value does not improve sufficiently after damping updating, the mode-by-mode damping refinement is repeated with adjusted damping ratio bounds until the FRF peak behaviour converges to an acceptable level of agreement with EMA.

Validation and comparative assessment are performed by comparing FE predictions and EMA results using the same correlation metrics across all FE model stages. The updated FE model is evaluated as the final best model because it provides the lowest error when compared with EMA for both specimens. Comparison across the initial FE model, tensile-test-based FE model, modal-updating-based FE model, and updated FE model is used to show the contribution of each step to overall improvement. Tensile results are used to support interpretation of stiffness-related findings while EMA remains the primary reference for vibration behaviour. This approach prepares the results structure required for Chapter 4.

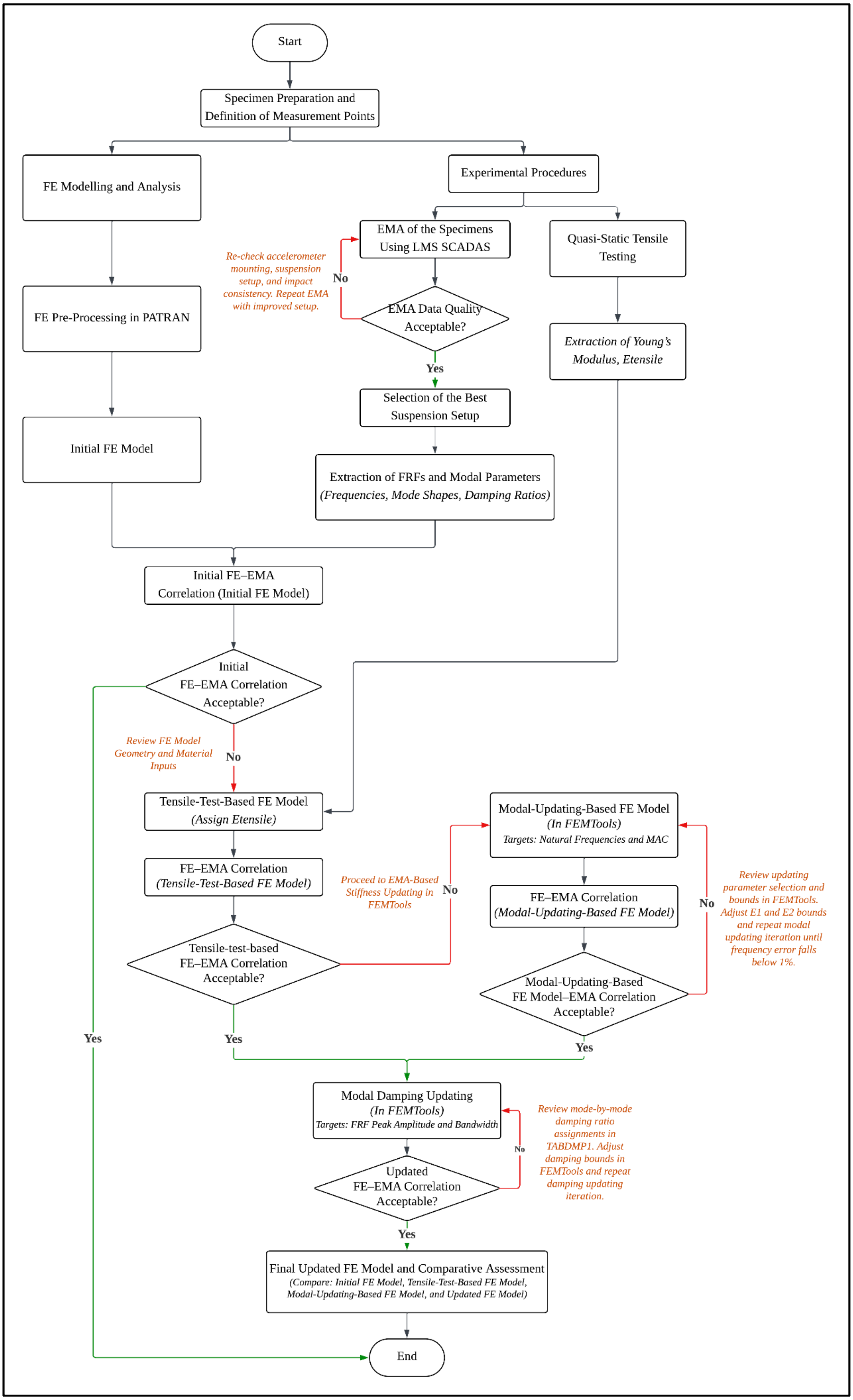

Figure 3.1 Flowchart of the Proposed Methodology

3.3 Specimen Description

This study uses two specimen types to support evaluation of Young's modulus determination for dynamic prediction, namely the tobacco composite strip and the steel dog-bone specimen. The tobacco composite strip is selected as the primary specimen because it represents the material system of interest in this study. The steel dog-bone specimen is included as a secondary specimen to support verification of the testing and modelling procedures using a conventional isotropic material. Both specimen types are evaluated using the same overall workflow so that comparisons are based on consistent test intent. This section provides an overview of the specimens before detailed procedures are presented in later sections.

TCP is selected as the primary specimen in this study because it represents a bio-based composite material with non-uniform fibre-matrix distribution that introduces variability in effective stiffness and modal damping, making it a practically relevant and technically challenging case for FRF-based FE model updating (Ardani et al., 2026). The tobacco fibres used in TCP are derived from processed tobacco plant material and are incorporated into a polymeric matrix during panel fabrication, resulting in a composite whose dynamic properties are sensitive to local variations in fibre content and fibre orientation. This material variability means that nominally identical specimens can exhibit measurable differences in natural frequencies and FRF peak characteristics, which directly motivates the need for a structured updating approach that can account for specimen-specific damping behaviour rather than assuming a single representative value.

The steel dog-bone specimen is included as a verification case because its isotropic and well-characterised elastic behaviour provides a controlled reference against which the EMA procedure, FE modelling workflow, and updating strategy can be evaluated before application to the more variable TCP specimens. This pairing of specimens therefore serves a dual purpose: TCP provides the primary case study for the proposed damping updating methodology, while steel provides the verification baseline that confirms the reliability of the experimental and numerical procedures employed throughout the study.

TCP is treated as an effective homogeneous orthotropic continuum within the FE model in this study, where the updated elastic moduli (E1 and E2) and modal damping ratios represent volume-averaged effective dynamic properties that best reproduce the globally measured FRF behaviour across the specimen. This homogenisation approach is consistent with standard practice in FE-EMA correlation studies for composite materials, and its limitation is acknowledged in that the effective properties identified through modal updating may not uniquely represent local microstructural variability. The use of three specimens per material type is intended to provide a practical assessment of the scatter introduced by this variability, and any systematic differences between specimens are interpreted in terms of the updating outcomes rather than attributed to a single representative material model. This approach is therefore sufficient to demonstrate the validity of the proposed staged updating methodology across specimens with different effective property sets.

The tobacco composite strip specimens used in this study were cut from TCP sheets produced through a compression moulding process in which processed tobacco fibres were mixed with a polymeric binder and consolidated under controlled temperature and pressure. The strips were cut to the target dimensions using a band saw with a guided fence to maintain consistent width and length across specimens, and the cut edges were inspected to ensure no significant edge damage or delamination was introduced during cutting. Specimen thickness was measured at multiple locations along the length using a digital vernier calliper, and any specimen showing thickness variation exceeding 5% of the nominal value was excluded. The steel dog-bone specimens were machined from a standard structural steel bar stock to the dog-bone geometry using conventional milling, and the gauge dimensions were verified against the target drawing before testing.

Three tobacco composite strip specimens are prepared for the purpose of supporting the repeatability and traceable comparison across the workflow. Each tobacco specimen is labelled as Tobacco Specimen 1 to 3 so that EMA, FE results, updating outputs and tensile results can be related to the correct test article. The three tobacco composite strip specimens used in this study are shown in Plate 3.1. The tobacco specimens are considered as independent samples during the course of investigation to avoid mixing the datasets. This specimen tracking approach is conducive for clear specimen-by-specimen interpretation of dynamic behaviour and modulus results.

Three steel dog-bone specimens are prepared for the purpose of providing the same number of specimen for verification and comparison. Each steel specimen is labelled as Steel Specimen 1 to 3 to keep track of it consistently between EMA, FE analysis and tensile testing. Plate 3.2 presents the three steel dog-bone specimens for this study. The steel specimens are included such that the same measurement strategy can be tested for a material for which the behaviour is well established. This gives more confidence in the experimental and numerical procedures applied in the overall workflow.

Specimen-specific density is calculated for every test article because the inertia properties have an effect on both predicted and measured modal response. Density is determined using the mass and calculated volume of each specimen in order to have the actual specimen weight and geometry reflected in the FE inputs. This density assignment is carried out separately for all tobacco specimens and all steel specimens to preserve traceability across samples. The specimen-specific densities are used as FE inputs when establishing the initial FE model in the modelling section. The density calculation method and final values are reported together with specimen property tables in the relevant sections.

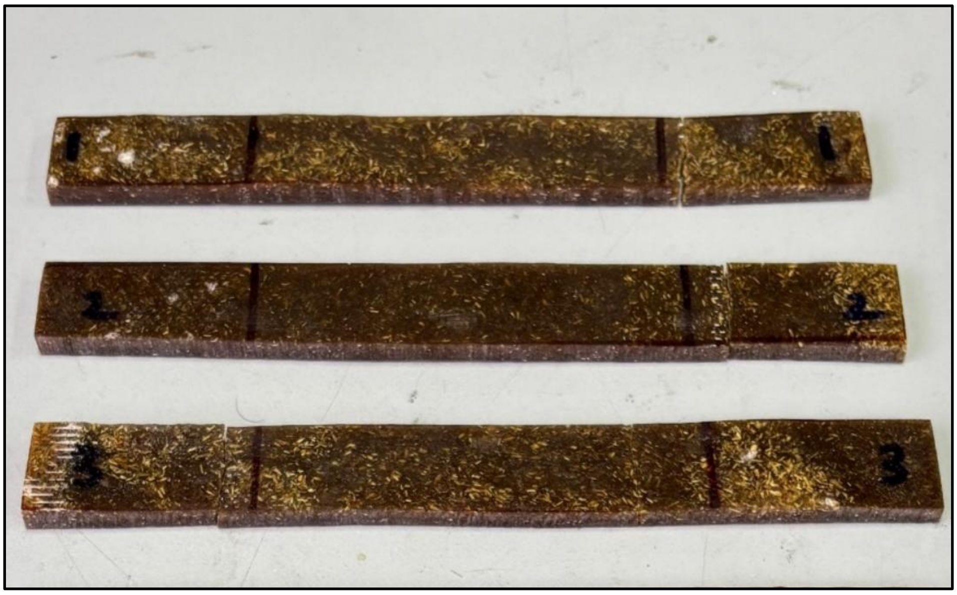

Plate 3.1 Tobacco Composite Strip Specimens Used in This Study (Tobacco Specimen 1 to 3)

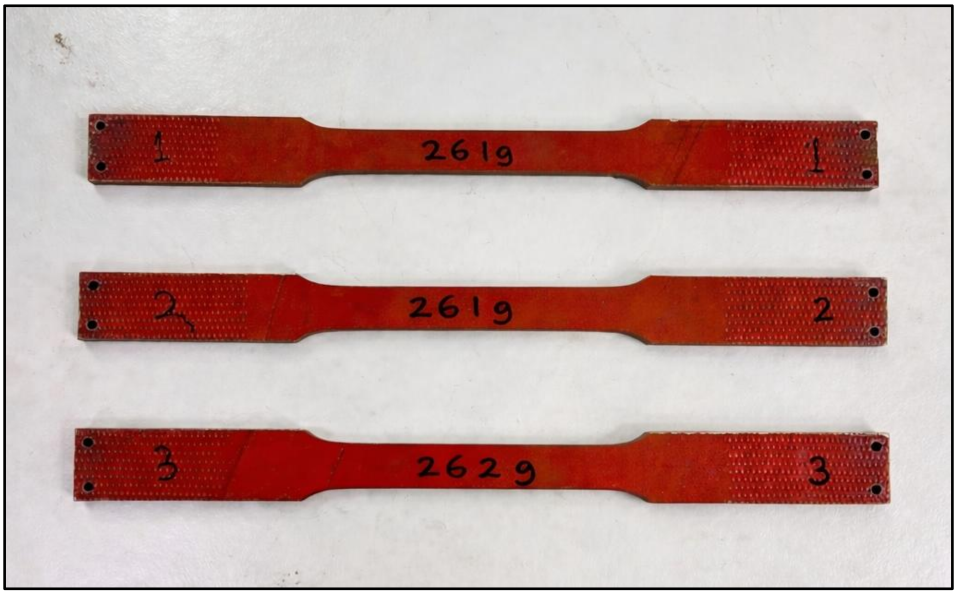

Plate 3.2 Steel Dog-Bone Specimens Used in This Study (Steel Specimen 1 to 3)

3.4 Experimental Modal Analysis (EMA)

EMA is conducted for the tobacco composite strip and the steel dog-bone specimen to obtain experimental FRFs and modal parameters required as reference targets for FE-EMA correlation and subsequent FEMU. Impact testing is used to provide broadband excitation so that FRFs can be measured over the frequency range of interest. Data acquisition and processing are performed using LMS SCADAS and Simcenter Testlab, as shown in Plate 3.3, to ensure consistency across both specimens. The excitation and sensing hardware used in the tests are shown in Plate 3.4 and Plate 3.5. The EMA outputs produced in this section form the experimental reference dataset used in later correlation and validation stages.

The suspension condition is controlled to approximate free-free boundary behaviour so that support influence on the measured response is minimised. For each specimen, three suspension configurations are evaluated, namely Horizontal 4-Corners, Horizontal 2-Corners, and Vertical 2-Corners. The overall configuration of the impact testing for these three setups is schematically shown in Figure 3.2, Figure 3.3 and Figure 3.4. The suitability of each configuration is judged from observation of the EMA results in terms of the quality of the FRF and mode shape clarity in the frequency range of interest. Based on these observations from both the tobacco composite strip and the steel dog-bone specimen, the Vertical 2-Corners configuration is chosen as the best suspension configuration since it gives better resonance peaks with less noise and smoother mode shapes for the first and second modes than the horizontal configurations.

Concerns about boundary condition induced damping were considered in the design of the EMA setup. Soft elastic cord suspension was used for all tests to approximate free-free conditions, and the suspension stiffness was selected so that the rigid body modes of the suspended specimen fell below 10 Hz, well below the first structural mode of interest for both specimen types. This separation ensures that the suspension does not introduce additional stiffness or damping into the frequency range used for modal parameter extraction. The suspension attachment points were positioned near the nodal regions of the first bending mode so that the cord contact force remained minimal during vibration, further reducing the risk of suspension-induced damping contamination in the identified modal damping ratios. Repeated FRF measurements taken without disturbing the suspension between impacts confirmed that the setup was stable and that the identified damping values were reproducible within the tested configuration.

Specimen geometry definition and measurement point selection are established to support repeatable FRF measurement and reliable mode shape extraction for both specimens. The detailed dimensions of the tobacco composite strip and the steel dog-bone specimen are presented in Figure 3.5 and Figure 3.7 to define the physical reference used throughout testing and modelling. The measurement points layout used for EMA is presented in Figure 3.6 for the tobacco composite strip and in Figure 3.8 for the steel dog-bone specimen to show the response locations used for mode shape construction. These measurement points are selected to avoid nodal regions and to provide adequate coverage of dominant deformation patterns. Consistent point labelling is maintained so that the experimental dataset can be matched directly with the corresponding FE response locations.

The data acquisition settings used in this study are summarised here to improve the technical completeness of the EMA procedure. All FRF measurements were acquired using LMS SCADAS with Simcenter Testlab configured with a frequency range of 0 to 1000 Hz for the tobacco composite strip and 0 to 4000 Hz for the steel dog-bone specimen, selected to capture the first two structural bending modes of each specimen type. A frequency resolution of 0.25 Hz was used for all measurements to ensure that resonance peaks are clearly resolved and that damping estimation from peak bandwidth is not compromised by insufficient frequency line density. Each FRF measurement was computed using an H1 estimator with a minimum of ten averages to reduce the influence of random noise on the estimated FRF magnitude and phase. An exponential window with a decay factor appropriate for the signal duration was applied to the response channel to reduce leakage, while a force window was applied to the impact channel to eliminate pre-trigger noise. Trigger level and pre-trigger delay were set consistently across all tests so that the impact event was fully captured from the onset of force application. Coherence was monitored in real time during acquisition and any measurement showing coherence below 0.9 in the frequency range of interest was discarded and repeated. The accelerometers were mounted using beeswax adhesive to minimise mass loading effects and to maintain consistent coupling stiffness across measurement points and specimens.

FRF estimation and data quality control are carried out to ensure that the measured dataset is suitable for correlation and modal damping updating. FRFs are computed from the measured force and acceleration signals using consistent processing settings so that comparisons across suspension configurations remain fair. Coherence and repeatability are monitored in order to verify that the measured responses are dominated by linear behaviour in the frequency band of interest. If the quality of the FRF is not acceptable, then the test is repeated with better setup consistency until stable FRFs are obtained. This quality control step is used to ensure that the extracted modal parameters are supported by reliable FRFs.

Modal parameter extraction is performed in order to get natural frequencies, mode shapes and modal damping ratios for both specimens. Natural frequencies are identified from resonance locations in the measured FRFs to support stiffness-related comparison in later stages. Mode shapes are assembled using responses at the defined measurement points so that mode pairing and MAC evaluation can be performed consistently. Modal damping ratios are estimated using Peak Picking and PolyMAX curve fitting procedures in Simcenter Testlab, where Peak Picking is applied when modes are well separated and PolyMAX is used when more robust damping estimation is required. The extracted modal dataset is then used as the experimental reference for FE-EMA correlation and for validation of the updated FE model.

Plate 3.3   Simcenter Testlab Impact Testing Software and LMS SCADAS Data Acquisition

Plate 3.4   Impact Hammer Used in EMA

Plate 3.5   Accelerometers Used in EMA

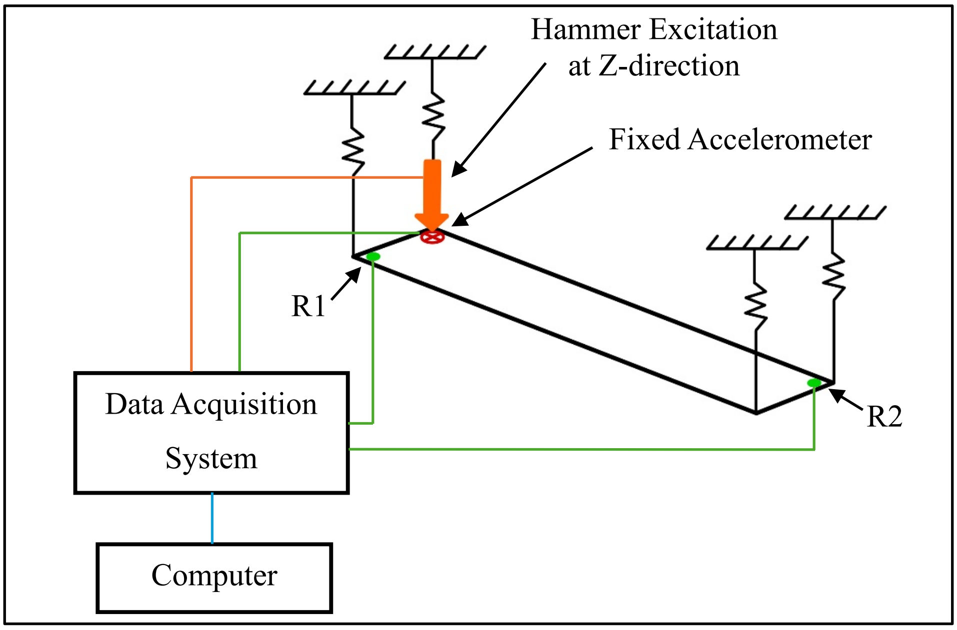

Figure 3.2 Schematic of Impact Testing Configuration for Horizontal 4-Corners Suspension

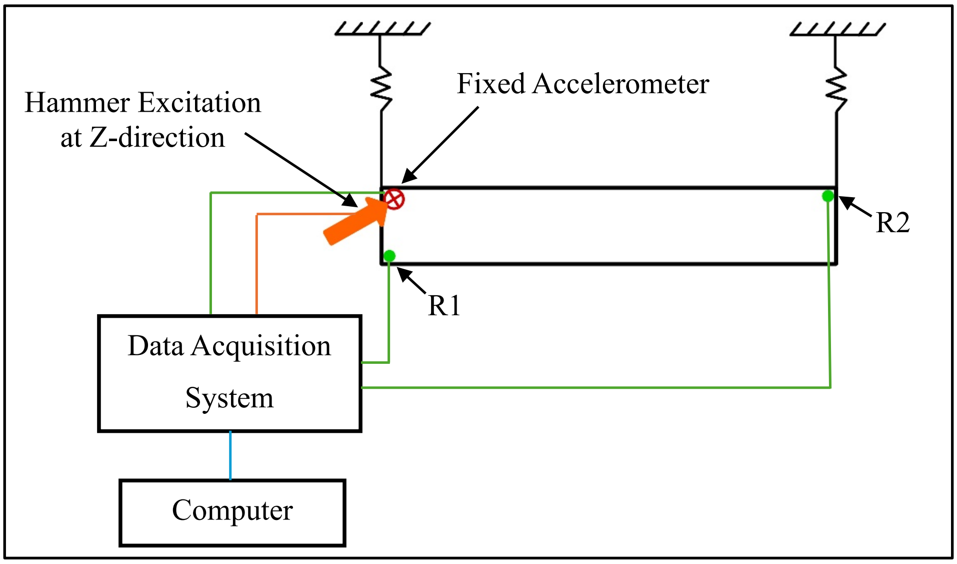

Figure 3.3 Schematic of Impact Testing Configuration for Horizontal 2-Corners Suspension

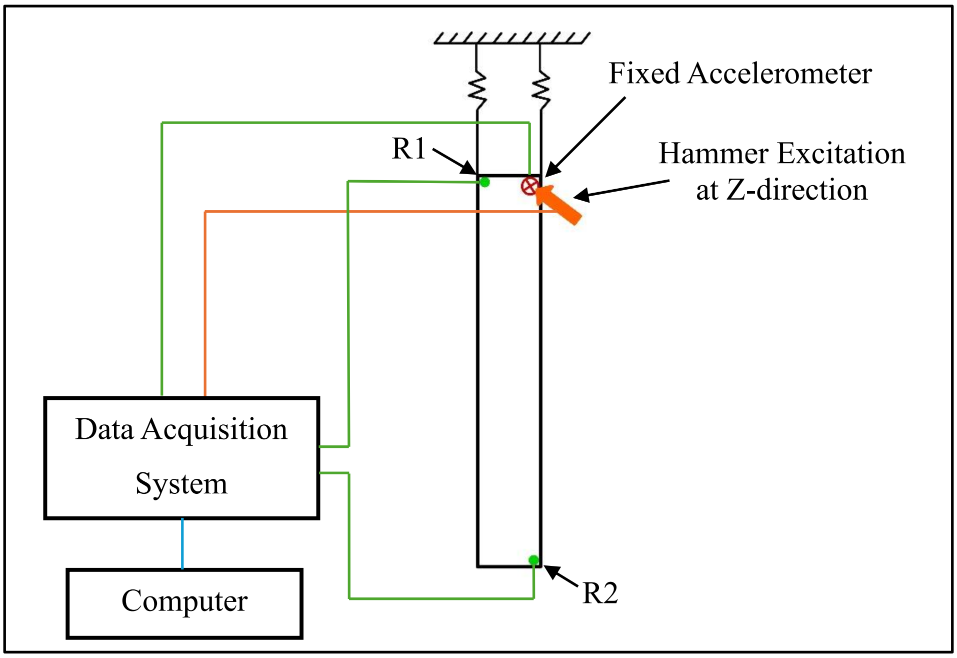

Figure 3.4 Schematic of Impact Testing Configuration for Vertical 2-Corners Suspension

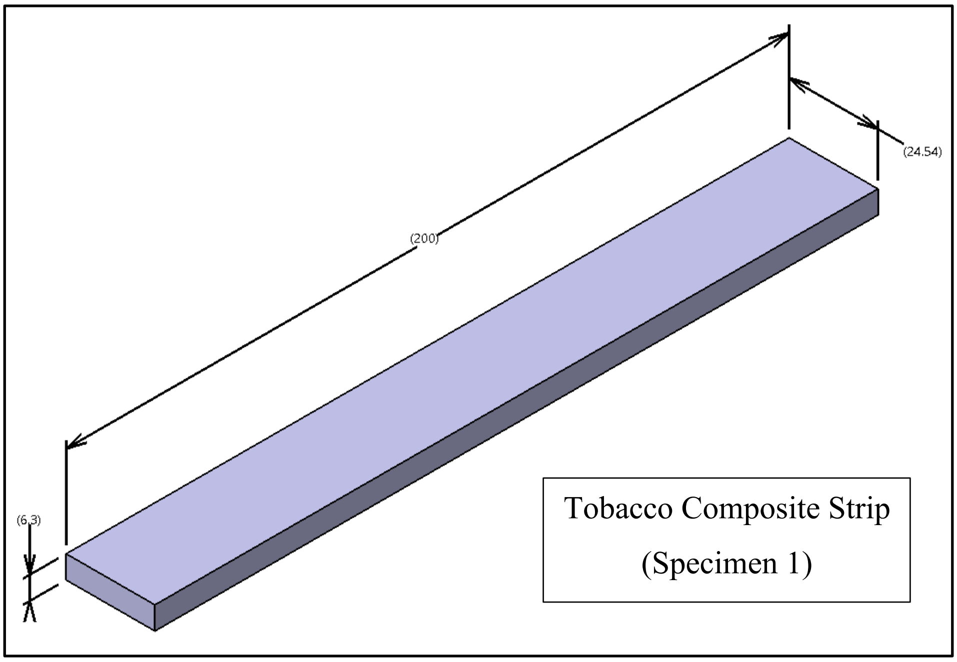
(200)
(24.54)
(6.3)
Tobacco Composite Strip
(Specimen 1)

(a)

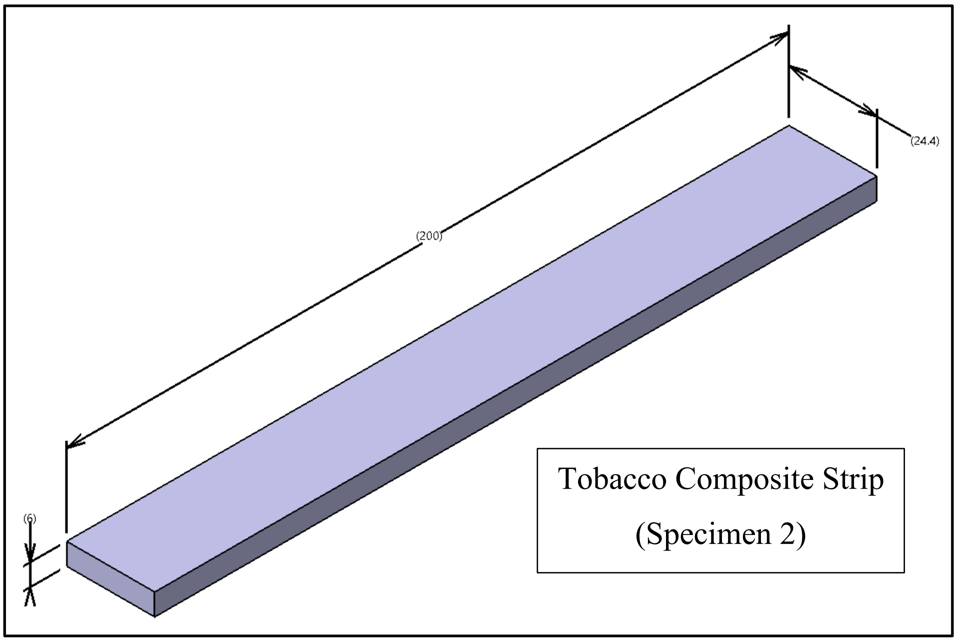
(200)
(24.4)
(6)
Tobacco Composite Strip
(Specimen 2)

(b)

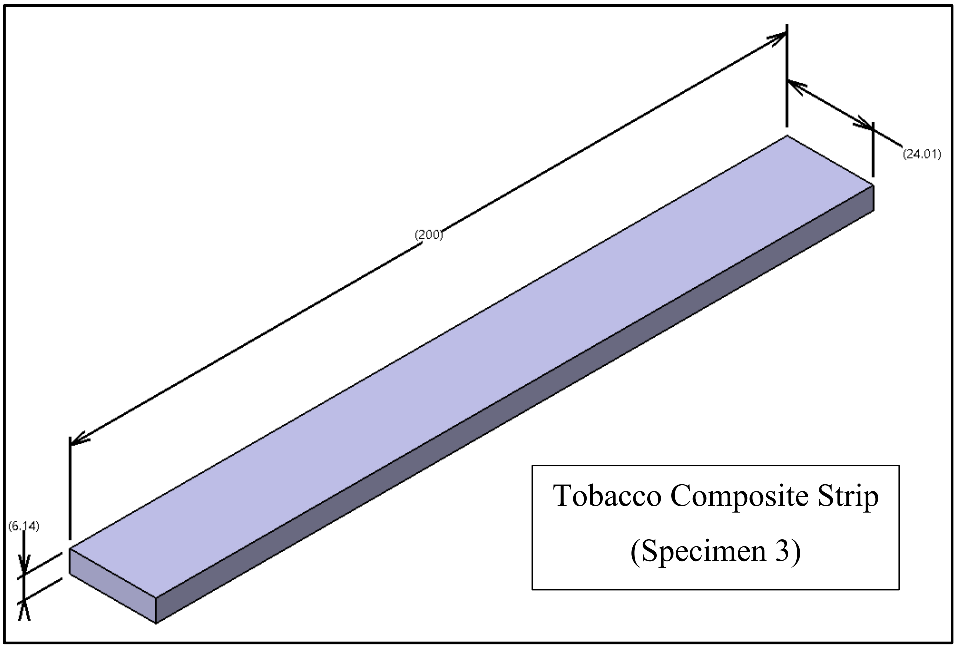

(c)

Figure 3.5 Detailed Dimensions of the Tobacco Composite Strip Specimen of (a) Specimen 1, (b) Specimen 2, (c) Specimen 3

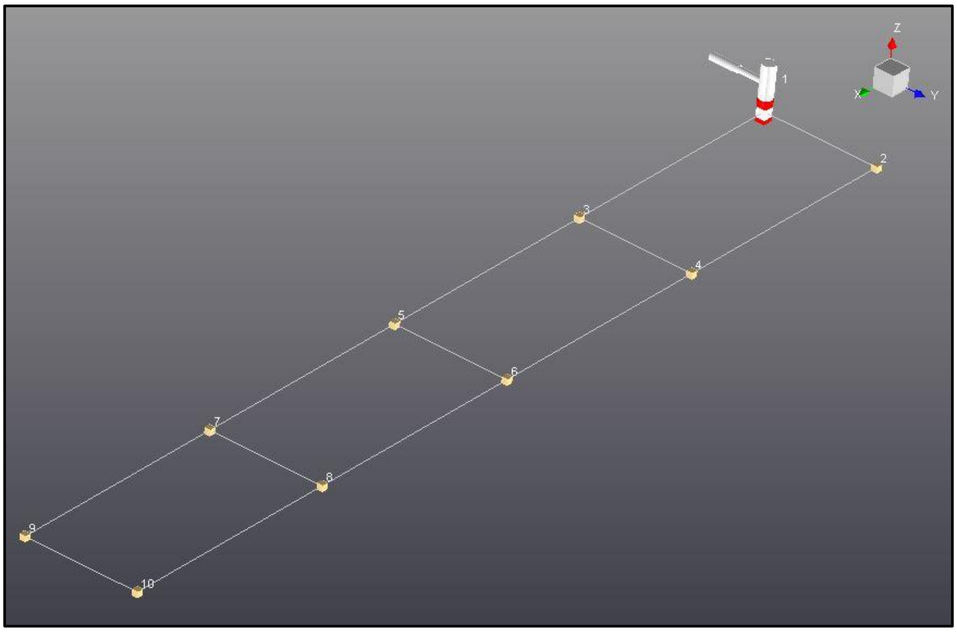

Figure 3.6 Measurement Points Layout for EMA of the Tobacco Composite Strip Specimen (10 Points)

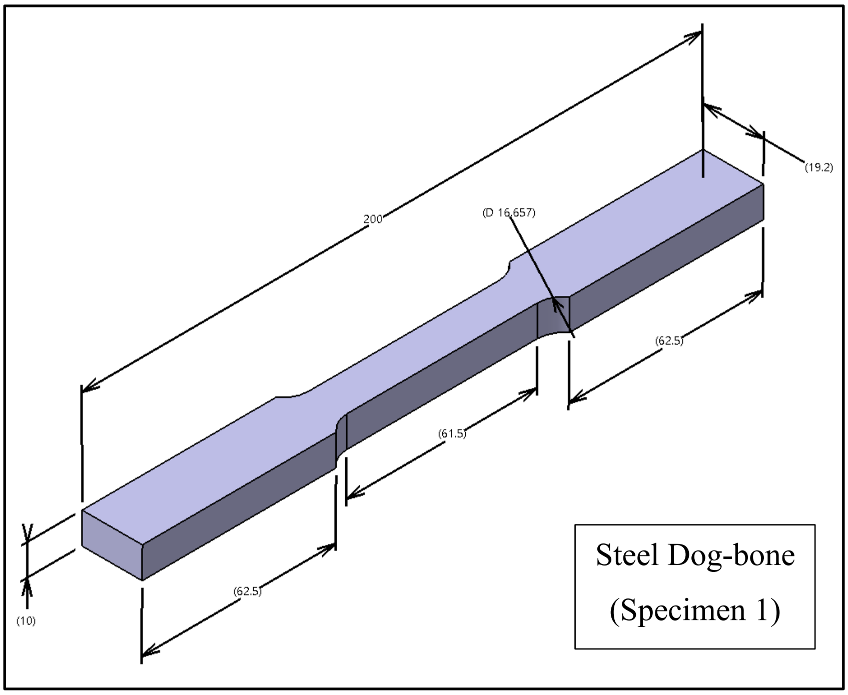
200
(19.2)
(D 16.657)
(62.5)
(61.5)
(62.5)
(10)
Steel Dog-bone
(Specimen 1)

(a)

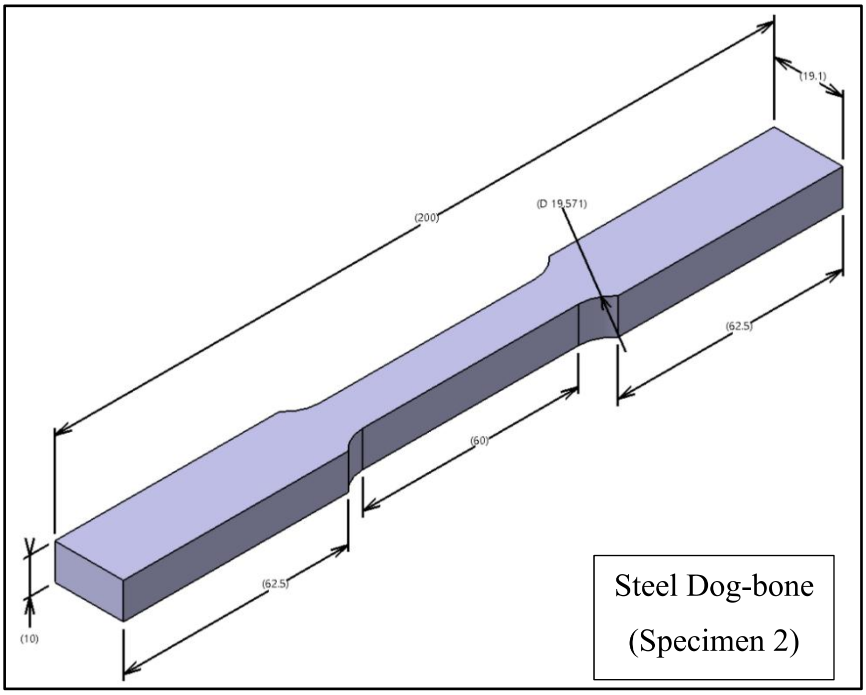
(200)
(19.1)
(D 19.571)
(62.5)
(60)
(62.5)
(10)
Steel Dog-bone
(Specimen 2)

(b)

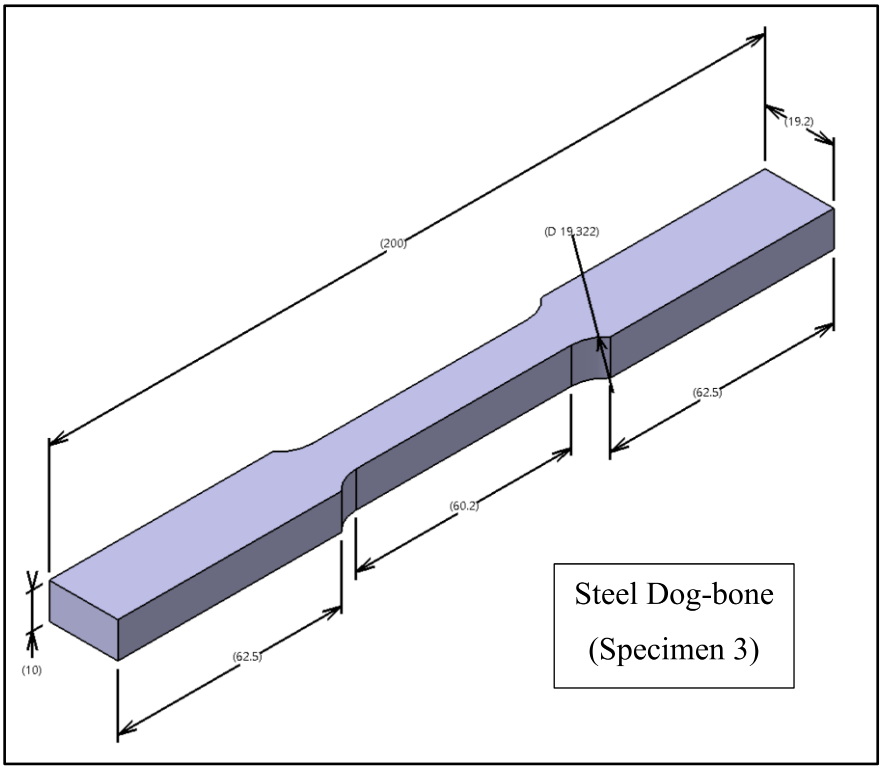

(c)

Figure 3.7 Detailed Dimensions of the Steel Dog-Bone Specimen of (a) Specimen 1, (b) Specimen 2, (c) Specimen 3

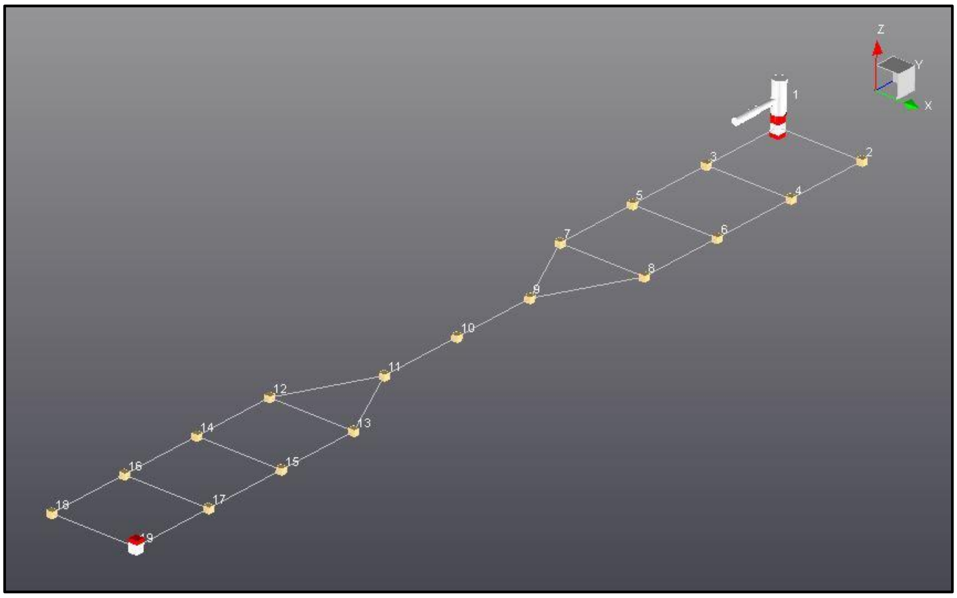

Figure 3.8 Measurement Points Layout for EMA of the Steel Dog-Bone Specimen (19 Points)

3.5 Tensile Testing

Tensile testing is performed to obtain quasi-static Young's modulus values for comparison with the stiffness representation identified through EMA-based FEMU for the tobacco composite strip and the steel dog-bone specimen. This tensile route is treated as a destructive reference method, and the tests are therefore conducted only after EMA is completed to avoid affecting the measured dynamic response. The tensile-derived modulus is denoted as E_{tensile} and is used to develop the tensile-test-based FE model for comparative assessment against the EMA-based model stages. This section provides an overview of the tensile testing approach, while specimen-specific details are presented in the designated tensile section.

Tensile testing for the tobacco composite strip is carried out using a low-capacity servo-hydraulic universal testing machine that is suitable for composite specimens. The tests are performed using a Shimadzu ServoPulser EHF-series servo-hydraulic universal testing machine, and the machine used is shown in Plate 3.6. The maximum capacity of 10 kN is selected to match the expected force range of the tobacco composite strip and to maintain stable load control during testing. The crosshead speed is set to 1 mm/min to obtain a stable stress–strain response for modulus evaluation. The measured outputs are recorded in the form of force and extension so that the stress–strain response can be constructed consistently.

Tensile testing for the steel dog-bone specimen is carried out using a higher-capacity universal electromechanical tensile machine to suit the higher stiffness and strength of steel. The tests are performed using a VEW2302A Universal Electromechanical Tensile Machine, and the machine used is shown in Plate 3.7. The maximum capacity of 60 kN is selected to ensure the specimen can be tested without approaching machine limits. The crosshead speed is set to 5 mm/min so that the steel stress–strain response can be evaluated consistently. The measured outputs are recorded as force and extension so that the resulting E_{tensile}values can be obtained for later comparison.

Plate 3.6 Shimadzu ServoPulser EHF-Series Servo-Hydraulic Universal Testing Machine Used for Tensile Testing of the Tobacco Composite Strip (10 kN Capacity)

Plate 3.7 VEW2302A Universal Electromechanical Tensile Machine Used for Tensile Testing of the Steel Dog-Bone Specimen (60 kN Capacity)

3.6 FE Modelling

3.6.1 FE Model Development

FE modelling is performed for the tobacco composite strip and the steel dog-bone specimen to generate numerical modal parameters and FRFs for comparison with EMA results. The tobacco composite strip is modelled as a 2D shell structure using PSHELL with CQUAD4 elements and MAT8, while the steel dog-bone specimen is modelled as a 3D solid structure using PSOLID with CTETRA elements and MAT1. The models are prepared in PATRAN and analysed using MSC NASTRAN so that a consistent modelling workflow is applied to both specimens. The initial material properties assigned to the initial FE model are listed in Table 3.1 for the tobacco composite strip and Table 3.2 for the steel dog-bone specimen. The FE model information, including element type and mesh cases, is summarised in Table 3.3.

Two MSC NASTRAN solution sequences are used in this study, namely SOL 103 for normal modes analysis and SOL 111 for modal frequency response analysis. The simplified NASTRAN input entries for each solution sequence, showing only the employed entries from the actual model files used in this study, are presented in Table 3.4 and Table 3.5 respectively. The intention is not to reproduce the complete Bulk Data File but to identify the key employed entries so that the analysis setup is fully traceable.

The TABDMP1 entry in SOL 111 is the key entry for modal damping representation in the frequency response analysis. It assigns an independent damping ratio to each mode rather than applying a global proportional damping coefficient, and this entry directly supports the mode-by-mode damping updating strategy used in the damping updating stage of this study. When EMA-based or FEMTools-refined damping ratios are assigned, they are entered into the TABDMP1 table and the SOL 111 analysis is re-executed to produce updated FRF predictions for comparison with EMA.

The FE model geometry and mesh representation are presented to show how the two specimens are discretised for analysis. The tobacco composite strip FE model is shown in Figure 3.9 to represent the shell-based discretisation used for the strip specimen. The steel dog-bone FE model is shown in Figure 3.10 to represent the solid-based discretisation used for the dog-bone specimen. These FE model views provide the modelling reference for the modal and FRF analyses performed in the next subsection.

Table 3.1
Initial MAT8 Properties for the Tobacco Composite Strip

No. of Specimen	Young's Modulus, E1 (GPa)	Young's Modulus, E2 (GPa)	Poisson's Ratio, v12	Density, ρ (kg/m³)
1				1164.83
2	2.55	2.55	0.33	1194.56
3				1153.25

Table 3.2
Initial MAT1 Properties for the Steel Dog-Bone

No. of Specimen	Young's Modulus, E (GPa)	Poisson's Ratio, ν	Density, ρ (kg/m³)
1			7844.32
2	210	0.30	7790.53
3			7812.89

Table 3.3
FE Model Information for the Tobacco Strip and Steel Dog-Bone Specimens

Specimen	No. of Specimen	Model Type	Property Card	Element Type	Material Card	Mesh Size (mm)	No. of Elements	No. of Nodes
Tobacco Composite Strip	1	2D	PSHELL	2D CQUAD4	MAT8	10	60	88
						5	200	250
						1	5000	5226
	2					10	40	67
						5	200	250
						1	4800	5025
	3					10	40	67
						5	200	250
						1	4800	5025
Steel Dog-Bone	1	3D	PSOLID	3D CTETRA	MAT1	10	1208	364
						5	3796	977
						1	140828	29728
	2					10	1635	455
						5	3760	967
						1	143064	30139
	3					10	1186	353
						5	3869	978
						1	141280	29839

Table 3.4
Simplified NASTRAN Input Entries for SOL 103 (Normal Modes Analysis)

Section	Entry	Description
Case Control	SOL 103	Solution sequence for normal modes analysis
	CEND	End of Executive Control
	ECHO = NONE	Suppresses echo of Bulk Data in output
	SUBCASE 1	Defines a single analysis subcase
	METHOD = 1	References EIGRL eigenvalue extraction method
	VECTOR(SORT1, REAL) = ALL	Requests mode shape output for all modes
	SPCFORCES(SORT1, REAL) = ALL	Requests SPC reaction force output
	BEGIN BULK	Start of Bulk Data Section

Bulk Data	PARAM, PRTMAXIM, YES	Prints maximum values in output
	PARAM, COUPMASS, -1	Activates consistent mass matrix formulation
	PARAM, POST, -1	Enables results export for post-processing
	EIGRL	Eigenvalue extraction (1 to 1000 Hz, 10 modes, MASS normalisation)
	MAT8	Orthotropic material card for TCP (E1, E2, G12, v12, density)
	PSHELL	Shell property card referencing MAT8
	CQUAD4	2D quadrilateral shell elements at 1 mm mesh
	GRID	Node coordinate definitions
	ENDDATA	End of Bulk Data Section

Table 3.5
Simplified NASTRAN Input Entries for SOL 111 (Modal Frequency Response Analysis)

Section	Entry	Description
Case Control	SOL 111	Solution sequence for modal frequency response analysis
	CEND	End of Executive Control
	ECHO = NONE	Suppresses echo of Bulk Data in output
	SUBCASE 1	Defines a single analysis subcase
	METHOD = 1	References EIGRL eigenvalue extraction method
	FREQUENCY = 1	References FREQ1 frequency set
	SPC = 1	References single point constraint set
	DLOAD = 10	References dynamic load definition
	SDAMPING = 20	References TABDMP1 modal damping table
	ACCELERATION(SORT2, PHASE) = ALL	Requests acceleration FRF output at all DOFs
	BEGIN BULK	Start of Bulk Data Section
Bulk Data	PARAM, POST, -1	Enables results export for post-processing
	EIGRL	Same eigenvalue extraction settings as SOL 103
	FREQ1	Defines frequency range and increment for FRF output
	TABDMP1	Modal damping table assigning damping ratio per mode
	MAT8 or MAT1	Orthotropic (TCP) or isotropic (steel) material card
	PSHELL or PSOLID	Shell or solid property card for respective specimen
	CQUAD4 or CTETRA	Shell or solid element definitions
	RLOAD1	Frequency-dependent dynamic load definition at excitation DOF
	DAREA	Load application point and unit force amplitude
	GRID	Node coordinate definitions
	ENDDATA	End of Bulk Data Section

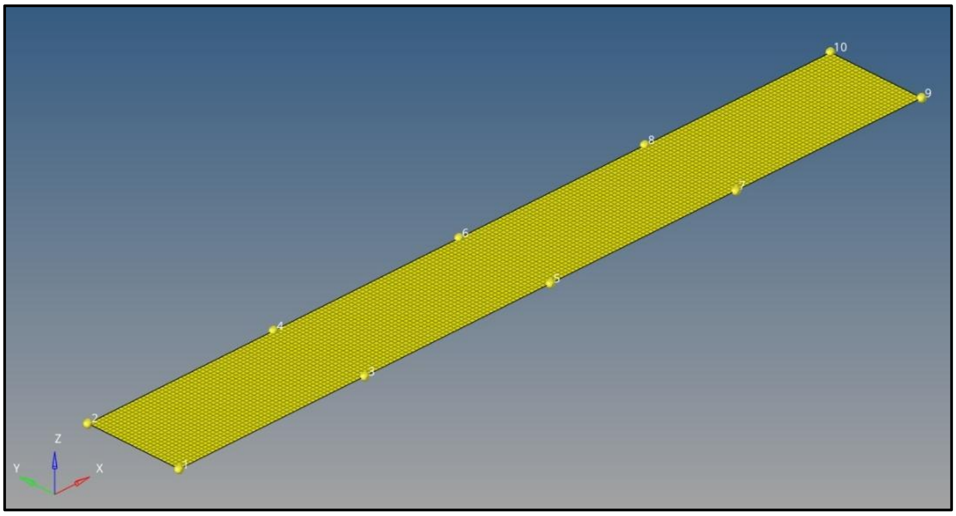

Figure 3.9 FE Model of the Tobacco Composite Strip

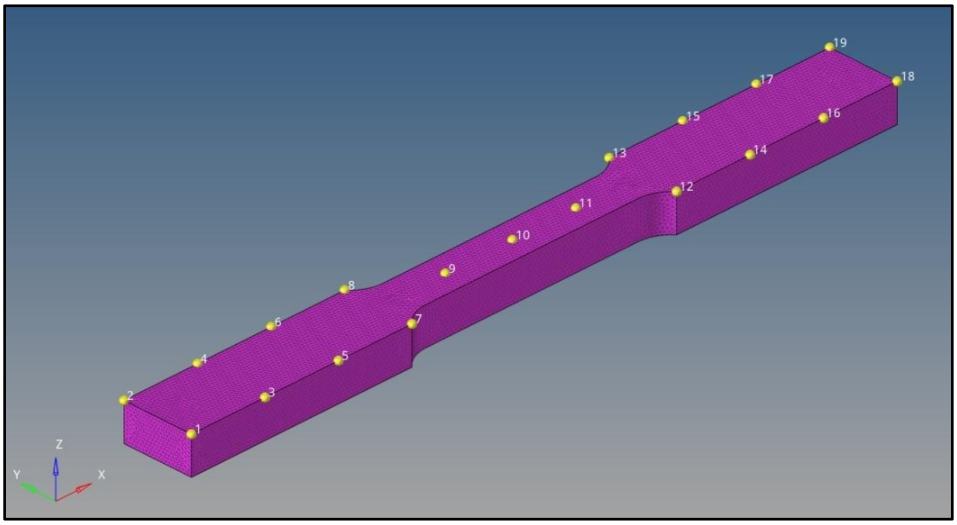

Figure 3.10 FE Model of the Steel Dog-Bone Specimen

3.6.2 Modal and FRF Analysis

Modal and FRF analyses are performed using the initial FE model to generate numerical outputs in forms suitable for FE–EMA correlation. Modal analysis is carried out to obtain predicted natural frequencies and mode shapes that will later be compared with EMA for mode pairing and MAC evaluation. FRF analysis is then performed using the same excitation and response definitions used in EMA so that predicted FRFs can be compared directly with measured FRFs. Initial damping is applied using baseline assumptions so that damping-related mismatch can be identified before modal damping updating is implemented. The predicted outputs from this stage serve as the baseline numerical dataset for the correlation step.

3.6.3 Mesh Convergence

Mesh convergence analysis is performed using one selected specimen for each specimen to decide a suitable mesh size for subsequent FE analyses, where Tobacco Specimen 1 and Steel Specimen 1 are used as the representative cases. Three mesh sizes are evaluated, namely 10 mm, 5 mm, and 1 mm, to observe the change in predicted natural frequencies as the mesh is refined. The convergence trend for the tobacco composite strip is presented in Figure 3.11, while the convergence trend for the steel dog-bone specimen is presented in Figure 3.12. For the tobacco composite strip, the Mode 1 error changes from 7.33% at 10 mm (60 elements) to 6.83% at 5 mm (200 elements) and 6.67% at 1 mm (5000 elements). The change in error between the 5 mm and 1 mm meshes is 0.16%, which is below the 0.5% stopping criterion, confirming that the 1 mm mesh has achieved a converged solution and is selected for all subsequent analyses. For the steel dog-bone specimen, the Mode 1 error reduces from 22.63% at 10 mm (1208 elements) to 13.04% at 5 mm (3796 elements) and 1.20% at 1 mm (140828 elements). The change in error between the 5 mm and 1 mm meshes is 11.84%, which exceeds the stopping criterion, indicating that further refinement would still yield improvement. However, the 1 mm mesh achieves a very low absolute error of 1.20% and represents a substantial reduction from the coarser meshes, and the associated computational cost at finer refinement is not justified for the level of accuracy required in this study; therefore, 1 mm is selected as the mesh for subsequent work and this limitation is acknowledged.

It is also noted that for the heterogeneous TCP material, the 1 mm mesh element size is substantially smaller than the typical tobacco fibre or flake dimensions within the composite, which means that the FE model does not resolve individual fibre-scale features but instead treats the material as a homogeneous effective medium at the element level. This is consistent with the effective continuum modelling approach adopted in this study, where the updating process identifies effective orthotropic properties that best reproduce the globally measured dynamic response rather than attempting to resolve microstructural features directly. The element size relative to fibre dimensions is not a limiting factor in this context because the correlation and updating targets are globally measured modal parameters and FRFs rather than local strain fields.

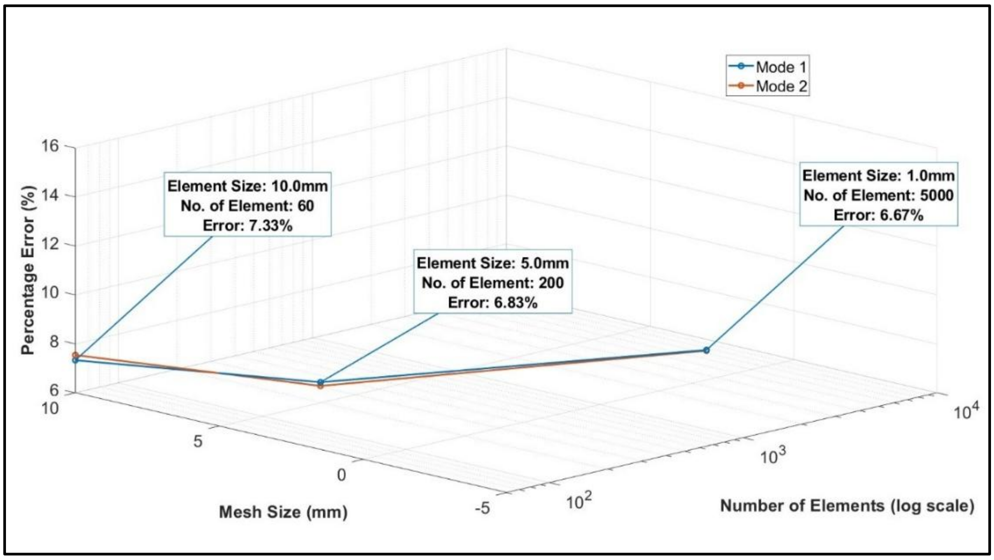

Figure 3.11 Mesh Convergence Plot for the Tobacco Composite Strip (Specimen 1) Showing Percentage Error in Natural Frequencies at Different Mesh Sizes

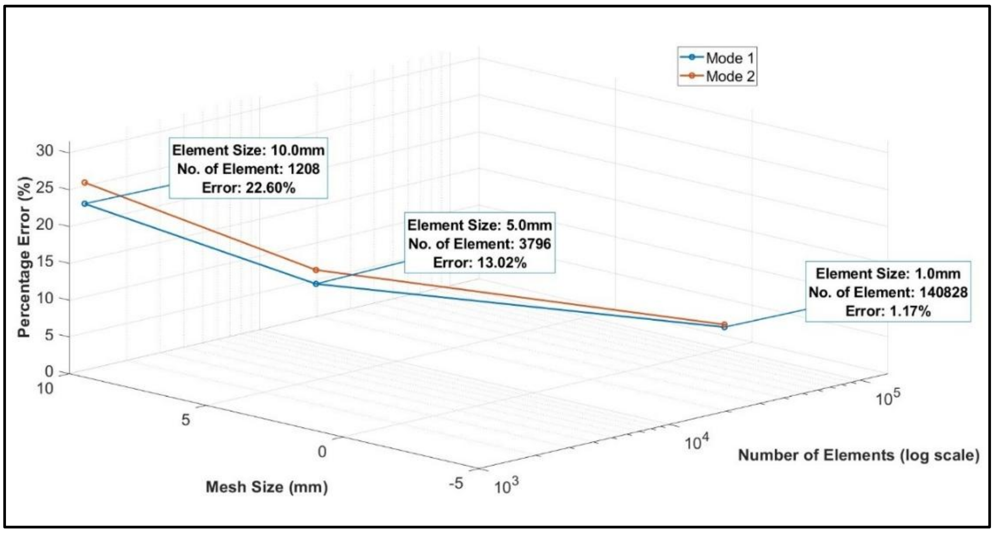

Figure 3.12 Mesh Convergence Plot for the Steel Dog-Bone Specimen (Specimen 1) Showing Percentage Error in Natural Frequencies at Different Mesh Sizes

3.7 FE–EMA Correlation

FE–EMA correlation is performed to quantify the agreement between numerical predictions and experimental results for the tobacco composite strip and the steel dog-bone specimen using consistent correlation measures. The correlation is carried out by comparing EMA-extracted natural frequencies, mode shapes, and FRFs with the corresponding predictions from the initial FE model. Natural frequency error is used to evaluate resonance location agreement so that stiffness-related mismatch can be identified clearly. Mode shape agreement is evaluated using MAC so that correct mode pairing and deformation patterns can be verified. FRF comparison is then used to evaluate resonance peak behaviour and overall frequency-domain agreement, which is sensitive to both stiffness and damping representation. The correlation outcomes from this baseline stage provide the reference mismatch pattern that guides development of the tensile-test-based FE model, the modal-updating-based FE model, and the final updated FE model.

Natural frequency correlation is applied first because frequency mismatch provides direct evidence of stiffness-to-mass imbalance in the FE model relative to the tested specimen. Frequency error is computed between FE and EMA for the paired modes within the frequency range selected for the study. The frequency error trend is examined to identify whether the initial FE model is systematically over-stiff or under-stiff relative to EMA. This frequency-based evaluation is also used to check whether the same set of modes is consistently observed across the three suspension configurations during EMA. The identified frequency mismatch pattern is then used as the first indicator for stiffness-related parameter adjustment in later model development steps.

Mode shape correlation is performed because matching frequencies alone does not confirm that the FE model captures the same deformation patterns as the measured structure. MAC is used to quantify the similarity between FE and EMA mode shapes and to support correct mode pairing. Modes with low MAC are treated carefully because poor mode shape agreement can indicate modelling deficiencies or incorrect pairing rather than small parameter differences. The mode shape correlation results are used to confirm that the selected measurement points and the FE response locations provide compatible spatial resolution for shape comparison. This step ensures subsequent updating uses properly paired modes as targets rather than forcing agreement on mismatched deformation patterns.

FRF correlation is performed to evaluate frequency-domain agreement beyond resonance locations, particularly the resonance peak behaviour used later for modal damping updating. Predicted FRFs from FE are compared with measured FRFs using the same input–output definitions so that amplitude and bandwidth behaviour can be assessed consistently. Differences in resonance peak amplitude and bandwidth are interpreted as indicators of damping mismatch when resonance locations and mode pairing are already reasonable. FRF comparison is also used to confirm that the FE model can represent both resonance and off-resonance trends within the chosen frequency range. This FRF-based evaluation provides the evidence needed to justify modal damping updating toward the final updated FE model.

The correlation results are used as the decision basis to move from baseline prediction to improved FE representations using clearly defined model stages. The initial FE model correlation establishes the baseline mismatch pattern that the tensile-test-based FE model and modal-updating-based FE model are intended to reduce. The tensile-test-based FE model is evaluated to observe how assigning tensile-derived stiffness affects frequency and mode shape agreement relative to EMA. The modal-updating-based FE model is evaluated to reduce stiffness-related mismatch using EMA modal targets before damping refinement is applied. Modal damping updating is then guided by FRF correlation so that the updated FE model achieves very low error when compared with EMA.

3.8 FE Model Updating Strategy

FEMU is implemented to improve agreement between FE predictions and EMA results for the tobacco composite strip and the steel dog-bone specimen in a traceable sequence of model stages. The updating sequence starts from the initial FE model and progresses through the tensile-test-based FE model and the modal-updating-based FE model before modal damping updating is applied. Each stage is defined to produce a clear output so that the influence of stiffness input, modal updating, and damping updating can be evaluated separately. The final model after modal damping updating is referred to as the updated FE model and represents the best FE agreement with EMA with very low error. This section describes how targets and parameters are organised across the updating stages.

The tensile-test-based FE model is developed to introduce a quasi-static stiffness input into the FE model using Young's modulus obtained from tensile testing. Tensile-derived modulus is assigned as the material stiffness input so that the FE model reflects stiffness measured under quasi-static loading. This model stage is used as a comparative stiffness route to observe how tensile-based stiffness influences predicted natural frequencies and mode shapes relative to EMA. The tensile-test-based FE model is not treated as the final target model because the main vibration reference remains the EMA dataset. The outcomes from this stage support interpretation of stiffness representation prior to modal updating.

The modal-updating-based FE model is developed to reduce stiffness-related mismatch using EMA modal targets as the updating reference. Updating targets include natural frequencies and mode shapes so that resonance locations and deformation patterns are improved together rather than corrected by frequency matching alone. MAC is used to support mode pairing and to ensure that parameter updates improve agreement for the correct modes. The updating parameters are selected to represent physically meaningful stiffness-related properties so that the updated values remain interpretable for both specimens. This stage gives a model with better modal agreement which produces a stable base for damping refinement.

Modal damping updating is performed to improve FRF peak behaviour after stiffness-related agreement has been improved using the modal-updating-based FE model. Damping updating targets are FRF peak amplitude and bandwidth so that resonance characteristics can be closed to EMA more closely within the selected frequency range. The damping parameters are set so as to minimise mismatch in peak behaviour, and keep the resonance locations identified by the stiffness-driven resonance achieved by modal updating. FRF agreement is determined using the same input-output definitions as are used in EMA so that improvements represent true response matching and not comparison setup changes. This damping updating stage is directly connected with the final updated FE model.

The updated FE model is determined if the correlation metrics show very low error against EMA for both the specimens. Improvement is evaluated consistently using natural frequency error, MAC and FRF agreement in order to evaluate the model performance in modal and frequency domain behaviours. The updated FE model is then used as the primary FE representation in the Results chapter as it is the one with the best agreement with EMA. Comparative discussion is supported by showing how the agreement is changed from the initial FE model to the tensile-test-based FE model, then to the modal-updating-based FE model, and finally to the updated FE model. This is the structure that helps make the updating process traceable and consistent with the research objectives.

3.9 Validation of Updated FE Model

Validation is done to verify that the updated FE model gives very small error in comparison with EMA for the tobacco composite strip and the steel dog-bone specimen.

The same correlation measures are used as in the previous method and again, the improvement is measured in a consistent way through all stages of the FE model. Natural frequency agreement is verified to ensure that the locations of the predicted resonance conditions by the updated FE model are in good agreement with EMA. Mode shape agreement is checked using MAC to confirm that the updated FE model reproduces the measured deformation patterns for the paired modes. FRF agreement is also checked to confirm that resonance peak behaviour improves after modal damping updating.

Validation is conducted comparatively to show how agreement improves from the initial FE model to the updated FE model through clearly defined intermediate stages. The initial FE model is used as the baseline reference to represent the starting mismatch before any updating is carried out. The tensile-test-based FE model is evaluated to show the influence of quasi-static stiffness input on predicted dynamic behaviour. The modal-updating-based FE model is evaluated to demonstrate improvements in natural frequency agreement and MAC when EMA modal targets are used. The updated FE model is then validated as the final best model because it provides the lowest error across the selected correlation measures.

3.10 Concluding Remarks

This chapter presented the research methodology adopted to achieve the objectives of this study through an integrated workflow applied to the tobacco composite strip and the steel dog-bone specimen. The workflow began with specimen definition and EMA to obtain FRFs and modal parameters as the experimental reference dataset. FE modelling was then performed using the initial FE model, including mesh convergence checks to support selection of modelling resolution.

Tensile testing was carried out after EMA to obtain E_{tensile} for development of the tensile-test-based FE model as a comparative stiffness route. FE–EMA correlation and FE model updating were then carried out to produce the modal-updating-based FE model and the final updated FE model after modal damping updating.

The outputs prepared using this methodology provide the basis for the results and discussion presented in Chapter 4.

CHAPTER 4
RESULTS AND DISCUSSION

4.1 Introduction

This chapter presents the results and discussion of the experimental and numerical investigations conducted for the tobacco composite strip and the steel dog-bone specimen, with emphasis on improving damping representation so that FE-predicted FRFs match EMA results. The chapter begins by reporting the EMA outcomes that define the experimental reference dataset for subsequent correlation and updating. The initial FE model results are then presented to establish the baseline numerical response before any stiffness or damping refinement is applied. Correlation results are reported by comparing EMA with the initial FE model, the tensile-test-based FE model, and the modal-updating-based FE model to show how resonance frequency mismatch is reduced across the model stages. The chapter then focuses on damping updating and reports how the updated FE model improves resonance peak behaviour using FRF-based measures.

The results are structured into the following key sections:

4.2 Correlation Results for the EMA–Initial FE Model

4.3 Correlation Results for the EMA–Tensile-Test-Based FE Model

4.4 Correlation Results for the EMA–Modal-Updating-Based FE Model

4.7 Damping Updating Results for the Updated FE Model

4.8 Concluding Remarks

The results are organised to maintain traceability across the three specimens for each specimen type so that specimen-to-specimen variability is not masked by combining datasets. Tobacco Specimen 1 to 3 are presented consistently across the EMA, correlation, and updating outcomes for the tobacco composite strip. Steel Specimen 1 to 3 are presented in the same manner to support verification of the same workflow using a conventional isotropic material. The same comparison format is applied in each section so that changes in agreement can be attributed clearly to stiffness input, modal updating, or damping updating. This structure ensures that the updated FE model reported later represents the best agreement with EMA with very low error for the selected response measures.

4.2 Correlation Results for the EMA−Initial FE Model

This section shows the baseline correlation between EMA and the initial FE model of the tobacco composite strip and steel dog-bone specimen to quantify the initial mismatch before any stiffness or damping updating is applied. The correlation is reported using FRF comparison, natural frequency comparison, and mode shape agreement so that frequency-domain and modal-domain consistency can be assessed together. The baseline correlation is reported for three tobacco specimens and three steel specimens to preserve specimen-by-specimen traceability. The outputs from this section define the mismatch level that motivates the next model stage.

The FRF comparison is used to evaluate the baseline agreement in resonance peak behaviour between EMA and the initial FE model under a consistent damping assumption. For FRF generation, the initial FE model uses an assumed damping ratio of 0.01 for both the tobacco composite strip and the steel dog-bone specimen so that the baseline comparison is not influenced by specimen-specific damping tuning. Figure 4.1 compares EMA and initial FE FRFs for the tobacco composite strip for Specimen 1 to 3, where the SAC values are 0.24, 0.26, and 0.32, indicating weak baseline FRF agreement. Figure 4.2 compares EMA and initial FE FRFs for the steel dog-bone specimen for Specimen 1 to 3, where the SAC values are 0.80, 0.52, and 0.52, indicating moderate-to-good baseline FRF agreement compared with tobacco. These SAC trends show that FRF mismatch is more severe for the tobacco composite strip at the baseline stage.

The initial FE model uses a uniform modal damping ratio of 0.01 for all modes of both specimen types. This value is selected as a conservative and neutral baseline assumption that is consistent with the lower bound of damping ratios commonly reported for lightly damped composite structures under free-free test conditions, where modal damping ratios typically fall in the range of 0.01 to 0.05 for the first few bending modes. The purpose of this assumption is not to represent the actual damping of either specimen but to provide a consistent and repeatable starting condition for FRF generation so that the baseline FRF comparison is not biased by specimen-specific damping tuning at the initial stage. Stiffness updating in FEMTools is performed using modal targets, specifically natural frequencies and mode shapes, and is therefore independent of the assumed damping ratio. The damping ratio of 0.01 affects only the amplitude and bandwidth of the predicted FRF peaks in the baseline comparison, while the natural frequency positions used as stiffness updating targets are unaffected by this assumption. This separation confirms that the stiffness updating process is physically justified and is not compromised by the initial damping assumption.

The tobacco composite strip is modelled using MAT8, which defines an orthotropic material in MSC NASTRAN with independent elastic moduli in two in-plane directions (E1 and E2), a single in-plane Poisson's ratio (v12), an in-plane shear modulus (G12), and density. In this study, E1 and E2 are treated as the primary updating parameters because the first two bending modes of a strip specimen are predominantly governed by the in-plane longitudinal and transverse bending stiffness, which are controlled by E1 and E2 respectively. The shear modulus G12 and Poisson's ratio v12 are retained at their initial values throughout updating because the selected modes do not exhibit significant shear-dominated deformation and their sensitivity to G12 and v12 is low within the tested frequency band. The material is described as orthotropic rather than fully anisotropic because the MAT8 formulation assumes material symmetry in the three principal material directions, which is consistent with the fibre-matrix composite structure of TCP where the dominant stiffness directions are aligned with and transverse to the predominant fibre orientation (Michal et al., 2024). Although TCP exhibits microstructural heterogeneity, the orthotropic effective continuum assumption is a standard and defensible simplification for panel-like composites at the structural scale, and the updating process identifies effective values of E1 and E2 that best reproduce the globally measured dynamic response rather than attempting to represent all directional properties independently.

Natural frequency comparison is used to quantify resonance location mismatch between EMA and the initial FE model for the tobacco composite strip. Table 4.1 lists the EMA natural frequencies and the corresponding initial FE natural frequencies for Mode 1 and Mode 2 for tobacco Specimen 1 to 3, combined with the frequency error and SAC. The Mode 1 error falls in the range of 2.96% to 5.83% and Mode 2 error falls in the range of 3.09% to 5.94%, which shows that there is consistent stiffness-related mismatch in the first two modes. This frequency mismatch indicates that stiffness parameters have to be improved before peak matching can be interpreted with confidence.

Natural frequency comparison is also used to quantify the baseline resonance location mismatch for the steel dog-bone specimen using the same reporting approach. Table 4.2 shows the EMA natural frequencies and corresponding initial FE natural frequencies for Mode 1 and Mode 2 for steel Specimen 1 to 3, along with the frequency error and SAC. The Mode 1 error ranges from 1.17% to 2.06% and the Mode 2 error from 1.35% to 2.02%, which is a lower degree of mismatch than tobacco but is not zero. The higher SAC values observed in steel FRFs compared to tobacco further support that stiffness mismatch is still present even with comparatively better FRF agreement.

Mode shape agreement is checked to verify whether the initial FE model is able to reproduce the measured deformation patterns of the first two modes. Table 4.3 shows tobacco mode shapes and MAC values for tobacco Specimen 1 to 3, where Mode 1 MAC values are 0.95, 0.90, and 0.67, and Mode 2 MAC values are 0.71, 0.79, and 0.47. Table 4.4 gives steel mode shapes and MAC values for steel Specimen 1 to 3, in which the Mode 1 MAC values are 0.80, 0.68, and 0.88, and the Mode 2 MAC values are 0.86, 0.80, and 0.91. These MAC values indicate a general trend of better mode shape agreement for steel and weaker agreement for tobacco, particularly for Mode 2. This mode shape trend is consistent with the low SAC values observed for tobacco and indicates the need for further improvement of the baseline model.

Overall, the EMA-initial FE model correlation shows noticeable mismatch in resonance locations and resonance peak behaviour for both specimens, with a stronger mismatch trend for the tobacco composite strip. The tobacco FRFs show low SAC values and several-percent frequency errors across both modes, which confirms that the baseline model is not yet adequate for FRF-based validation. The steel results show better FRF agreement based on SAC, but frequency error remains non-zero and still requires stiffness refinement. This baseline mismatch motivates the next model stage where $E_{Tensile}$ is assigned into the initial FE model to form the tensile-test-based FE model for further correlation with EMA.

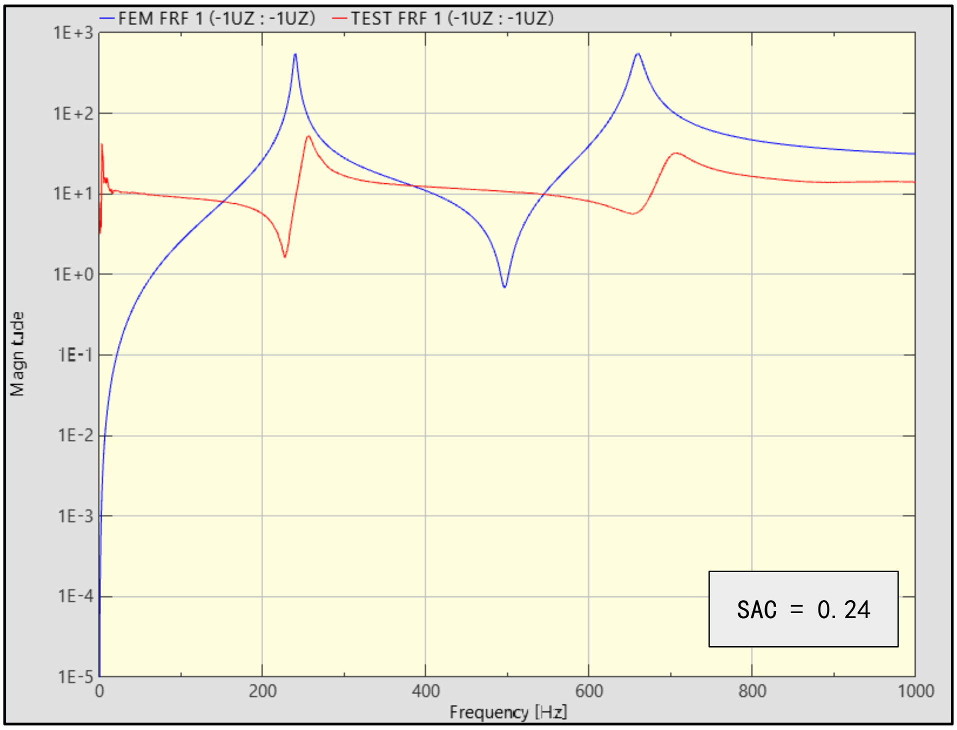
FEM FRF 1 (-1UZ : -1UZ)
TEST FRF 1 (-1UZ : -1UZ)
1E+3
1E+2
1E+1
1E+0
1E-1
1E-2
1E-3
1E-4
1E-5
Magnitude
0
200
400
600
800
1000
Frequency [Hz]
SAC = 0.24

(a)

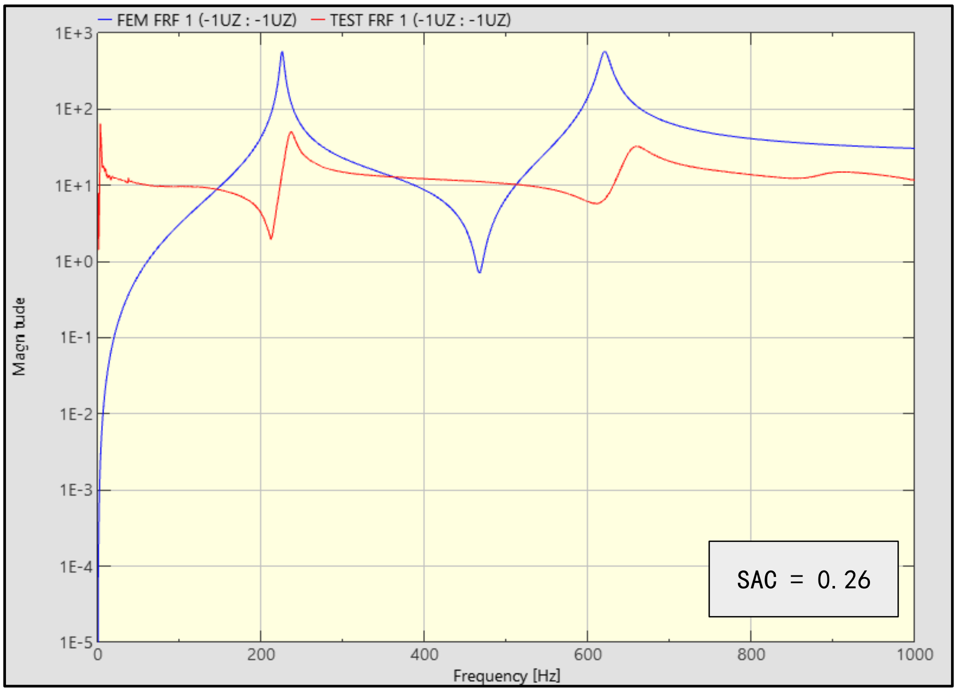
FEM FRF 1 (-1UZ : -1UZ)
TEST FRF 1 (-1UZ : -1UZ)
1E+3
1E+2
1E+1
1E+0
1E-1
1E-2
1E-3
1E-4
1E-5
Magnitude
0
200
400
600
800
1000
Frequency [Hz]
SAC = 0.26

(b)

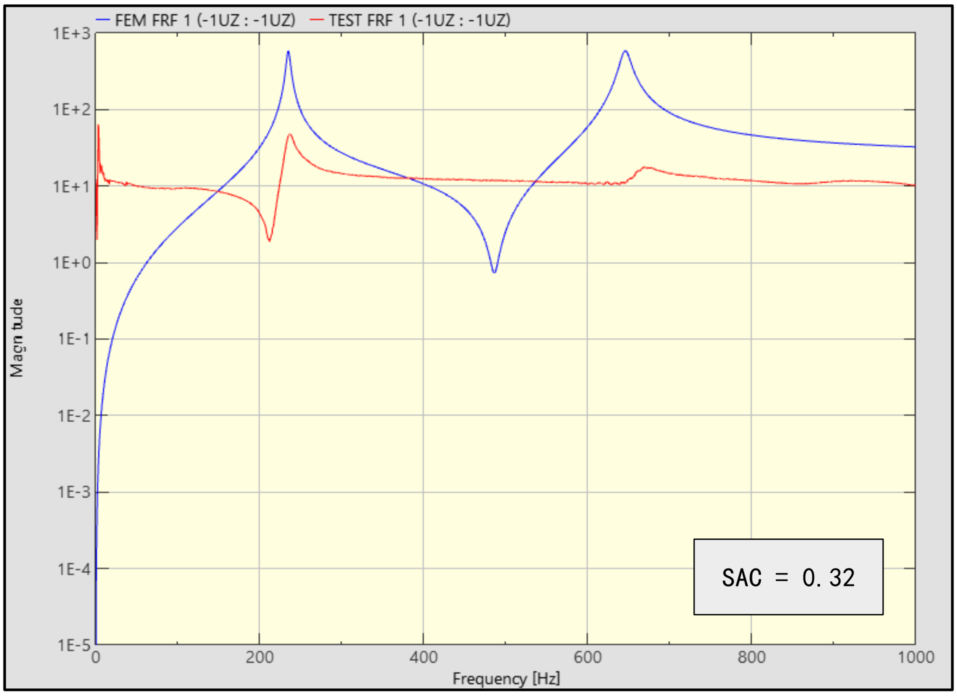

(c)

Figure 4.1 FRF Comparison Between EMA and the Initial FE Model for the Tobacco Composite Strip for (a) Specimen 1, (b) Specimen 2, and (c) Specimen 3

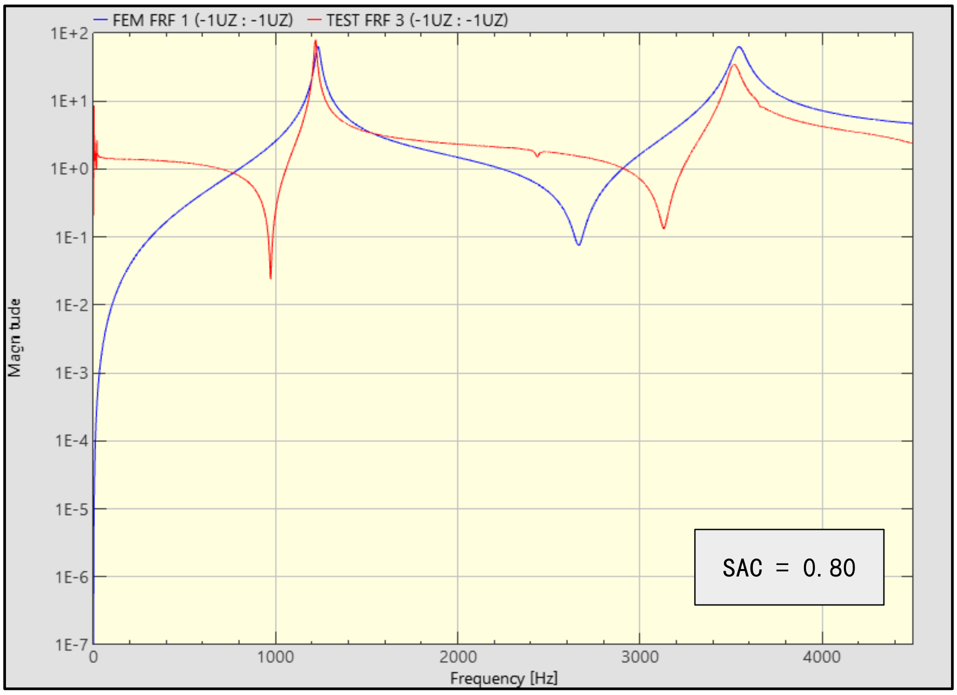

(a)

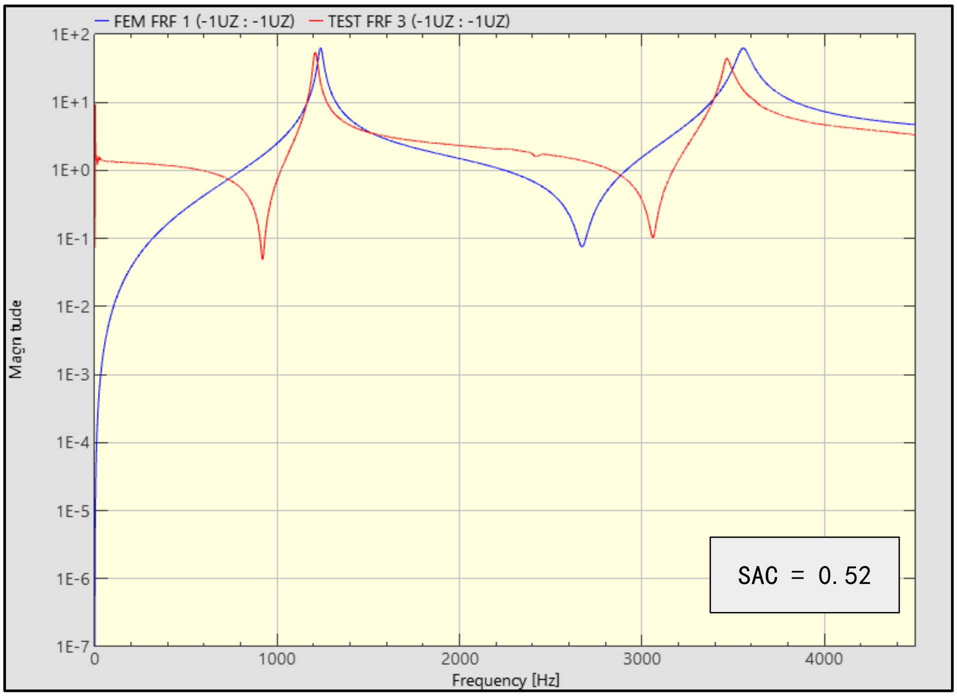

(b)

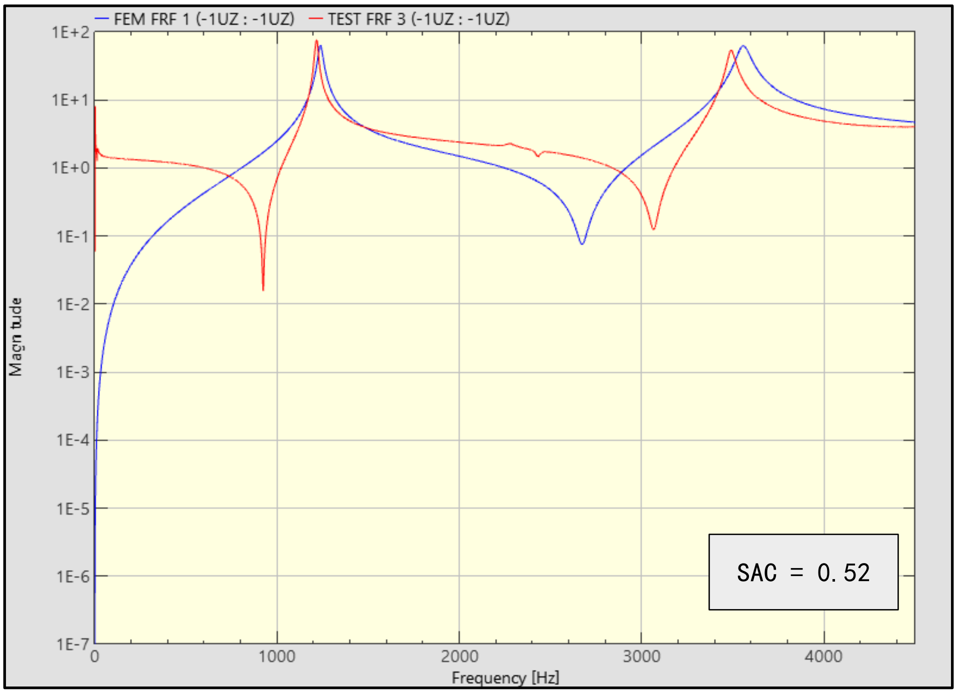

(c)

Figure 4.2 FRF Comparison Between EMA and the Initial FE Model for the Steel Dog-Bone Specimen for (a) Specimen 1, (b) Specimen 2, and (c) Specimen 3

Table 4.1
EMA and Initial FE Natural Frequencies and SAC for the Tobacco Composite Strip

No. of Specimen	Mode	EMA (Hz)	Initial FE (Hz)	Error (%)	SAC
1	1	254.637	239.800	5.83	0.24
	2	700.848	659.212	5.94	
2	1	235.029	225.520	4.05	0.26
	2	653.210	620.224	5.05	
3	1	241.897	234.736	2.96	0.32
	2	665.950	645.398	3.09	

Table 4.2
EMA and Initial FE Natural Frequencies and SAC for the Steel Dog-Bone

No. of Specimen	Mode	EMA (Hz)	Initial FE (Hz)	Error (%)	SAC
1	1	1217.132	1231.398	1.17	0.80
	2	3485.558	3538.379	1.52	
2	1	1212.258	1237.269	2.06	0.52
	2	3502.897	3550.322	1.35	
3	1	1214.842	1237.197	1.84	0.52
	2	3482.420	3552.650	2.02	

Table 4.3
EMA and Initial FE Mode Shapes and MAC Values for the Tobacco Composite Strip

Mode	**EMA**						**FE**
	Specimen 1	**MAC**	**Specimen 2**	**MAC**	**Specimen 3**	**MAC**	
1	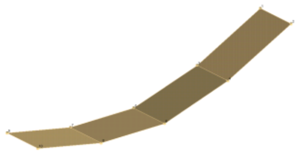	0.95	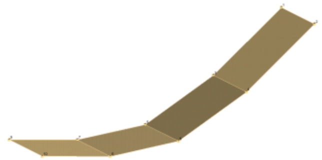	0.90	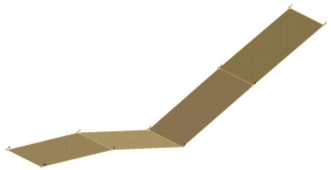	0.67	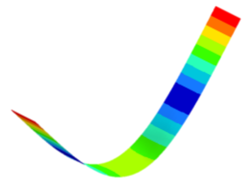
2	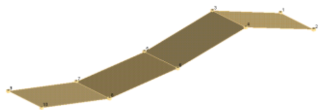	0.71	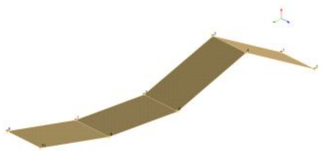	0.79	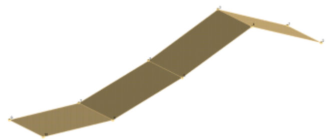	0.47	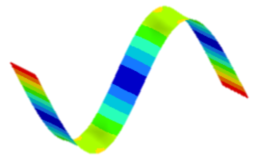

Table 4.4
EMA and Initial FE Mode Shapes and MAC Values for the Steel Dog-Bone Specimen

Mode	**EMA**						**FE**
	Specimen 1	**MAC**	**Specimen 2**	**MAC**	**Specimen 3**	**MAC**	
1	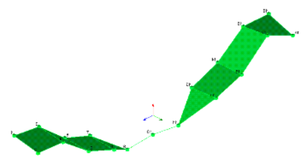	0.80	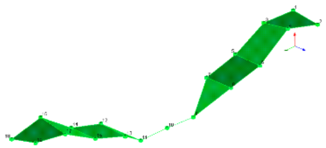	0.68	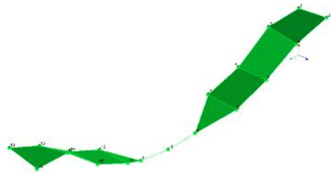	0.88	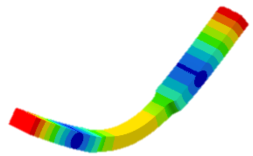
2	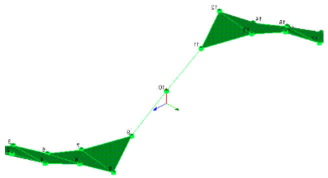	0.86	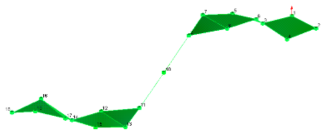	0.80	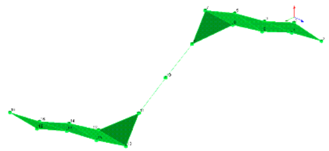	0.91	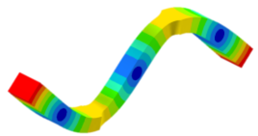

4.3 Correlation Results for the EMA–Tensile-Test-Based FE Model

This section presents the correlation between EMA and the tensile-test-based FE model to evaluate the effect of using quasi-static Young's modulus as the stiffness input for dynamic prediction. The tensile-test-based FE model is formed by assigning the tensile-derived modulus, $E_{Tensile}$, into the initial FE model while maintaining the same FE modelling setup used in the baseline comparison. This section focuses on FRF agreement and natural frequency agreement for Mode 1 and Mode 2 because the purpose of this model stage is to evaluate stiffness input influence rather than to refine mode shapes. Results are reported for three tobacco specimens and three steel specimens to maintain consistent specimen tracking across the study.

The tensile-derived modulus values used to construct the tensile-test-based FE model are summarised to establish the stiffness input applied in this model stage. Figure 4.3 presents the stress-strain curves for tobacco composite strip specimens, which yield $E_{Tensile}$ = 2.262 GPa, 2.190 GPa, and 2.296 GPa for Specimen 1 to 3. Figure 4.4 presents the stress-strain curves for the steel dog-bone specimens, where $E_{Tensile}$ = 4.889 GPa, 4.892 GPa, and 5.232 GPa are reported for Specimen 1 to 3. Table 4.5 compiles these tensile-derived Young's modulus values to give a direct relation between the stiffness input in the quasi-static regime and the later correlation in the dynamic regime. These tensile results are also recorded in Appendix 1 for traceability from Specimen 1 to 3.

The tensile-derived steel modulus values of 4.889 GPa, 4.892 GPa, and 5.232 GPa differ substantially from the well-established literature value for structural steel, which is typically in the range of 190 to 210 GPa. This large discrepancy is attributed to the strain measurement method used in the tensile test, where crosshead displacement was recorded as the extension input rather than a dedicated local strain measurement device such as an extensometer or strain gauge. Crosshead displacement captures the total system compliance, including grip seating, machine compliance, and any initial specimen slip within the grips, all of which contribute apparent extension that is not true gauge strain. At the small deformation levels in the linear elastic region of steel, these compliance contributions are disproportionately large relative to the true elastic strain, resulting in an apparent initial slope of the stress-strain curve that is far lower than the true material modulus. The modulus values reported in Table 4.5 for steel are therefore treated as apparent quasi-static stiffness outputs from the specific tensile test procedure used and are not claimed to represent the intrinsic elastic modulus of the steel material. For the purpose of FE modelling, the steel dog-bone initial FE model uses the established isotropic modulus of 210 GPa as the baseline material input, which is consistent with the known material properties of structural steel and is supported by the well-converged mesh study confirming that the FE model can reproduce the EMA-measured natural frequencies to within 1.20% after stiffness updating. The tensile-test-based FE model for steel is therefore included as a methodological comparison step to demonstrate the limitation of quasi-static stiffness transfer to dynamic prediction, rather than as a proposed route for dynamic model improvement.

FRF comparison is used to evaluate whether stiffness substitution using $E_{Tensile}$ improves agreement with EMA resonance behaviour compared with the baseline initial FE model. Figure 4.5 compares the EMA FRFs with the tensile-test-based FE FRFs for the tobacco composite strip for Specimen 1 to 3, where the SAC values are 0.20, 0.20, and 0.25. Figure 4.6 compares the EMA FRFs with the tensile-test-based FE FRFs for the steel dog-bone specimen for Specimen 1 to 3, where the SAC values are 0.35, 0.33, and 0.25. These SAC values indicate that FRF agreement remains weak at this stage, which is expected because damping has not yet been refined and the resonance locations can still be far from the EMA results when stiffness is not dynamically consistent. The FRF overlays therefore show that stiffness substitution alone does not deliver reliable FRF peak matching for either specimen.

Natural frequency comparison is used to quantify the effect of $E_{Tensile}$ on resonance location mismatch for both specimens to support direct stiffness-input evaluation. Table 4.6 reports that the tobacco composite strip frequency errors range from 7.84% to 12.01% across Mode 1 and Mode 2 after assigning $E_{Tensile}$, indicating that quasi-static stiffness substitution does not improve resonance location agreement for the tobacco specimens. Table 4.7 reports that the steel dog-bone frequency errors range from 83.67% to 84.65% across Mode 1 and Mode 2 after assigning $E_{Tensile}$, which shows that the quasi-static modulus values produce a large underestimation of dynamic stiffness and shift resonance locations substantially. This outcome confirms that the tensile-test-based FE model is not suitable as a final predictive model for dynamic behaviour and should be treated as a comparative step that highlights stiffness transfer limitations. The findings motivate the next stage, where FEMTools is used to update stiffness parameters directly using EMA modal targets to form the modal-updating-based FE model.

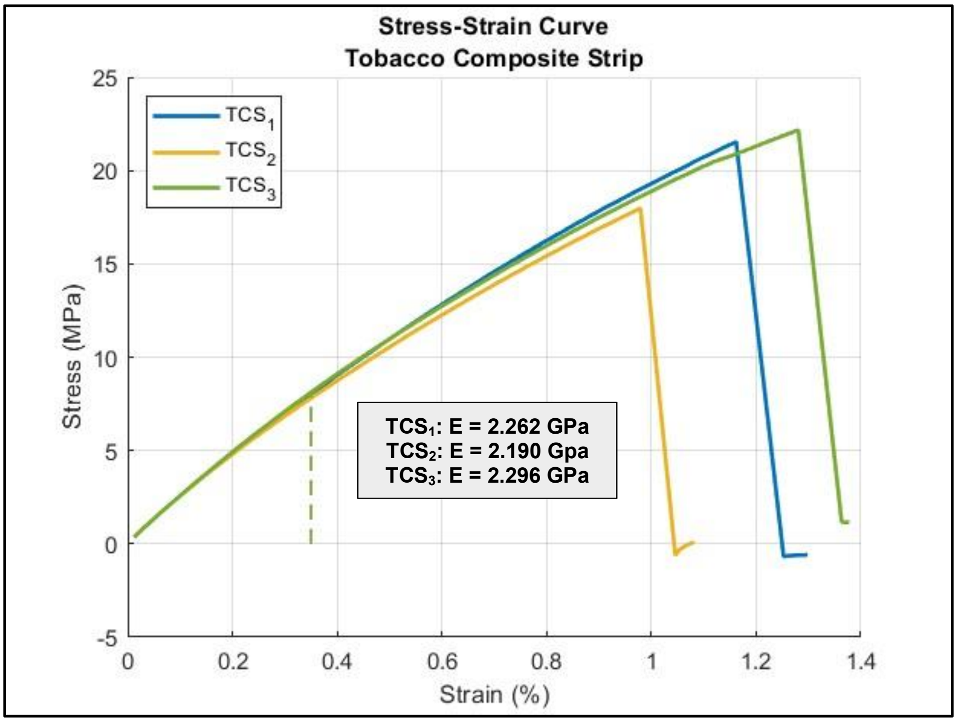

Figure 4.3 Stress–Strain Curves for Tobacco Composite Strip Specimens and Tensile-Derived Young's Modulus Values

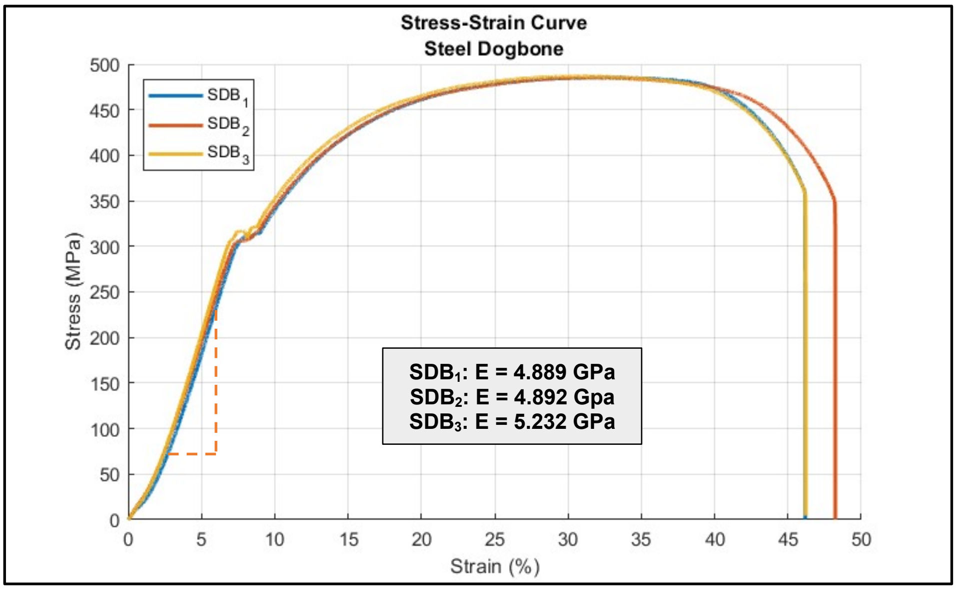

Figure 4.4 Stress–Strain Curves for Steel Dog-Bone Specimens and Tensile-Derived Young's Modulus Values

Table 4.5
Tensile-Derived Young's Modulus Values Used in the Tensile-Test-Based FE Model

No. of Specimen	Young Modulus, $E_{Tensile}$ (GPa)	
	Tobacco Composite Strips	**Steel Dog-Bone**
1	2.262	4.889
2	2.190	4.892
3	2.296	5.232

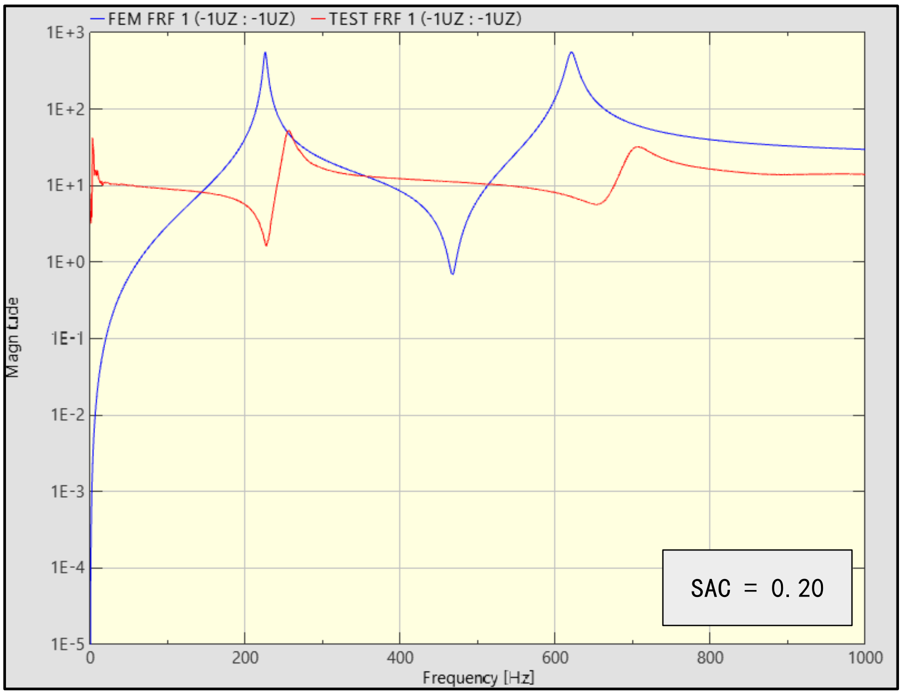
FEM FRF 1 (-1UZ : -1UZ)
TEST FRF 1 (-1UZ : -1UZ)
Magnitude
Frequency [Hz]
SAC = 0. 20
(a)

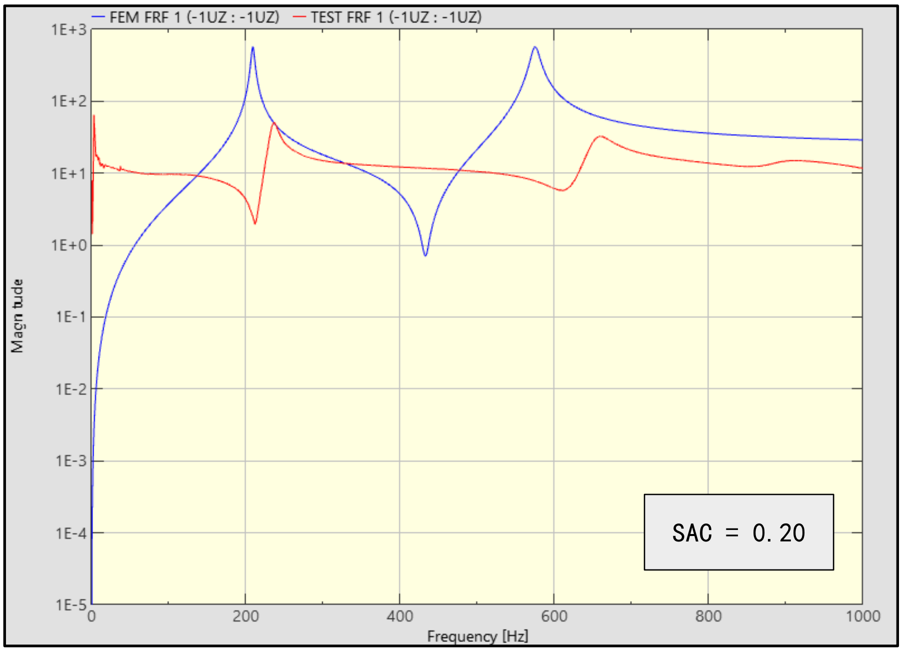
FEM FRF 1 (-1UZ : -1UZ)
TEST FRF 1 (-1UZ : -1UZ)
Magnitude
Frequency [Hz]
SAC = 0. 20
(b)

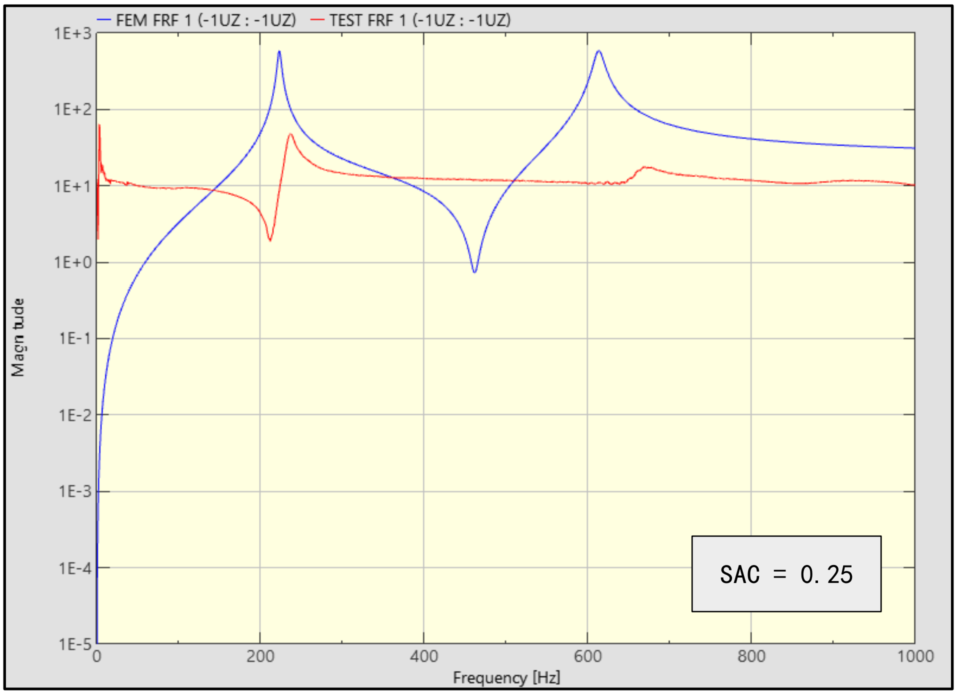

(c)

Figure 4.5 FRF Comparison Between EMA and the Tensile-Test-Based FE Model for the Tobacco Composite Strip for (a) Specimen 1, (b) Specimen 2, and (c) Specimen 3

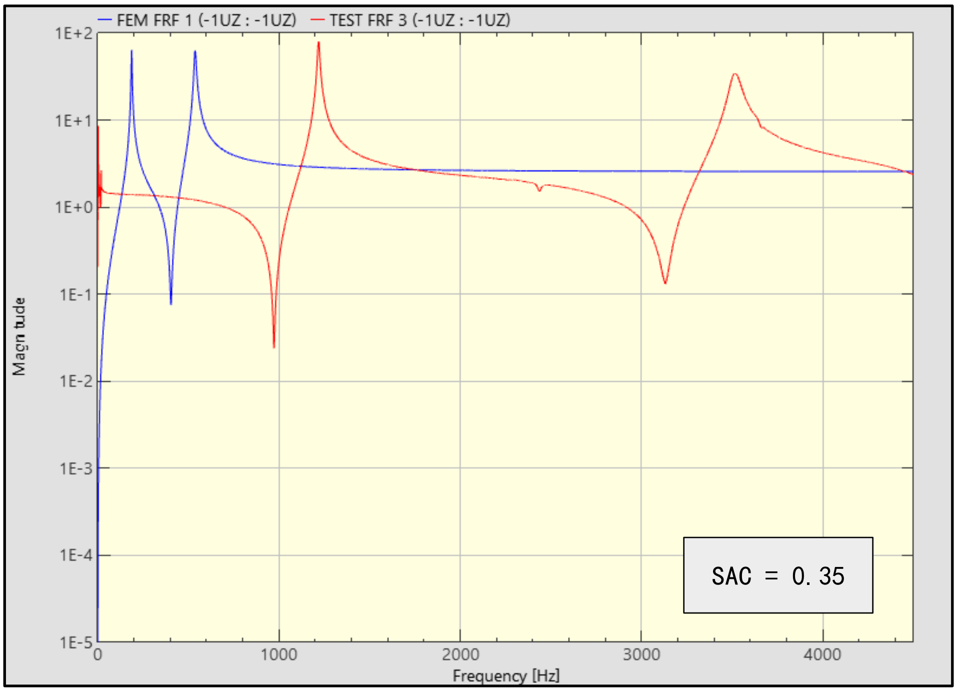

(a)

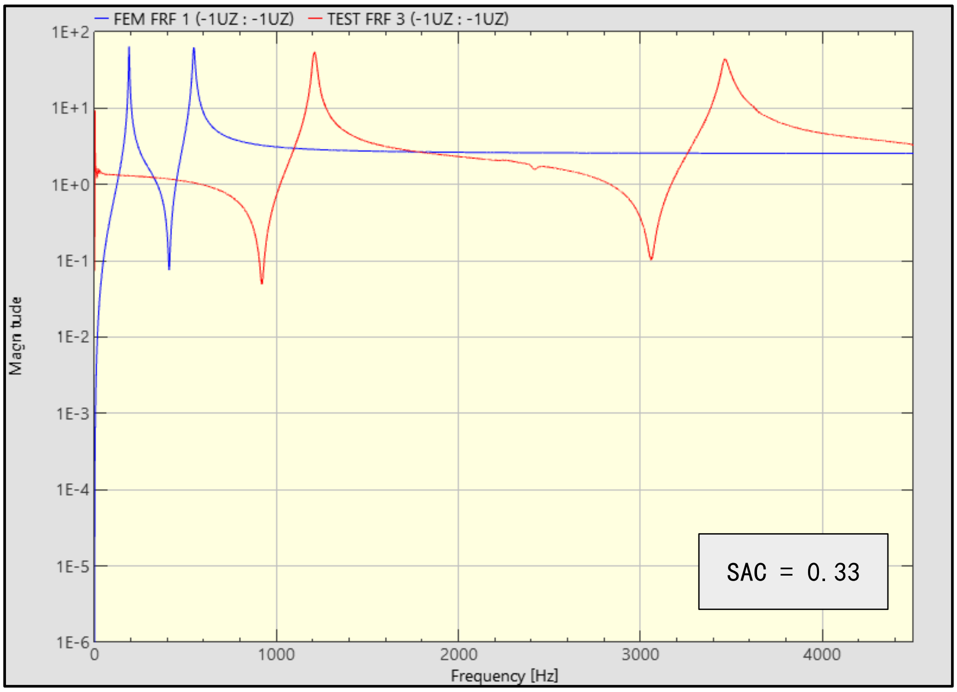

(b)

(c)

Figure 4.6 FRF Comparison Between EMA and the Tensile-Test-Based FE Model for the Steel Dog-Bone Specimen for (a) Specimen 1, (b) Specimen 2, and (c) Specimen 3

Table 4.6
EMA and Tensile-Test-Based FE Natural Frequencies, Frequency Errors and SAC for the Tobacco Composite Strip

No. of Specimen	Mode	EMA (Hz)	Tensile-Test-Based FE (Hz)	Error (%)	SAC
1	1	254.637	225.753	11.34	0.20
	2	700.848	620.596	11.45	
2	1	235.029	208.995	11.08	0.20
	2	653.210	574.778	12.01	
3	1	241.897	222.933	7.84	0.25
	2	665.950	612.945	7.96	

Table 4.7
EMA and Tensile-Test-Based FE Natural Frequencies, Frequency Errors and SAC for the Steel Dog-Bone

No. of Specimen	Mode	EMA (Hz)	Tensile-Test-Based FE (Hz)	Error (%)	SAC
1	1	1217.132	186.855	84.65	0.35
	2	3485.558	536.922	84.60	
2	1	1212.258	189.956	84.33	0.33
	2	3502.897	545.075	84.44	
3	1	1214.842	198.091	83.69	0.25
	2	3482.420	568.826	83.67	

4.4 Correlation Results for the EMA−Modal-Updating-Based FE Model

This section presents the correlation between EMA and the modal-updating-based FE model to show how resonance locations improve after stiffness-related parameters are updated in FEMTools using modal targets. This stage focuses on reducing natural frequency errors for Mode 1 and Mode 2 so that resonance locations align with EMA before damping is treated as an updating target. The results are reported using updated material parameters, FRF overlays, and natural frequency errors for the tobacco composite strip and the steel dog-bone. Specimen-by-specimen reporting is maintained for Specimen 1 to 3 for both specimen types.

The updated stiffness-related parameters are summarised to define the property set used to form the modal-updating-based FE model for each specimen. For the tobacco composite strip, Table 4.8 reports the updated orthotropic properties, where E1 is 2.875 GPa, 2.799 GPa, and 2.704 GPa and E2 is 2.881 GPa, 2.792 GPa, and 2.703 GPa for Specimen 1 to 3, with v12 remaining close to 0.330 to 0.332. For the steel dog-bone, Table 4.9 reports the updated isotropic properties, where E is 204.202 GPa, 202.781 GPa, and 201.866 GPa for Specimen 1 to 3, with v remaining close to 0.299 to 0.301. These updated values show that stiffness correction is achieved mainly through modulus adjustment while Poisson's ratio remains essentially unchanged. This parameter update provides the stiffness basis needed for resonance alignment in the frequency response comparison.

The FRF overlays show that resonance positions move closer to EMA after modal updating, while peak behaviour remains different because damping has not been updated at this stage. Figure 4.7 compares the EMA FRFs with the modal-updating-based FE FRFs for the tobacco composite strip, and the SAC values for Specimen 1 to 3 improve to 0.46, 0.41, and 0.34. Figure 4.8 presents the corresponding comparison for the steel dog-bone, and the SAC values for Specimen 1 to 3 are 0.62, 0.70, and 0.61. These FRF plots show clearer alignment in resonance frequency locations compared with earlier model stages, especially for the steel specimen where the overall FRF shape agreement is stronger. However, the remaining differences in peak amplitude and bandwidth indicate that damping representation still limits FRF peak matching even after stiffness alignment.

The natural frequency comparisons quantify the resonance alignment achieved by the modal-updating-based FE model for both specimens. Table 4.10 reports that the tobacco composite strip frequency errors are reduced to 0.00% to 0.52% for Mode 1 and 0.06% to 0.52% for Mode 2 across Specimen 1 to 3. Table 4.11 reports that the steel dog-bone frequency errors are reduced to 0.11% to 0.33% for Mode 1 and 0.11% to 0.33% for Mode 2 across Specimen 1 to 3. These low errors confirm that stiffness-related mismatch has been reduced to a small level for both specimens. This resonance alignment allows the next section to treat damping as the main source of remaining FRF mismatch.

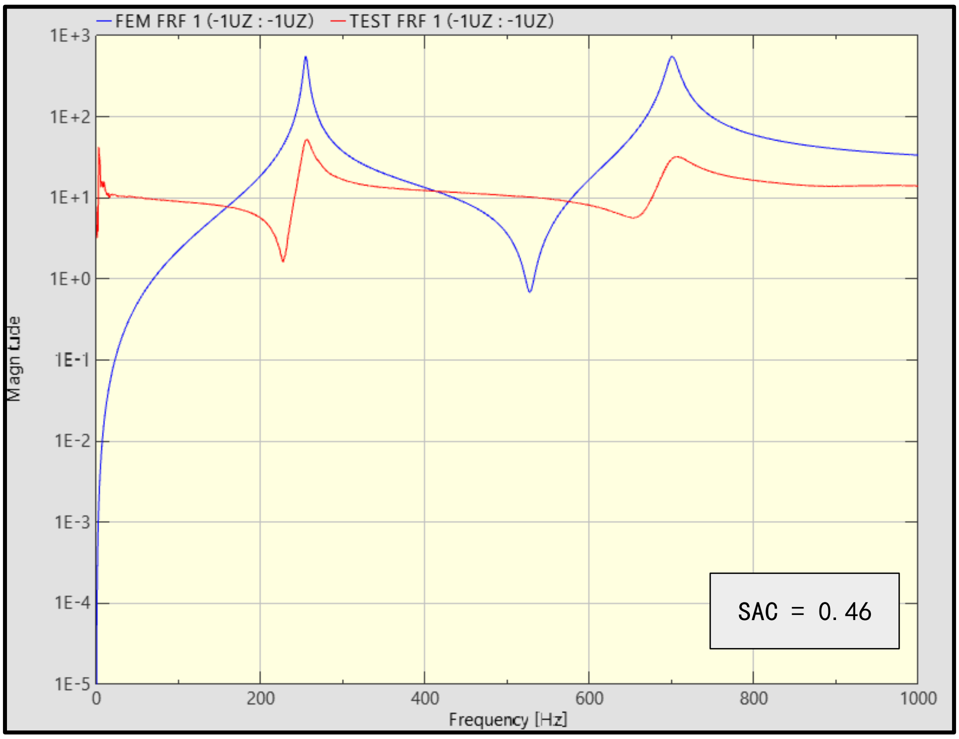

FEM FRF 1 (-1UZ : -1UZ)
TEST FRF 1 (-1UZ : -1UZ)
1E+3
1E+2
1E+1
1E+0
1E-1
1E-2
1E-3
1E-4
1E-5
Magnitude
0
200
400
600
800
1000
Frequency [Hz]
SAC = 0.46

(a)

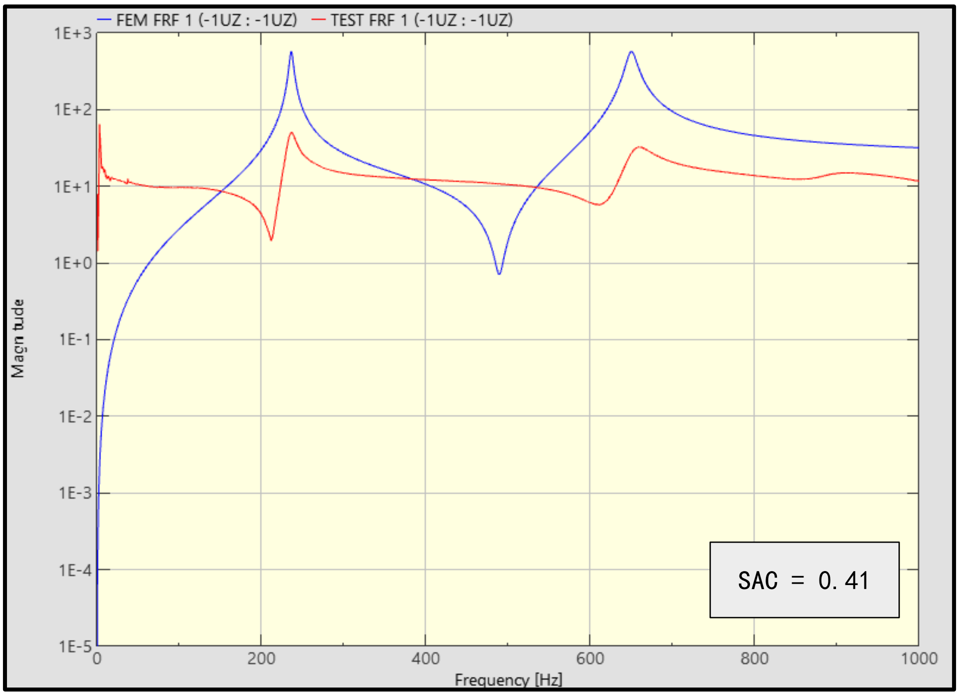

FEM FRF 1 (-1UZ : -1UZ)
TEST FRF 1 (-1UZ : -1UZ)
1E+3
1E+2
1E+1
1E+0
1E-1
1E-2
1E-3
1E-4
1E-5
Magnitude
0
200
400
600
800
1000
Frequency [Hz]
SAC = 0.41

(b)

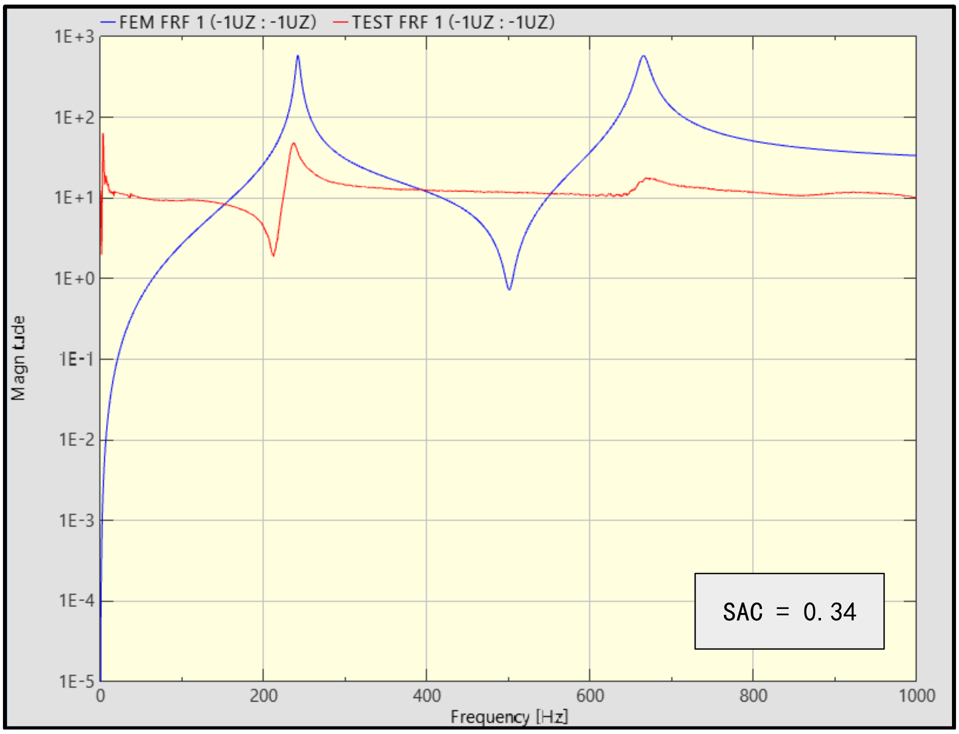

(c)

Figure 4.7 FRF Comparison Between EMA and the Modal-Updating-Based FE Model for the Tobacco Composite Strip for (a) Specimen 1, (b) Specimen 2, and (c) Specimen 3

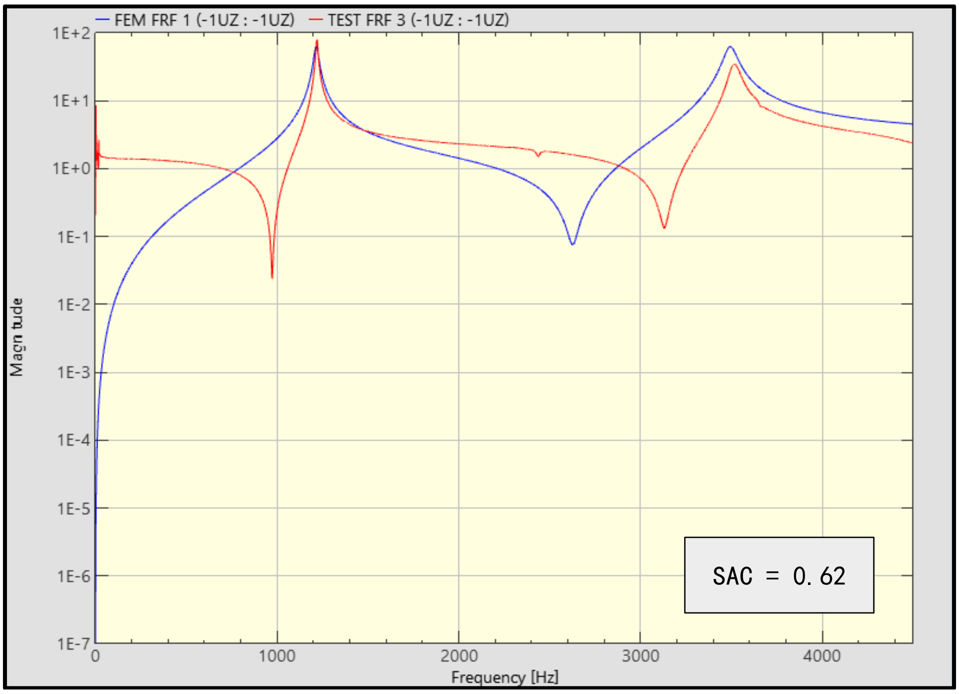

(a)

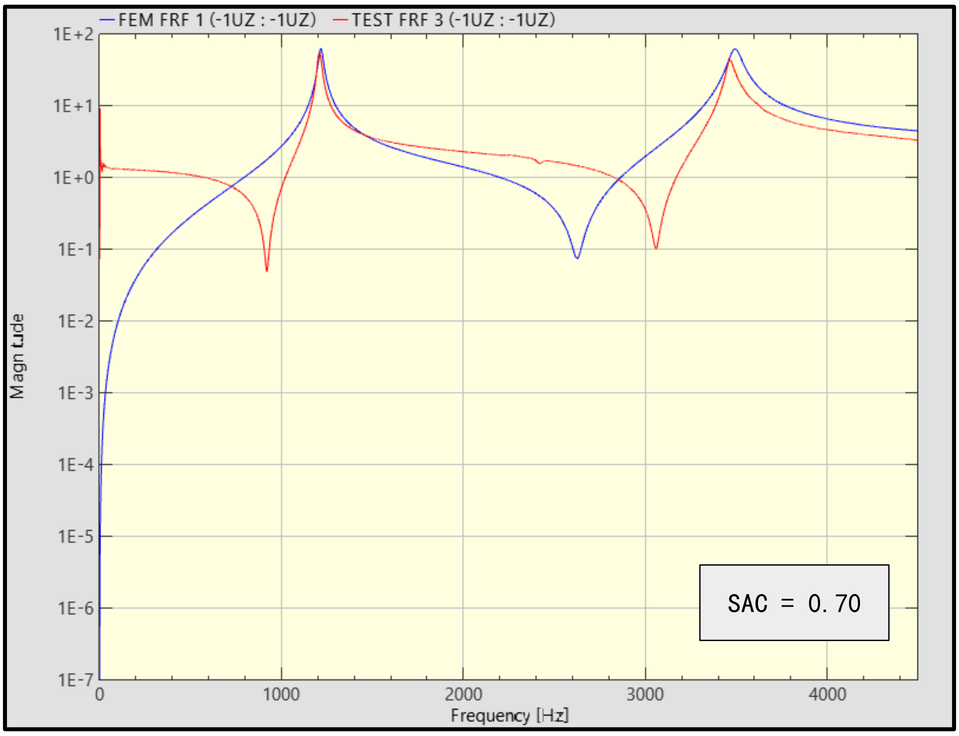

(b)

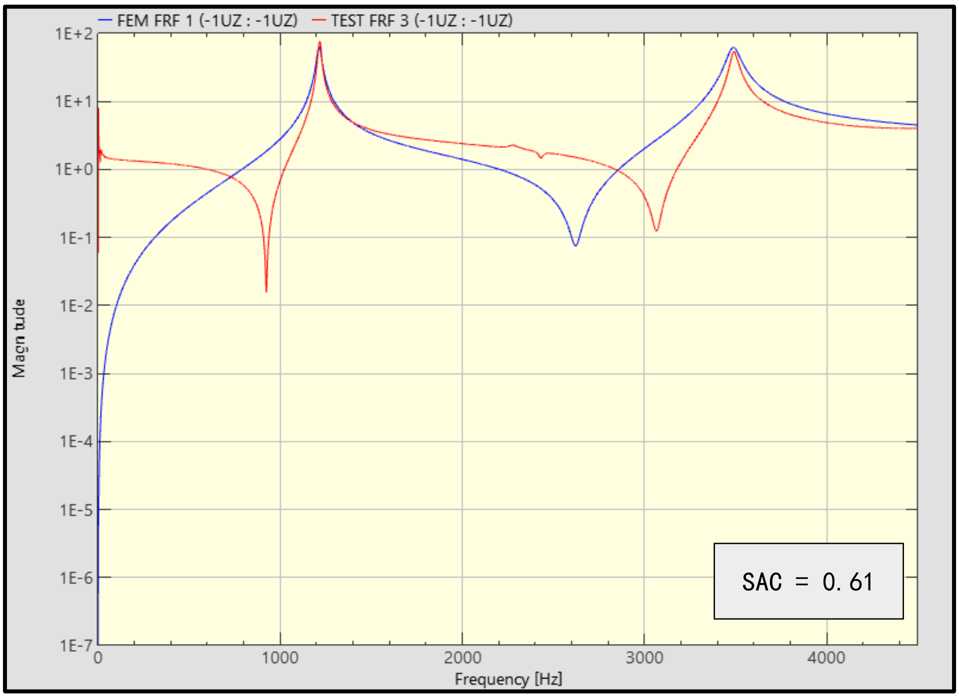

(c)

Figure 4.8 FRF Comparison Between EMA and the Modal-Updating-Based FE Model for the Steel Dog-Bone for (a) Specimen 1, (b) Specimen 2, and (c) Specimen 3

Table 4.8

Updated Material Parameters for the Tobacco Composite Strip From Modal Updating

No. of Specimen	Young's Modulus, E1 (GPa)	Young's Modulus, E2 (GPa)	Poisson's Ratio, ν12
1	2.875	2.881	0.330
2	2.799	2.792	0.332
3	2.704	2.703	0.330

Table 4.9

Updated Material Parameters for the Steel Dog-Bone From Modal Updating

No. of Specimen	Young's Modulus, E (GPa)	Poisson's Ratio, ν
1	204.202	0.301
2	202.781	0.299
3	201.866	0.301

Table 4.10

EMA and Modal-Updating-Based FE Natural Frequencies and Frequency Errors for the Tobacco Composite Strip

No. of Specimen	Mode	EMA (Hz)	Modal-Updating-Based FE (Hz)	Error (%)	SAC
1	1	254.637	254.781	0.06	0.46
	2	700.848	700.430	0.06	
2	1	235.029	236.261	0.52	0.41
	2	653.210	649.809	0.52	
3	1	241.897	241.893	0.00	0.34
	2	665.950	665.107	0.13	

Table 4.11

EMA and Modal-Updating-Based FE Natural Frequencies and Frequency Errors for the Steel Dog-Bone

No. of Specimen	Mode	EMA (Hz)	Modal-Updating-Based FE (Hz)	Error (%)	SAC
1	1	1217.132	1214.860	0.19	0.62
	2	3485.558	3492.070	0.19	
2	1	1212.258	1216.260	0.33	0.70
	2	3502.897	3491.50	0.33	
3	1	1214.842	1213.560	0.11	0.61
	2	3482.420	3486.090	0.11	

4.5 Damping Updating Results for the Updated FE Model

This section presents the damping updating results used to improve FRF peak behaviour after the natural frequencies have been aligned using the modal-updating-based FE model. For the earlier FE stages up to the modal-updating-based FE model, a constant damping ratio of 0.01 is applied for both the tobacco composite strip and the steel dog-bone to generate numerical FRFs using a consistent baseline. The EMA modal damping ratios are first assigned into the modal-updating-based FE model to form the EMA-based damping FE case. This step allows the effect of measured damping on FRF peaks to be checked directly. The outcome of this step is then used to decide whether additional damping updating in FEMTools is needed to obtain the updated FE model.

The EMA-based damping step checks whether inserting the measured modal damping ratios is enough to reproduce the measured FRF peaks for both specimens. Figure 4.9 compares the EMA FRF with the EMA-based damping FE case for the tobacco composite strip, and Figure 4.10 shows the same comparison for the steel dog-bone. The SAC values for the tobacco composite strip under EMA-based damping are 0.65, 0.60, and 0.51 for Specimen 1 to 3, as reported in Table 4.12. The SAC values for the steel dog-bone are 0.72, 0.55, and 0.58 for Specimen 1 to 3, as reported in Table 4.13. These results show that assigning EMA damping improves FRF agreement for both specimens, although mismatch in peak height and peak width still remains for the tobacco composite strip. This comparison confirms that measured damping improves correlation, but peak matching still needs further refinement depending on the specimen.

Damping updating in FEMTools is then applied to refine the damping values until the FRF peak behaviour matches the measured response more closely. This step follows the theory set out in Chapter 2, where damping controls peak bandwidth and amplitude through the damping term in the equation of motion and through the FRF formulation in Equation 2.1 and Equation 2.10. Once the natural frequencies are matched through stiffness updating, the remaining differences in peak sharpness come mainly from damping rather than stiffness. This matches the modal FRF dependence on modal damping ratio shown in Equation 2.12. Damping is therefore treated as an updating target only after stiffness alignment is done, so that peak-related mismatch can be corrected without disturbing the matched natural frequencies. This is the basis for using FRF-based targets in FEMTools during the damping updating stage.

The final result is shown by the FRF comparisons between EMA and the updated FE model for both specimens. Figure 4.11 shows that the updated FE model improves FRF peak height and peak width agreement for the tobacco composite strip, with SAC values increasing to 0.90, 0.89, and 0.88 for Specimen 1 to 3, as reported in Table 4.14. Figure 4.12 shows the updated FE comparison for the steel dog-bone, with SAC values of 0.90, 0.73, and 0.63 for Specimen 1 to 3, as reported in Table 4.15. These results confirm that damping refinement improves peak behaviour once natural frequency alignment is already done, matching the role of damping described in Equation 2.10 and Equation 2.12. The updated FE model therefore gives the best overall agreement with EMA within the tested frequency range and selected modes.

The high SAC values in the final updated FE model show strong overall FRF agreement across the tested frequency range. In Equation 2.12, the modal damping ratio controls the sharpness and amplitude of each resonance peak, so when the identified damping ratios are set correctly, the FRF shape matches the measured response closely. High SAC values therefore show that both the resonance locations and the shapes of the FRF peaks are accurately reproduced by the updated FE model, matching the result expected from the staged stiffness and damping updating procedure. The SAC metric checks the complex-valued FRF across all frequency lines in the comparison range, so a value close to 1.00 confirms that the model matches both magnitude and phase across the full range, not only near the resonance peaks. This method works best for composite strip or panel structures tested under approximate free-free conditions, where the main response is governed by the first two bending modes and the goal is to improve FRF peak amplitude and bandwidth using damping values taken from test data. The method needs further adjustment for structures with different boundary conditions in service, higher numbers of modes close together, or cases where damping changes strongly with frequency. Therefore, the high SAC values obtained in this study provide confidence that the updated modal parameters successfully reproduce the measured dynamic response within the calibrated frequency range.

The updated modal damping ratio of 0.425 reported in Table 4.14 for Tobacco Specimen 3 Mode 2 is much higher than the EMA-based damping ratio of 0.025 used at the earlier stage. This value comes from the FEMTools damping updating process, which reduces the mismatch in FRF peak amplitude and bandwidth by adjusting the damping ratio until the predicted FRF peak matches the measured peak. Therefore, the value obtained through FRF curve fitting should be interpreted as an equivalent modal damping ratio rather than as a material property of the tobacco composite itself. This interpretation is consistent with the established view that modal damping identified through EMA and FE model updating represents the combined energy dissipation associated with a vibration mode rather than the damping behaviour of the material alone (Ewins, 2000; Maia & Silva, 1997). Accordingly, the updated value accounts for the cumulative influence of several dissipative mechanisms that are not explicitly represented in the FE model, such as energy loss at the fibre matrix interface, simplification of the boundary conditions, fixture or support losses, local material heterogeneity, resin content variation, and possible local micro slip or microcracking. Since the high updated damping ratio occurs only for Specimen 3 Mode 2, while the remaining updated modal damping ratios remain within a comparatively consistent range, this result is considered to represent a localised, mode specific calibration parameter rather than the general damping behaviour of the tobacco composite material. Two specimens can therefore show closely matching FRF amplitude at resonance even though the physical mechanisms contributing to the identified damping ratios differ, since the equivalent modal damping ratio is independently identified for each specimen through FRF matching rather than being prescribed as a single material constant. . The second bending mode of TCP is known to be sensitive to how fibres are arranged in each specimen, so higher damping ratios are expected where fibre clusters or higher resin concentration line up with the high-strain zones of that mode shape. The higher damping ratio found for Specimen 3 Mode 2 is consistent with the known variation between TCP specimens. Therefore, differences in the local strain energy distribution associated with Mode 2 may require different equivalent modal damping ratios to reproduce the experimentally observed FRF. Therefore, the higher updated damping ratio identified for Specimen 3 Mode 2 is interpreted as a mode specific equivalent damping parameter required to achieve accurate FE and experimental FRF correlation, rather than direct evidence of unusually high material damping.

The frequency separation between the identified modes supports the continued use of the real-mode normal mode superposition formulation in Equation 2.12 for the frequency range considered in this study. The proportional damping assumption behind Equation 2.12 depends on how much coupling is introduced through the off-diagonal terms of the damping matrix. Although a relatively high modal damping ratio may increase the possibility of modal interaction, the first two identified bending modes remain well separated in frequency, thereby limiting significant modal overlap within the calibrated frequency range. (Ewins, 2000). This point is supported by Karaağaçlı and Çelik (2024), who identified modal damping ratios of up to 30% for the actuation mechanism of a guided missile control fin. They found that the mode shape stayed mostly real-valued, since the mode of interest was well separated in frequency from the other modes, giving system behaviour close to proportional damping even at a high damping level. A similar frequency separation is present in the tobacco composite specimens in this study, where Mode 1 and Mode 2 are separated by several hundred hertz for all three specimens, for example 254.64 Hz and 700.85 Hz for Specimen 1. Although the updated damping ratio for Specimen 3 Mode 2 is higher than those of the remaining modes, no evidence of significant modal interaction was observed within the analysed frequency range, and the updated FE model continued to provide good agreement with the measured FRFs, as demonstrated by the corresponding SAC value of 0.88 . On this basis, using the classical real-mode solver MSC NASTRAN SOL 111 with TABDMP1 is considered appropriate for reproducing the measured FRFs within the calibrated frequency range adopted in this study. Nevertheless, the relatively high updated damping ratio also indicates a limitation of the present proportional damping representation, and future work should investigate more advanced damping formulations, such as complex modal analysis, viscoelastic damping models, or direct frequency response formulations, for cases involving stronger dissipative behaviour.

To show the differences between specimens in the identified damping ratios, Table 4.16 summarises the mean and standard deviation of the EMA-based and updated modal damping ratios across the three specimens, for each specimen type and each mode. The standard deviation values confirm that TCP shows much greater variation between specimens in damping than the steel dog-bone, which is consistent with the greater microstructural variability typically observed in natural fibre composites. However, these updated modal damping ratios should be interpreted as equivalent modal parameters identified through model updating rather than direct material damping properties. The observed variation therefore reflects the combined influence of specimen to specimen variability together with other unmodelled dissipative mechanisms represented by the updating process. This statistical result supports the robustness of the proposed updating framework by demonstrating its ability to accommodate the variability in equivalent modal damping required to reproduce the measured FRFs of different TCP specimens.

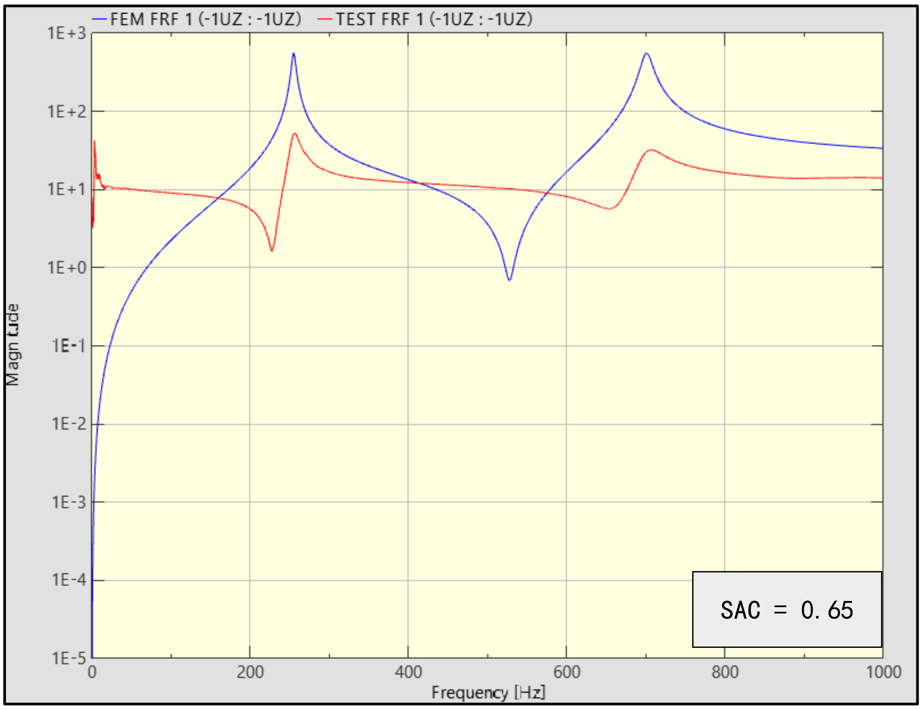
FEM FRF 1 (-1UZ : -1UZ)
TEST FRF 1 (-1UZ : -1UZ)
1E+3
1E+2
1E+1
1E+0
1E-1
1E-2
1E-3
1E-4
1E-5
Magnitude
0
200
400
600
800
1000
Frequency [Hz]
SAC = 0.65

(a)

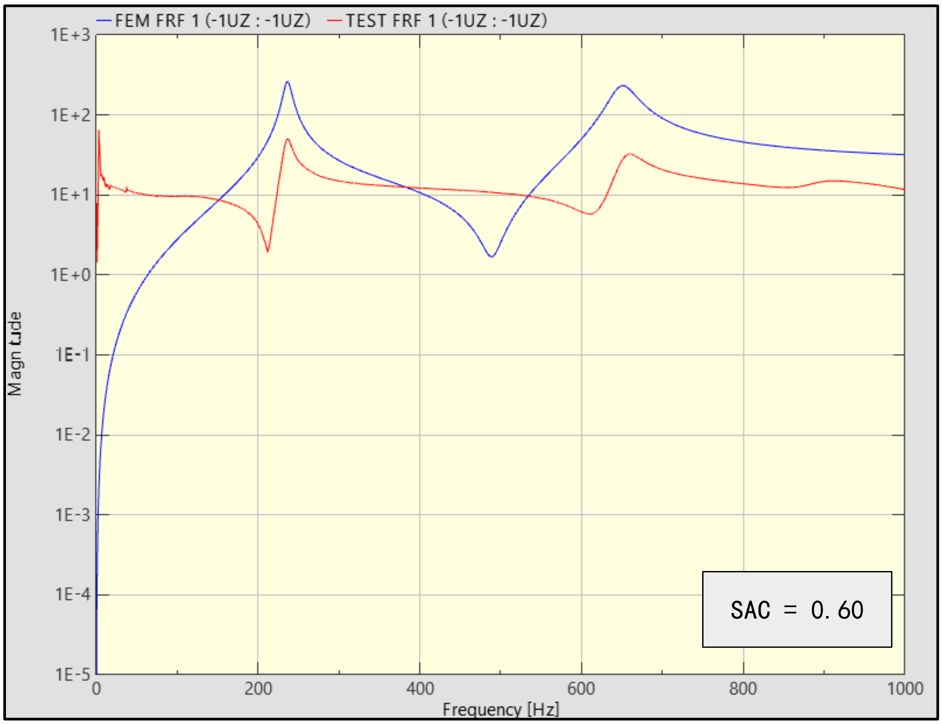
FEM FRF 1 (-1UZ : -1UZ)
TEST FRF 1 (-1UZ : -1UZ)
1E+3
1E+2
1E+1
1E+0
1E-1
1E-2
1E-3
1E-4
1E-5
Magnitude
0
200
400
600
800
1000
Frequency [Hz]
SAC = 0.60

(b)

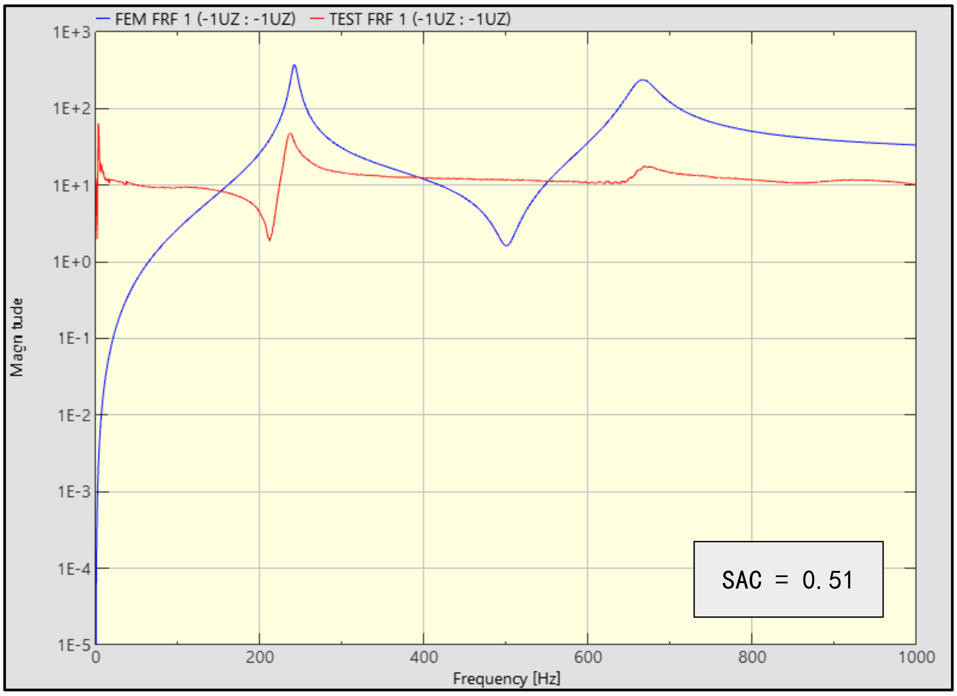

(c)

Figure 4.9 FRF Comparison Between EMA and the Modal-Updating-Based FE Model With EMA-Based Damping for the Tobacco Composite Strip for (a) Specimen 1, (b) Specimen 2, and (c) Specimen 3

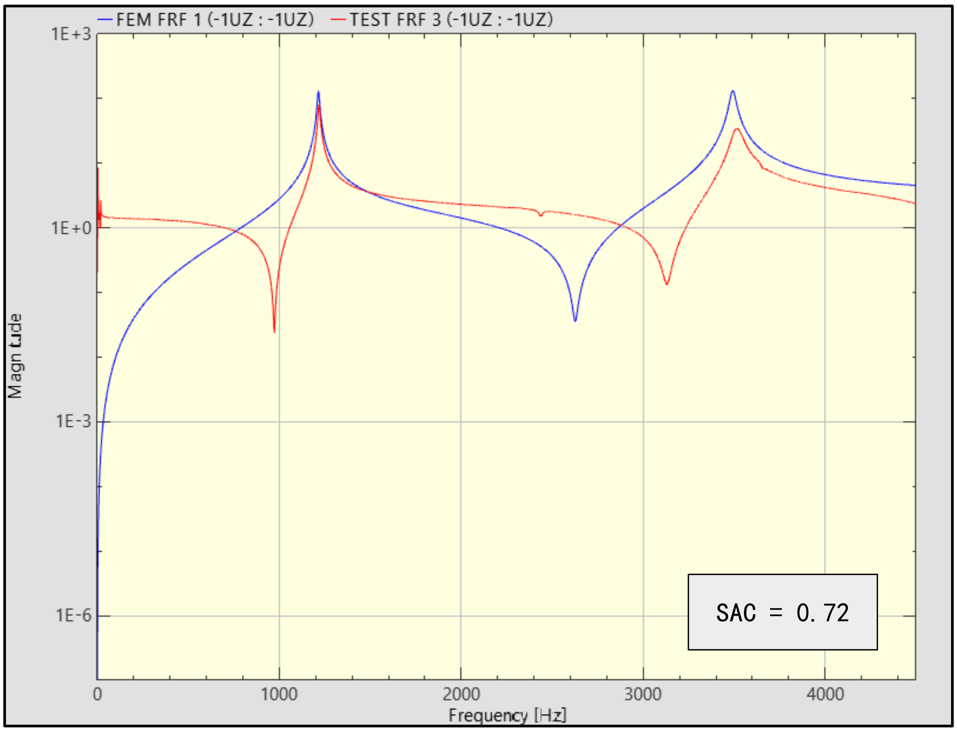

(a)

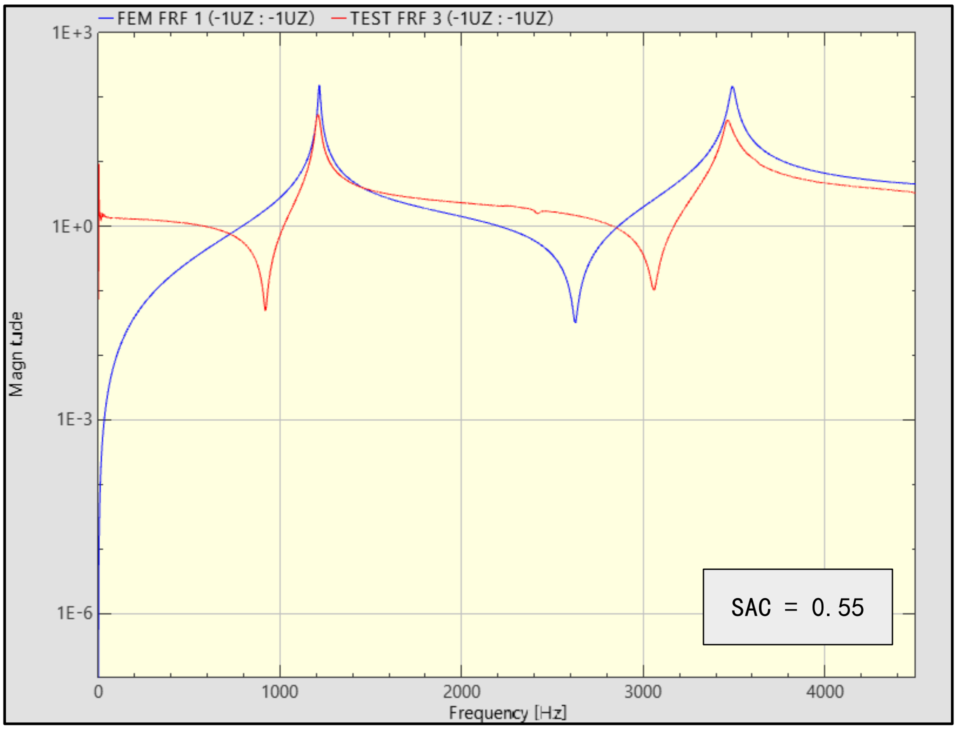

(b)

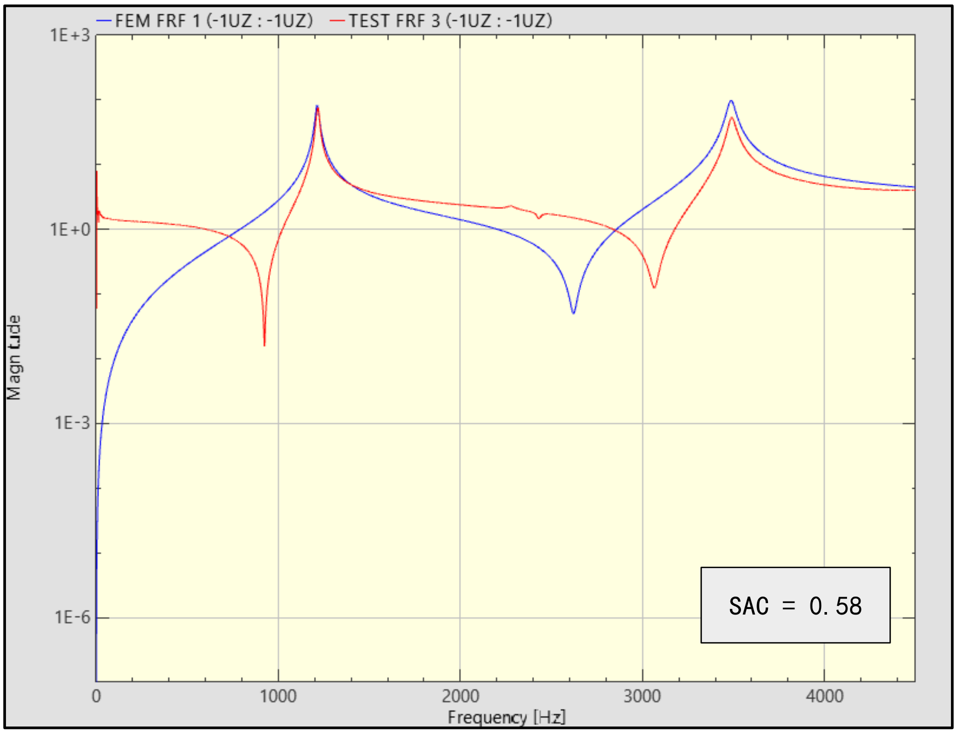

(c)

Figure 4.10 FRF Comparison Between EMA and the Modal-Updating-Based FE Model With EMA-Based Damping for the Steel Dog-Bone for (a) Specimen 1, (b) Specimen 2, and (c) Specimen 3

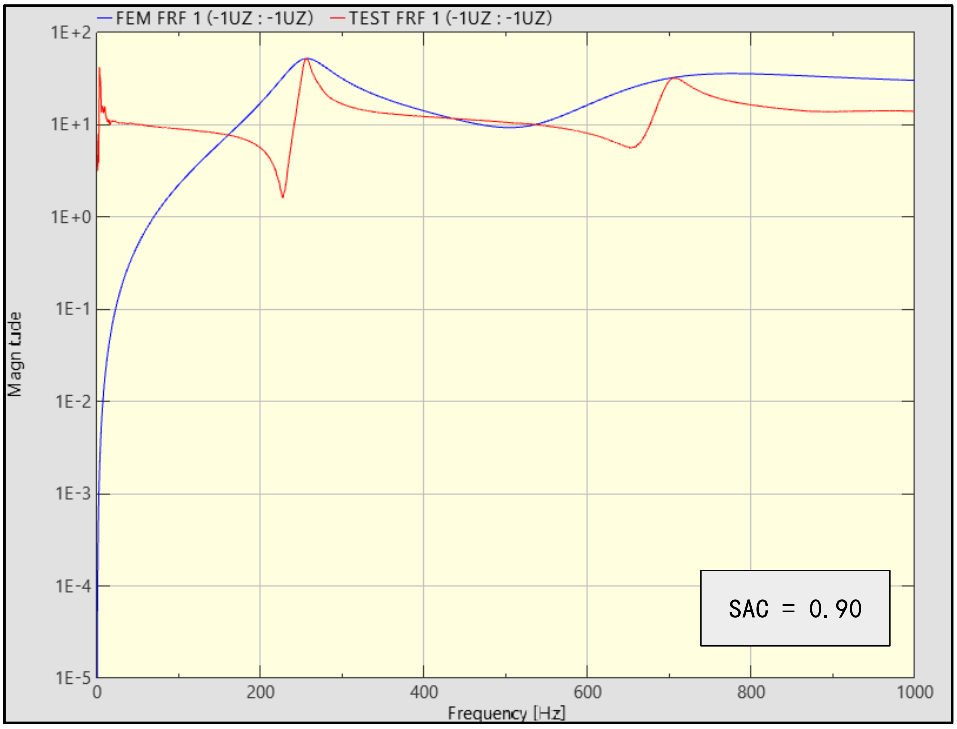

FEM FRF 1 (-1UZ : -1UZ)
TEST FRF 1 (-1UZ : -1UZ)
1E+2
1E+1
1E+0
1E-1
1E-2
1E-3
1E-4
1E-5
Magnitude
0
200
400
600
800
1000
Frequency [Hz]
SAC = 0.90

(a)

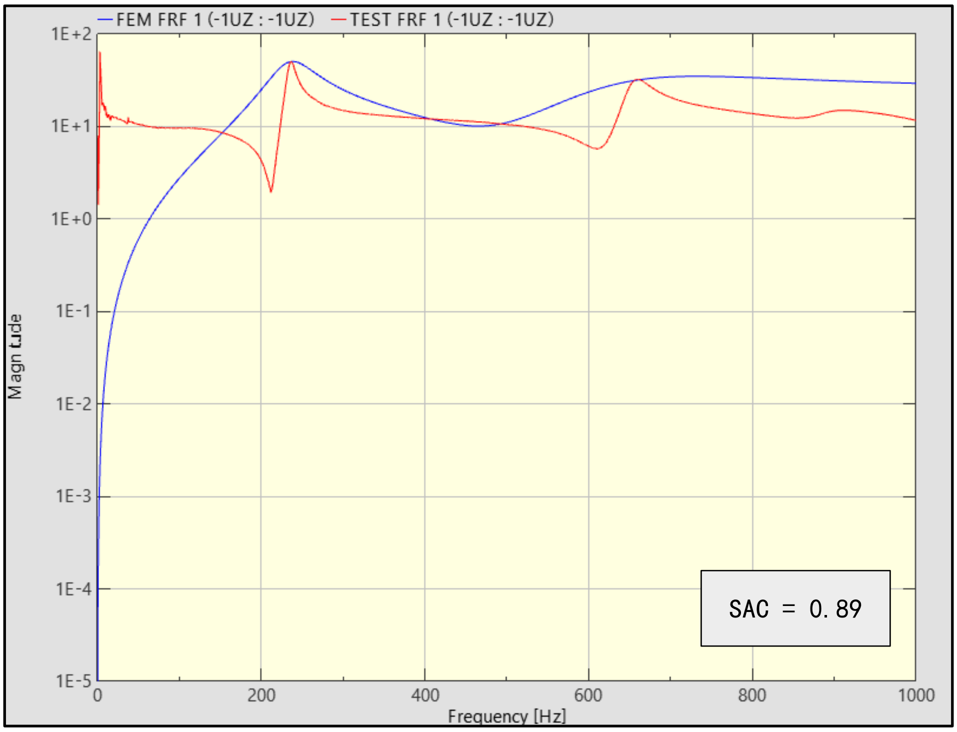

FEM FRF 1 (-1UZ : -1UZ)
TEST FRF 1 (-1UZ : -1UZ)
1E+2
1E+1
1E+0
1E-1
1E-2
1E-3
1E-4
1E-5
Magnitude
0
200
400
600
800
1000
Frequency [Hz]
SAC = 0.89

(b)

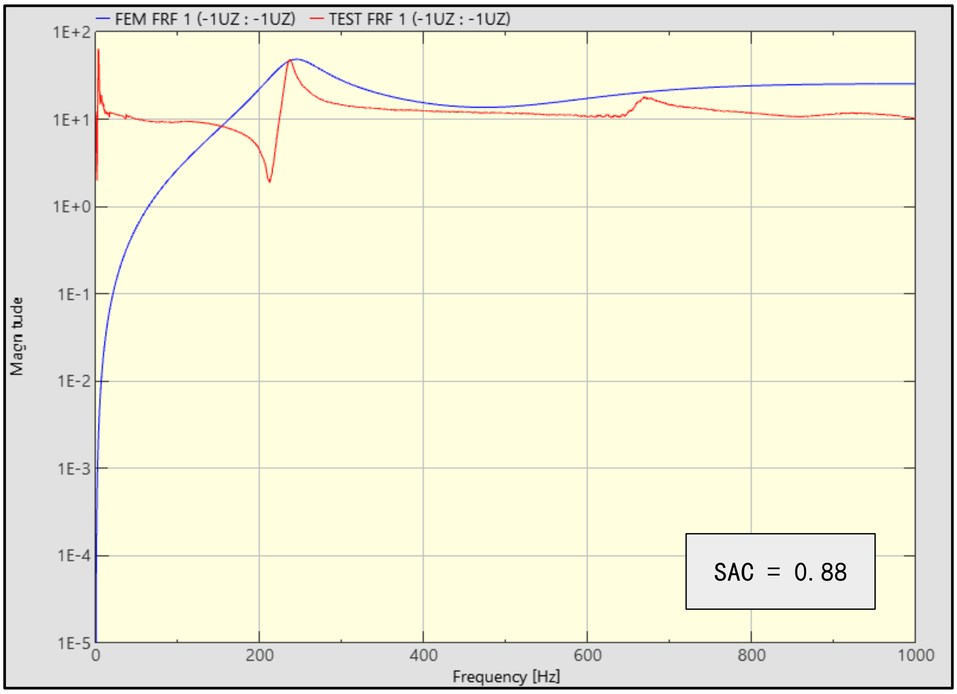

(c)

Figure 4.11 FRF Comparison Between EMA and the Updated FE Model for the Tobacco Composite Strip for (a) Specimen 1, (b) Specimen 2, and (c) Specimen 3

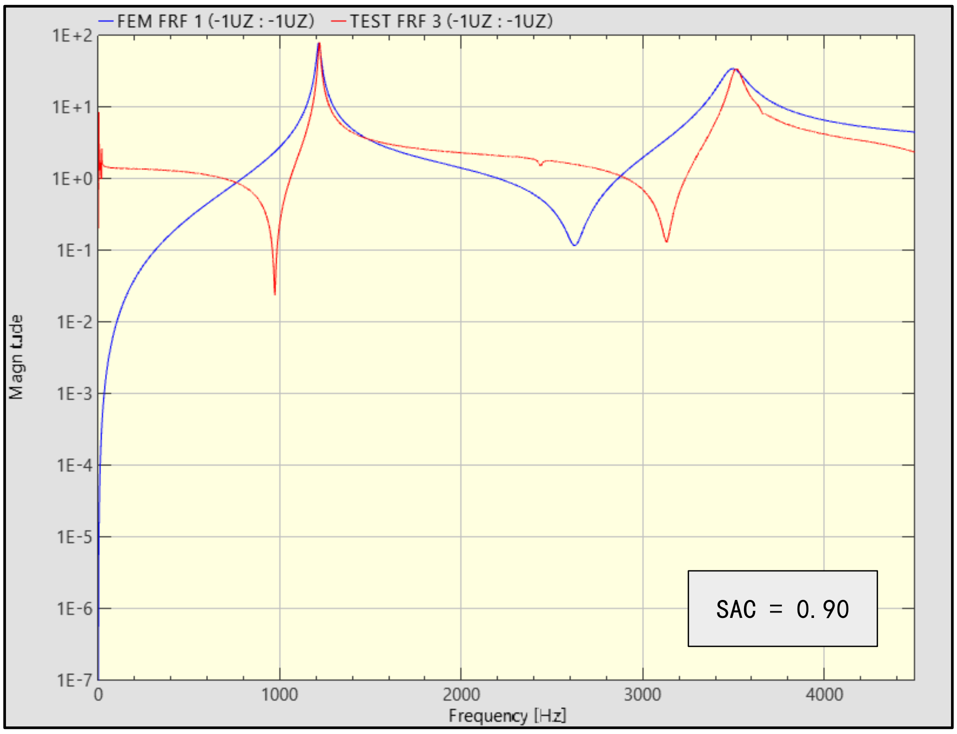

(a)

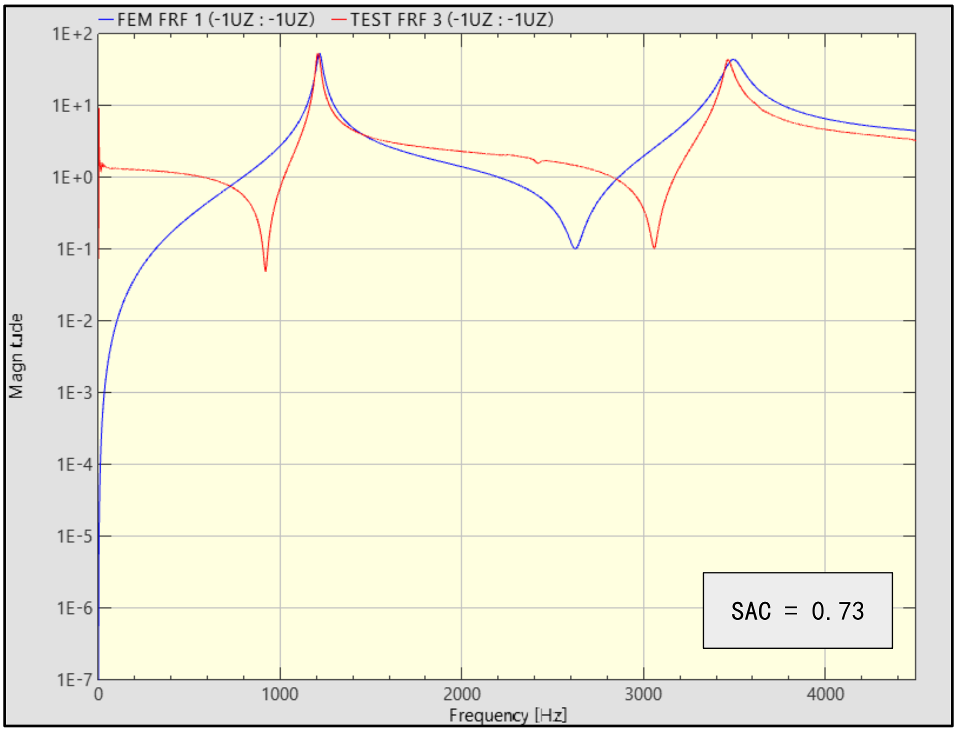

(b)

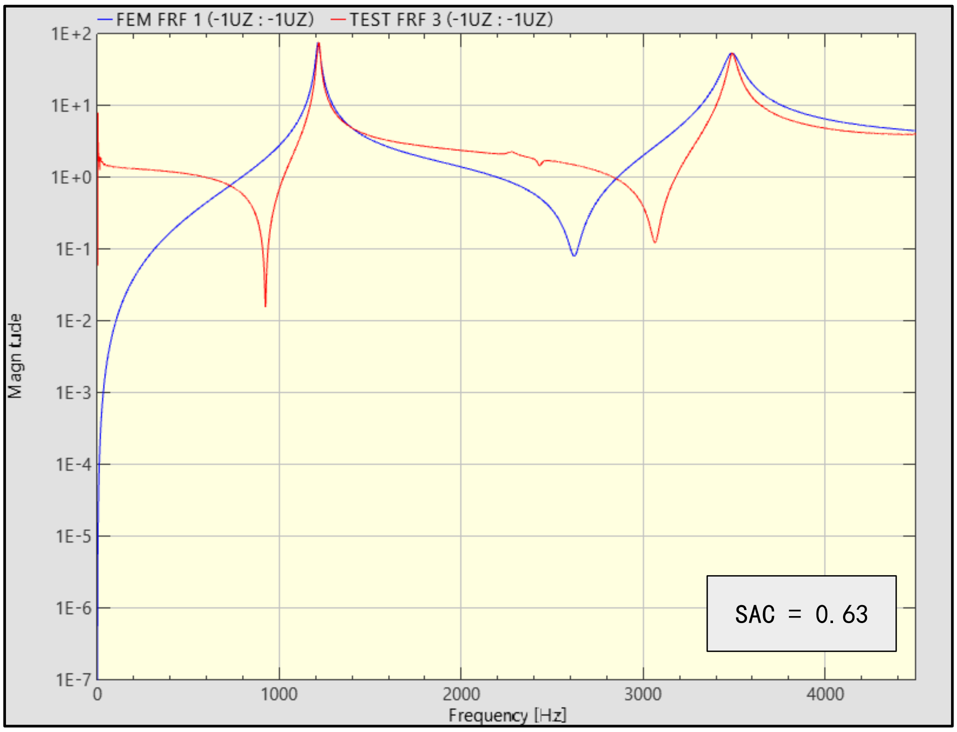

(c)

Figure 4.12 FRF Comparison Between EMA and the Updated FE Model for the Steel Dog-Bone for (a) Specimen 1, (b) Specimen 2, and (c) Specimen 3

Table 4.12
EMA and Modal-Updating-Based FE Natural Frequencies, EMA-Based Damping, Frequency Errors and SAC for the Tobacco Composite Strip

No. of Specimen	Mode	EMA (Hz)	Modal-Updating-Based FE (Hz)	EMA-Based Damping	Error (%)	SAC
1	1	254.637	254.781	0.022	0.06	0.65
	2	700.848	700.430	0.026	0.06	
2	1	235.029	236.261	0.022	0.52	0.60
	2	653.210	649.807	0.025	0.52	
3	1	241.897	241.893	0.016	0.00	0.51
	2	665.950	665.107	0.025	0.13	

Table 4.13
EMA and Modal-Updating-Based FE Natural Frequencies, EMA-Based Damping, Frequency Errors and SAC for Steel Dog-Bone

No. of Specimen	Mode	EMA (Hz)	Modal-Updating-Based FE (Hz)	EMA-Based Damping	Error (%)	SAC
1	1	1217.132	1214.860	0.005	0.19	0.72
	2	3485.558	3492.070	0.005	0.19	
2	1	1212.258	1216.260	0.004	0.33	0.55
	2	3502.897	3491.450	0.004	0.33	
3	1	1214.842	1213.560	0.008	0.11	0.58
	2	3482.420	3486.090	0.006	0.11	

Table 4.14
EMA and Updated FE Natural Frequencies, EMA-Based and Updated Modal Damping, Frequency Errors and SAC for the Tobacco Composite Strip

No. of Specimen	Mode	EMA (Hz)	Updated FE (Hz)	EMA-Based Damping	Updated Modal Damping	Error (%)	SAC
1	1	254.637	254.781	0.022	0.107	0.06	0.90
	2	700.848	700.430	0.026	0.196	0.06	
2	1	235.029	236.261	0.022	0.115	0.52	0.89
	2	653.210	649.807	0.025	0.214	0.52	
3	1	241.897	241.893	0.016	0.123	0.00	0.88
	2	665.950	665.107	0.025	0.425	0.13	

Table 4.15
EMA and Updated FE Natural Frequencies, EMA-Based and Updated Modal Damping, Frequency Errors and SAC for Steel Dog-Bone

No. of Specimen	Mode	EMA (Hz)	Updated FE (Hz)	EMA-Based Damping	Updated Modal Damping	Error (%)	SAC
1	1	1217.132	1214.860	0.005	0.008	0.19	0.90
	2	3485.558	3492.070	0.005	0.018	0.19	
2	1	1212.258	1216.260	0.004	0.012	0.33	0.73
	2	3502.897	3491.450	0.004	0.014	0.33	
3	1	1214.842	1213.560	0.008	0.008	0.11	0.63
	2	3482.420	3486.090	0.006	0.115	0.11	

Table 4.16
Mean and Standard Deviation (SD) of EMA-Based and Updated Modal Damping Ratios Across Specimens

Specimen Type	**Mode**	**EMA-Based Damping Mean**	**EMA-Based Damping SD**	**Updated Damping Mean**	**Updated Damping SD**
Tobacco Composite Strip	1	0.020	0.003	0.115	0.008
	2	0.025	0.001	0.278	0.120
Steel Dog-Bone	1	0.006	0.002	0.009	0.002
	2	0.005	0.001	0.049	0.055

4.6 Concluding Remarks

This chapter presented the results of EMA, FE modelling, correlation, and FE model updating for the tobacco composite strip and the steel dog-bone specimen to support development of a damping updating scheme for TCP. EMA results established the experimental reference FRFs and modal parameters used consistently throughout the correlation and updating stages. Baseline correlation showed that the initial FE model did not reproduce the measured response with sufficiently low error, thereby justifying further refinement of stiffness and damping representation. The use of a uniform initial damping ratio of 0.01 was shown to be a physically justified and neutral starting assumption that does not compromise the stiffness updating process, which relies solely on modal frequency and mode shape targets.

The tensile-test-based FE model provided a quasi-static stiffness comparison route, but it did not eliminate mismatch in dynamic response. The substantially lower steel modulus values obtained from tensile testing were explained as a consequence of crosshead displacement-based strain measurement, which captures system-level compliance rather than true gauge strain, and the established steel modulus of 210 GPa was retained for dynamic FE modelling. The orthotropic material assumption for TCP was justified on the basis that the first two bending modes are governed by in-plane elastic moduli E1 and E2, and the MAT8 formulation provides a defensible effective continuum representation at the structural scale.

CHAPTER 5
CONCLUSION

5.1 Introduction

This chapter summarises the main research findings and conclusions of this study based on the results presented in Chapters 3 and 4. The conclusions are organised directly according to the three research objectives so that the attainment of each objective is demonstrated through quantitative evidence drawn from the experimental and numerical results. The chapter also highlights the main findings that support the formulated damping updating scheme for TCP, with verification using the steel dog-bone specimen. Finally, recommendations for future work are provided to strengthen damping representation, improve the efficiency of FRF-based updating, and extend the framework toward stochastic modelling approaches that account for the natural variability of bio-based composite materials.

5.2 Conclusions

This study achieved its aim of developing and validating a systematic staged FE model updating framework for TCP by formulating a four-stage updating sequence comprising the initial FE model, the tensile-test-based FE model, the modal-updating-based FE model, and the final updated FE model. The framework explicitly separates stiffness-related parameter updating from modal damping calibration, with EMA measurements serving as the experimental reference throughout all stages. The decoupling of stiffness and damping updating is the central methodological contribution of this study, as it prevents physically unwarranted stiffness corrections from being used to compensate for damping-related peak mismatch. This separation maintains the physical traceability of each correction step and provides a structured basis for interpreting the source of FRF mismatch at each stage.

The use of an initial uniform modal damping ratio of 0.01 was shown to be a physically justified and neutral starting assumption that does not compromise the stiffness updating process, which relies exclusively on modal frequency and mode shape targets. The orthotropic material assumption for TCP using MAT8 with E1 and

E2 as the primary updating parameters was justified on the basis that the first two bending modes are governed by in-plane bending stiffness. This representation provides a defensible effective continuum model at the structural scale, consistent with standard practice in FE-EMA correlation studies for composite materials.

In the stiffness calibration stage, the modal-updating-based FE model achieved natural frequency errors below 0.52% for all TCP specimens and below 0.33% for all steel specimens, meeting the target of below 1% for both specimen types. Prior to stiffness calibration, the tensile-test-based FE model produced frequency errors of 7.84% to 12.01% for TCP and 83.67% to 84.65% for steel, demonstrating that quasi-static stiffness input alone is insufficient for dynamic prediction. The substantially lower steel modulus values from tensile testing were attributed to system-level compliance captured through crosshead displacement rather than true gauge strain, and the established value of 210 GPa was retained for dynamic FE modelling.

In the damping calibration stage, direct assignment of EMA-measured modal damping ratios improved SAC values to 0.51 to 0.65 for TCP and 0.55 to 0.72 for steel, confirming the benefit of measured damping over the initial uniform assumption. Subsequent damping refinement in FEMTools further improved SAC values for TCP to 0.88, 0.89, and 0.90 for Specimens 1 to 3, representing a substantial improvement from the baseline values of 0.24, 0.26, and 0.32. For the steel dog-bone, EMA-based damping assignment alone was sufficient to achieve an SAC of 0.90 for Specimen 1, confirming that the two-step damping approach correctly identifies when further refinement is required.

Validation was carried out through systematic comparison of all four FE model stages against EMA using natural frequency error, MAC, and SAC as consistent correlation metrics. The mean SAC improved from 0.27 at the initial FE model stage to 0.89 at the final updated FE model stage for TCP, and from 0.61 to 0.75 for steel, demonstrating measurable and traceable improvement at each step. MAC values for the first bending mode of TCP were consistently above 0.90 for two of three specimens and above 0.67 for all specimens, supporting the reliability of mode pairing throughout the updating stages.

The updated modal damping ratios for TCP, with Mode 1 values of 0.107 to 0.123 and Mode 2 values of 0.196 to 0.425 across the three specimens, confirm that TCP exhibits substantially higher and more variable damping than steel. The inter-specimen standard deviation of the updated damping ratio for TCP Mode 2 was 0.120, compared with 0.055 for steel Mode 2, quantitatively confirming the higher damping variability of bio-based composites. The elevated updated damping ratio of 0.425 for Tobacco Specimen 3 Mode 2 was shown to be physically consistent with the viscoelastic energy dissipation characteristics of TCP and is not a modelling artefact.

Overall, the results confirm that the updated FE model provides the best agreement with EMA after stiffness alignment and damping refinement are completed in the correct sequence. The study demonstrates that a damping-focused staged updating strategy is necessary for TCP because damping is the dominant contributor to FRF peak mismatch once resonance frequencies are aligned. The workflow developed in this study provides a traceable and reproducible approach to improving dynamic prediction reliability for composite structures where damping variability is significant.

5.3 Main Findings of This Study

The following list summarises the main findings of this study in direct correspondence with the research objectives and research questions:

1. A systematic staged FE model updating framework that explicitly decouples stiffness-related parameter updating from modal damping calibration was successfully developed and demonstrated for TCP, using EMA as the experimental reference throughout all stages.
2. The initial FE model exhibited significant mismatch with EMA in resonance location and resonance peak behaviour, with natural frequency errors of 2.96% to 5.83% and SAC values of 0.24 to 0.32 for TCP, confirming that baseline stiffness representation and assumed damping were insufficient for accurate FRF prediction.
3. The tensile-test-based FE model demonstrated that quasi-static stiffness alone does not ensure accurate dynamic prediction, as frequency errors worsened to 7.84% to 12.01% for TCP and 83.67% to 84.65% for steel when tensile-derived moduli were assigned. The large steel discrepancy was attributed to system-level compliance captured through crosshead displacement rather than true gauge strain.
4. The modal-updating-based FE model achieved natural frequency errors below 0.52% for TCP and below 0.33% for steel, meeting the target of below 1% and

establishing a stable base for isolating damping-related effects on FRF peak characteristics.

5. Direct assignment of EMA modal damping ratios improved SAC values from 0.34 to 0.46 at the modal-updating-based stage to 0.51 to 0.65 for TCP and 0.55 to 0.72 for steel, demonstrating that measured damping provides meaningful improvement but is not always sufficient to reproduce FRF peak behaviour for highly damped TCP specimens.
6. The tobacco composite strip required additional damping updating beyond EMA damping insertion to accurately reproduce resonance peak amplitude and bandwidth, with final SAC values of 0.88 to 0.90 achieved after FEMTools damping refinement, validating the necessity of the two-step damping calibration approach for TCP.
7. The elevated updated damping ratio of 0.425 for Tobacco Specimen 3 Mode 2 was shown to be physically consistent with the high and variable energy dissipation characteristics of TCP arising from non-uniform fibre-matrix distribution and viscoelastic mechanisms at the fibre-matrix interface.
8. The inter-specimen standard deviation of updated damping ratios for TCP Mode 2 was 0.120, compared with 0.055 for steel Mode 2, quantitatively confirming that TCP exhibits substantially higher damping variability than isotropic metallic structures and highlighting the importance of specimen-specific damping calibration for bio-based composites.

5.4 Recommendations for Future Work

Although this study has successfully developed and validated a staged damping updating scheme for TCP using EMA as the reference, several improvements and extensions can be pursued in future work:

1. Extension to Stochastic Modelling for Bio-Based Composite Variability
   The deterministic updating framework developed in this study identifies a single set of effective stiffness and damping parameters for each specimen. Future work should extend this framework toward stochastic or probabilistic modelling approaches that explicitly account for the natural variability in fibre distribution, fibre content, and fibre-matrix adhesion quality inherent to bio-based

composites such as TCP. A stochastic FE model updating formulation, in which E1, E2, and modal damping ratios are treated as random variables with distributions characterised from multi-specimen EMA data, would enable the prediction of FRF response bounds rather than single deterministic predictions. This extension would more faithfully represent the physical behaviour of TCP in engineering applications where specimen-to-specimen variability is a design consideration.

2. Extension to Higher Modes and Wider Frequency Range
   Future work should extend the updating process to higher modes and a wider frequency band to test whether stiffness and damping updates remain stable when modal density increases. The current study is limited to the first two bending modes, and the validity of the identified effective orthotropic properties and damping ratios at higher modes has not been assessed.
3. Evaluation of Alternative Damping Models
   Future studies should involve comparison of different damping representations such as mode-dependent damping, proportional Rayleigh damping, and frequency-dependent viscoelastic damping models to identify the formulation that provides the best balance of accuracy, physical interpretability, and computational efficiency for TCP. The high and mode-dependent damping ratios identified in this study suggest that proportional damping assumptions are particularly unsuitable for TCP and that mode-specific or frequency-dependent representations may be more appropriate.
4. Improved Characterisation of TCP Variability
   Future work should increase specimen count beyond three per material type and incorporate measurable fabrication descriptors such as fibre volume fraction, fibre orientation distribution, and resin content measurements so that specimen-to-specimen damping scatter can be systematically related to microstructural parameters rather than treated as unexplained variability.
5. Sensitivity to Boundary Condition and Suspension Variation
   Future studies should determine the sensitivity of the identified damping ratios to small changes in suspension configuration and test setup, particularly because damping in TCP is extracted from FRF peak behaviour which is sensitive to boundary condition influence. This is especially important when the framework is applied outside the laboratory setting.

6. Application to More Complex TCP Structures

   Future work should apply the framework to TCP panels or TCP components with more realistic boundary conditions and geometry, allowing the staged damping updating scheme to be evaluated under conditions closer to practical engineering use and assessing how microstructural variability propagates to structural-scale FRF behaviour.

7. Machine Learning for Faster Model Updating

   Future work can investigate the use of machine learning to accelerate the damping updating iteration by learning the mapping between FE model parameters and EMA targets such as natural frequencies, MAC, and FRF peak features from the dataset generated in this study. A trained surrogate model could reduce the number of FEMTools iterations required for each specimen, which is particularly beneficial for damping updating where the sensitivity of FRF peak behaviour to damping changes can require many repeated evaluations.

5.5 Concluding Remarks

Accurate damping representation is essential for reproducing the FRF resonance peak behaviour of TCP when FE predictions are validated against EMA results. This study provided a structured and systematic FE-EMA correlation and damping updating framework that increases confidence in vibration prediction for TCP, particularly when FRF peak behaviour is the primary validation objective. The results demonstrated that resonance frequency agreement must be achieved first before peak amplitude and bandwidth can be fairly evaluated, because damping governs peak shape once resonance frequencies are already aligned. For steel, assigning EMA-based modal damping was generally sufficient to achieve acceptable FRF peak agreement, while TCP required additional damping updating to obtain the best match due to its stronger and more variable energy dissipation behaviour. The staged framework, with its explicit decoupling of stiffness alignment and damping calibration, provides a reproducible and physically defensible route for FRF-based FE model updating of bio-based composite structures and establishes a clear foundation for future extensions toward stochastic and higher-fidelity dynamic modelling approaches.

REFERENCES

Abdullah, N. A. Z., Sani, M. S. M., Rahman, M. M., & Zaman, I. (2017). Correlation of numerical and experimental analysis for dynamic behaviour of a body-in-white (BIW) structure. *MATEC Web of Conferences*, *90*, 01020.

Aggarwal, P. K. (2010). Dynamic (Vibration) Testing: Design Certification of Aerospace System. In *Encyclopedia of Aerospace Engineering*. Wiley.

Aleyaasin, M. (2025). Comparing the Accuracy and Sensitivity of Mesh-Free and Finite Element Methods in Vibration Analysis. *Dynamics*, *5*(2), 13.

Alkhatib, A. J. (2023). *Response of Thin-Walled Composite Polymer Structures Fabricated via Additive Manufacturing Technologies* (pp. 41–58).

Allemang, R. J., Patwardhan, R. S., Kolluri, M. M., & Phillips, A. W. (2022). Frequency response function estimation techniques and the corresponding coherence functions: A review and update. *Mechanical Systems and Signal Processing*, *162*, 108100.

Altun, B., Çalışkan, H., & Özşahin, O. (2023). Position-dependent FRF identification without force measurement in milling process. *The International Journal of Advanced Manufacturing Technology*, *128*(11–12), 4981–4996.

Ammar, M. M., Mohamed, M. I., Mahmoud, G. M., Hassan, S. R., Kumme, R., Zakaria, H. M., & Gaafer, A. M. (2022). A comparison between static and dynamic stiffness of force transducers for dynamic force calibrations. *Measurement*, *203*, 111945.

Ardani, A., Soltani, P., Taban, E., Selicati, V., & Berardi, U. (2026). Bio-composite Panels from upcycling cigarette butts: Acoustic and thermal characterization. *Sustainable Materials and Technologies*, *47*(9), e01867. https://doi.org/10.1038/s41569-021-00532-5

Arora, V., Adhikari, S., & Vijayan, K. (2023). FRF-based finite element model updating for non-viscous and non-proportionally damped systems. *Journal of Sound and Vibration*, *552*, 117639.

Arora, V., Singh, S. P., & Kundra, T. K. (2009a). Comparative study of damped FE model updating methods. *Mechanical Systems and Signal Processing*, *23*(7), 2113–2129.

Arora, V., Singh, S. P., & Kundra, T. K. (2009b). Finite element model updating with damping identification. *Journal of Sound and Vibration*, *324*(3–5), 1111–1123.

Azhar, A. S., Abdul Kudus, S., Jamadin, A., & Mustaffa, N. K. (2023). Comparison of

Modal Parameters of a Square Steel Plate Using Finite Element Method and Operational Modal Analysis. *International Journal of Integrated Engineering*, *15*(2).

Ballard, M. K., & Whitcomb, J. D. (2019). Effect of heterogeneity at the fiber–matrix scale on predicted free-edge stresses for a [0°/90°]s laminated composite subjected to uniaxial tension. *Journal of Composite Materials*, *53*(5), 625–639.

Banwell, G., Mohr, S., Rothberg, S., & Roberts, J. (2012). Using experimental modal analysis to validate a finite element model of a tennis racket. *Procedia Engineering*, *34*, 688–693.

Barazzutti, L. F., Gomes, H. M., & Drehmer, L. R. C. (2024). Sensitivity-Based Model Update for Estimating Generalized Proportional Damping Parameters in a Finite-Element Model. *ASCE-ASME Journal of Risk and Uncertainty in Engineering Systems, Part A: Civil Engineering*, *10*(2).

Berriet, R., & Link, M. (1994). *Updating of Modal Damping, Physical Stiffness and Mass Parameters from Measured Frequency Response Functions*.

Bhattacharjee, A., & Roy, H. (2020). Assessment of tensile and damping behaviour of hybrid particle/woven fibre/polymer composites. *Composite Structures*, *244*, 112231.

Bondsman, B., & Peplow, A. (2025). Experimental Modal Analysis and variability assessment in Cross-laminated Timber. *Mechanical Systems and Signal Processing*, *228*, 112466.

Brandt, A., Berardengo, M., Manzoni, S., & Cigada, A. (2017). Scaling of mode shapes from operational modal analysis using harmonic forces. *Journal of Sound and Vibration*, *407*, 128–143.

Brown, D. L., Allemang, R. J., & Phillips, A. W. (2025). Forty Years of Use and Abuse of Impact Testing: A Practical Guide to Making Good FRF Measurements. In *Experimental Techniques, Rotating Machinery, and Acoustics, Volume 8* (pp. 221–241). River Publishers.

Butaud, P., Maynadier, A., Brault, N., Placet, V., Ouisse, M., Foltête, E., & Rogueda-Berriet, C. (2013). Static and dynamic thermo mechanical characterization of a bio-compatible Shape Memory Polymer. *ICAST 2013, The 24th International Conference on Adaptive Structures Technologies*, 1–10.

Cai, F., Jo, S.-H., Ma, Y., Guo, H., Xu, Y., Xu, W., & Li, F. (2022). Effect of Four Groups of GO-CF/EP Composites with Ideal Infiltration Structure and Different

Layering Ways on Damping Properties. *Polymers*, *14*(12).

Castro, B. M., Monteiro, U. A., Gutiérrez, R. H. R., & Vaz, L. A. (2022). A framework for numerical and experimental correlation of mode shapes with low spatial resolution: a catamaran's case study. *Journal of the Brazilian Society of Mechanical Sciences and Engineering*, *44*(9), 418.

Charoensuk, K., & Sethaput, T. (2023). The Vibration Analysis Based on Experimental and Finite Element Modeling for Investigating the Effect of a Multi-Notch Location of a Steel Plate. *Applied Sciences*, *13*(21), 12073.

Chu, T., Nguyen, T., Yoo, H., & Wang, J. (2024). A review of vibration analysis and its applications. *Heliyon*, *10*(5), e26282.

Ciura, Ł., Wróbel, J., Boguski, J., & Wróbel, J. (2023). Investigation of 1/f noise sources with the coherence function. *Measurement*, *214*, 112772.

Deng, C., Wen, J., Tang, L., Cai, X., & Peng, F. (2024). The Accuracy of Frequency Estimation of Structure Vibration under Ambient Excitation: Problems, Causes, and Methods. *Buildings*, *14*(1), 198.

Dharmajan, N. B., & AlHamaydeh, M. (2025). State-of-the-Art Review of Structural Vibration Control: Overview and Research Gaps. *Applied Sciences*, *15*(14), 7966.

DICKENS, J. D. (2000). Dynamic Model of Vibration Isolator Under Static Load. *Journal of Sound and Vibration*, *236*(2), 323–337.

Du, Z., Lu, J., Sun, T., Liu, F., Wang, Y., He, W., Chen, A., & Zhu, L. (2025). A method for identifying inertia properties of vibration structure from experimental frequency response functions. *Measurement*, *256*, 118321.

Ebrahimi, F., & Ahari, M. F. (2024). Mechanics of Active Materials. *Comprehensive Mechanics of Materials, Volume 1-4*, *4*, V4-234-V4-268.

Ereiz, S., Duvnjak, I., & Fernando Jiménez-Alonso, J. (2022). Review of finite element model updating methods for structural applications. *Structures*, *41*, 684–723.

Ewins, D. J. (2000). *Modal Testing: Theory, Practice and Application* (2nd ed.). Research Studies Press Ltd.

Fahlovi, O., Kurnia, G., & Setyawan, H. (2024). Recent Developments in Vibration Analysis: An Innovative Way to Improve Machine Reliability. *International Journal of Mechanics, Energy Engineering and Applied Science (IJMEAS)*, *2*(3), 66–71.

Fazlali, B., Breite, C., Czél, G., Fiedler, B., Gibhardt, D., Hojo, M., Koerber, H., Kumar, R., Velasco, M. L., McEnteggart, I., Mikkelsen, L. P., Paris, F., Taketa, I., Wisnom, M. R., & Swolfs, Y. (2025). Round-robin programme for longitudinal tensile testing of unidirectional composites: results, conclusions, and recommendations. *Polymer Testing*, *152*, 108974.

Fazlali, B., Upadhyay, S., Ashokbhai Ashodia, S., Mesquita, F., Lomov, S. V., Carvelli, V., & Swolfs, Y. (2023). Specimen designs for accurate tensile testing of unidirectional composite laminates. *Composites Part A: Applied Science and Manufacturing*, *175*, 107799.

Flauder, S., Langhof, N., & Schafföner, S. (2025). The role of alignment for valid tensile testing of ceramic matrix composites. *Journal of the European Ceramic Society*, *45*(3), 117001.

Freddi, M., Pagliari, C., & Frizziero, L. (2025). Parametric Sensitivity Analysis of Suspension Design Using Response Surface Techniques. *Applied Sciences*, *15*(22), 11887.

Friswell, M. I., Inman, D. J., & Pilkey, D. F. (1998). Direct Updating of Damping and Stiffness Matrices. *AIAA Journal*, *36*(3), 491–493.

Gabbert, U., Zehn, M., & Wahl, F. (1995). *Improved results in structural dynamic calculations by linking finite element analysis (FEA) and experimental modal analysis (EMA)*. *84*.

Gazdagh, Z., & Vehovszky, B. (2021). Influence of frequency resolution in case of frequency response function measurement in structural dynamics. *Acta Technica Jaurinensis*, *14*(4), 508–520.

Giani, P., & Locarno, S. (2025). Tensile testing of polymeric materials: a model-based approach to estimate the material strength without position sensor. *Journal of Physics D: Applied Physics*, *58*(7), 075301.

Gibson, R. (2000). Modal vibration response measurements for characterization of composite materials and structures. *Composites Science and Technology*, *60*(15), 2769–2780.

Goharian, A. (2017). Biomechanics of plating fixation. *Trauma Plating Systems: Biomechanical, Material, Biological, and Clinical Aspects*, 89–112.

González, A., OBrien, E. J., & McGetrick, P. J. (2012). Identification of damping in a bridge using a moving instrumented vehicle. *Journal of Sound and Vibration*, *331*(18), 4115–4131.

Gülbahçe, E., & Çelik, M. (2022). Experimental modal analysis for the plate structures with roving inertial shaker method approach. *Journal of Low Frequency Noise,* *Vibration and Active Control*, *41*(1), 27–40.

Haris, N. I. N., Hassan, M. Z., Ilyas, R. A., Suhot, M. A., Sapuan, S. M., Dolah, R., Mohammad, R., & Asyraf, M. R. M. (2022). Dynamic mechanical properties of natural fiber reinforced hybrid polymer composites: a review. *Journal of Materials Research and Technology*, *19*, 167–182.

Hassan, M. H., & Ramle, M. S. (2018). *A Review of Experimental Modal Analysis and Finite Element Analysis*.

Huang, F.-L., Wang, X.-M., Chen, Z.-Q., He, X.-H., & Ni, Y.-Q. (2007). A new approach to identification of structural damping ratios. *Journal of Sound and Vibration*, *303*(1–2), 144–153.

Huang, J., Li, X., Zhang, J., Sun, Y., & Ren, J. (2022). Determining the Rayleigh damping parameters of flexible pavements for finite element modeling. *Journal of Vibration and Control*, *28*(21–22), 3181–3194.

Huňady, R., Lengvarský, P., Pavelka, P., Kaľavský, A., & Mlotek, J. (2021). Stiffness Estimation and Equivalence of Boundary Conditions in FEM Models. *Applied Sciences*, *11*(4), 1482.

Ichiki, A., & Tadokoro, Y. (2013). Signal-to-noise ratio improvement by stochastic resonance in moments in non-dynamical systems with multiple states. *Physics Letters A*, *377*(3–4), 185–188.

International, A. (2008). *ASTM D3039/3039M-Standard test method for tensile properties of polymer matrix composite materials*.

Janeliukstis, R., & Mironovs, D. (2021). Smart Composite Structures with Embedded Sensors for Load and Damage Monitoring – A Review. *Mechanics of Composite Materials*, *57*(2), 131–152.

Jeannin, T., Arnold, G., Bourmaud, A., Corn, S., De Luycker, E., Dumont, P. J. J., Ferreira, M., François, C., Grégoire, M., Harzallah, O., Heurtel, J., Joannès, S., Kervoelen, A., Labanieh, A. R., Le Moigne, N., Martoïa, F., Orgéas, L., Ouagne, P., Soulat, D., … Placet, V. (2024). A round-robin study on the tensile characterization of single fibres: A multifactorial analysis and recommendations for more reliable results. *Composites Part A: Applied Science and Manufacturing*, *185*, 108323.

Jiang, D., Huang, Z., Wang, G., Wang, Y., Zhu, R., & Hang, X. (2024). Reducing effects of boundary condition in modal testing of flexible structures. *Journal of Mechanical Science and Technology*, *38*(1), 89–99.

Jiang, X., & Jiang, F. (2020). Optimal strain sensors placement to analyze the modal parameters of the sorting arm. *Journal of Vibroengineering*, *22*(1), 145–155.

Jwo, D.-J., Wu, I.-H., & Chang, Y. (2019). Windowing Design and Performance Assessment for Mitigation of Spectrum Leakage. *E3S Web of Conferences*, *94*, 03001.

Kalusuraman, G., Kumaran, S. T., Balamurugan, K., Sivashanmugam, N., Sivaprakasam, P., Kurniawan, R., & Ezhilmaran, V. (2023). Vibration Studies on Fiber Reinforced Composites – a Review. *Journal of Natural Fibers*, *20*(1).

Kamei, K., & Khan, M. A. (2021). Current challenges in modelling vibrational fatigue and fracture of structures: a review. *Journal of the Brazilian Society of Mechanical Sciences and Engineering*, *43*(2), 77.

Karaağaçlı, T., & Çelik, F. K. (2024). Modal analysis of non-conservative systems with friction-induced strong nonlinear damping by using response-controlled testing. *Mechanical Systems and Signal Processing*, *221*, 111718. https://doi.org/10.1016/J.YMSSP.2024.111718

Kharchenko, S., Samborski, S., Kharchenko, F., Mitura, A., Paśnik, J., & Korzec, I. (2023). Identification of the Natural Frequencies of Oscillations of Perforated Vibrosurfaces with Holes of Complex Geometry. *Materials*, *16*(17), 5735.

Khoo, S. Y., Lian, Y. C., Ong, Z. C., Ismail, Z., & Noroozi, S. (2020). Feasibility study of performing experimental modal analysis with oblique impact testing using various oblique impact directions. *Alexandria Engineering Journal*, *59*(1), 457–473.

Ko, D.-H., & Boo, S.-H. (2022). Efficient Structural Dynamic Analysis Using Condensed Finite Element Matrices and Its Application to a Stiffened Plate. *Journal of Marine Science and Engineering*, *10*(12), 1958.

Kostic, S., Miljojkovic, J., Simunovic, G., Vukelic, D., & Tadic, B. (2022). Uncertainty in the determination of elastic modulus by tensile testing. *Engineering Science and Technology, an International Journal*, *25*, 100998.

Kowalski, S. (2025). Analysis of Automotive Suspension System Failures and Reliability Evaluation: A Study Based on V-SIM Simulation. *Applied Sciences*, *15*(2), 805.

Kranjc, T., Slavič, J., & Boltežar, M. (2013). The mass normalization of the displacement and strain mode shapes in a strain experimental modal analysis using the mass-change strategy. *Journal of Sound and Vibration*, *332*(26), 6968–6981.

Kumar, J., Panchore, V., Rajak, D. K., & Joshi, T. (2025). Dynamic Properties and Vibration Response of Polymer Matrix Composites: Mechanisms, Influences, and Applications in Engineering. *Polymers for Advanced Technologies*, *36*(1).

Kumar, P., Singh, S. P., & Sharma, S. (2023). *Damping in fiber reinforced composite materials*. Woodhead Publishing.

Kuś, W., Mucha, W., & Jiregna, I. T. (2025). Optimization of Sensor Positions and Orientations for Multiple Load Case Scenarios. *Applied Sciences*, *15*(13), 7463.

Kwon, K.-S., & Lin, R.-M. (2004). Frequency selection method for FRF-based model updating. *Journal of Sound and Vibration*, *278*(1–2), 285–306.

Langer, P., Jelich, C., Guist, C., Peplow, A., & Marburg, S. (2021). Simplification of Complex Structural Dynamic Models: A Case Study Related to a Cantilever Beam and a Large Mass Attachment. *Applied Sciences*, *11*(12), 5428.

Lázaro, M., Perez-Aparicio, J., & Gomez-Hernandez, J. (2010). An Analytical Approach to the Computation of the Frequency Response Function. In *Civil-Comp Proceedings* (Vol. 93).

Lee, D. (2023). Updating of the complete joint characteristics of finite element model via FRF-based substructuring of complex structures. *Journal of Mechanical Science and Technology*, *37*(7), 3437–3444.

Lee, U., & Shin, J. (2002). A frequency response function-based structural damage identification method. *Computers & Structures*, *80*(2), 117–132.

Lee, Y., Kim, H., Min, S., & Yoon, H. (2023). Structural damage detection using deep learning and FE model updating techniques. *Scientific Reports*, *13*(1), 18694.

Lenticchia, E., Miraglia, G., Cusicanqui Lopez, J. A., & Ceravolo, R. (2025). Sensitivity driven model updating: a multi-step procedure for structural assessment. *Journal of Building Engineering*, *109*, 112941.

Li, J., Deng, Z., Tang, Y., Wang, S., Yang, Z., Luo, H., Feng, W., & Zhang, B. (2024). Improved Bayesian Model Updating Method for Frequency Response Function with Metrics Utilizing NHBFT-PCA. *Mathematics*, *12*(13), 2076.

Li, K., Fang, J., Sun, B., Li, Y., & Cai, G. (2022). Structural Dynamic Model Updating with Automatic Mode Identification Using Particle Swarm Optimization. *Applied Sciences*, *12*(18), 8958.

Lim, H. C., Ong, Z. C., & Brandt, A. (2018). Implementation of phase controlled impact device for enhancement of frequency response function in operational modal testing. *Journal of the Franklin Institute*, *355*(1), 291–313.

Liu, T., Butaud, P., Placet, V., & Ouisse, M. (2021). Damping behavior of plant fiber composites: A review. *Composite Structures*, *275*, 114392.

Livingston, R., & Koohbor, B. (2022). Characterizing fiber-matrix debond and fiber interaction mechanisms by full-field measurements. *Composites Part C: Open Access*, *7*, 100229.

Loi, G., Aymerich, F., & Porcu, M. C. (2022). Influence of Sensor Position and Low-Frequency Modal Shape on the Sensitivity of Vibro-Acoustic Modulation for Impact Damage Detection in Composite Materials. *Journal of Composites Science*, *6*(7), 190.

Lu, G., Zhu, T., & Xu, Y. (2021). Low Velocity Impact Energy Monitoring and Recognition of Composite Laminates with Variable Thickness Based on Optical Fiber Sensor Network. *Applied Sciences*, *11*(2), 584.

Ma, L., Liu, F., Liu, D., & Liu, Y. (2021). Review of Strain Rate Effects of Fiber-Reinforced Polymer Composites. *Polymers*, *13*(17), 2839.

Mahat, S., Sharma, R., Jeong, H., & Liu, J. (2024). Natural frequency informed finite element modal analysis method for estimating elastic properties of solid materials. *Journal of Applied Physics*, *136*(10).

Maia, N. M. M., & Silva, J. M. M. (1997). *Theoretical and Experimental Modal Analysis*. Research Studies Press Ltd.

Manring, L. H., Schultze, J. F., Zimmerman, S. J., & Mann, B. P. (2022). Improving magnitude and phase comparison metrics for frequency response functions using cross-correlation and log-frequency shifting. *Journal of Sound and Vibration*, *539*, 117255.

Mares, C., Dratz, B., Mottershead, J. E., & Friswell, M. I. (2006). Model updating using Bayesian estimation. *International Conference on Noise and Vibration Engineering, ISMA2006, Katholieke Universiteit Leuven*, 18–20.

Mat Samudin, I., Mohd Radzuan, N. A., Sulong, A. B., Ma, Q., Azman, A. H., & Wan Zamri, W. F. H. (2025). Stress strain curve analysis of sheet based TPMS structures in quasi static compression test: A review. *Journal of Materials Research and Technology*, *36*, 5757–5796.

McClintock, F. A., Callaway, A. J., Clark, C. J., & Williams, J. M. (2024). Assessing the Impact of Sensor Orientation on Accelerometer-Derived Angles: A Systematic Analysis and Proposed Error Reduction. *Applied Sciences*, *14*(2), 842.

Mesogitis, T. S., Skordos, A. A., & Long, A. C. (2014). Uncertainty in the manufacturing of fibrous thermosetting composites: A review. *Composites Part A: Applied Science and Manufacturing*, *57*, 67–75.

Michal, P., Vaško, M., Sapieta, M., Majko, J., & Fiačan, J. (2024). The Impact of Internal Structure Changes on the Damping Properties of 3D-Printed Composite Material. *Applied Sciences*, *14*(13), 5701.

Mobarhan Zad, S., Rahai, M., Ranjbar, S., & Moghadas Nejad, F. (2026). Structural damage analysis using finite element model updating enhanced by response surface methodology. *Scientific Reports*, *16*(1), 1066.

Modak, S. V. (2023). *Analytical and Experimental Modal Analysis*. CRC Press.

Moens, D., & Vandepitte, D. (2005, April 18). Frequency Response Function Analysis of Structures with Fuzzy Modal Damping Parameters. *46th AIAA/ASME/ASCE/AHS/ASC Structures, Structural Dynamics and Materials Conference*.

Mohd Kahar, M. S. A., Wan Iskandar Mirza, W. I. I., Abdul Rani, M. N., & Yunus, M. A. (2024). Finite element modelling for the dynamic behaviour analysis of a structure with Hi-Lok fasteners. *Journal of Mechanical Engineering (JMechE)*, *21*(3), 231–246.

Mugabo, I., Barbosa, A. R., & Riggio, M. (2019). Dynamic Characterization and Vibration Analysis of a Four-Story Mass Timber Building. *Frontiers in Built Environment*, *5*.

Murčinková, Z., Adamčík, P., & Sabol, D. (2022). Dynamic Response of Components Containing Polymer Composites in the Resonance Region for Vibration Amplitudes up to 5g. *Polymers*, *14*(22), 5051.

Murčinková, Z., Postawa, P., & Winczek, J. (2022). Parameters Influence on the Dynamic Properties of Polymer-Matrix Composites Reinforced by Fibres, Particles, and Hybrids. *Polymers*, *14*(15), 3060.

Navarro-Quiles, A., Laudani, R., & Falsone, G. (2022). Effect of uncertain damping coefficient on the response of a SDOF system. *Probabilistic Engineering Mechanics*, *68*, 103238.

Ni, Y.-C., Lam, H.-F., & Zhang, F.-L. (2023). Assessing uncertainty in fast Bayesian modal identification based on seismic structural responses. *Mechanical Systems and Signal Processing*, *185*, 109686.

Nimityongskul, S., & Kammer, D. C. (2009). Frequency response based sensor placement for the mid-frequency range. *Mechanical Systems and Signal*

Processing, *23*(4), 1169–1179.

Nori, C. V., McCarty, T. A., & Mantena, P. R. (1996). Vibration analysis and finite element modeling for determining shear modulus of pultruded hybrid composites. *Composites Part B: Engineering*, *27*(3–4), 329–337.

Okolie, O., Faisal, N. H., Jamieson, H., Mukherji, A., & Njuguna, J. (2025). Structural integrity and failure mechanisms of thermoplastic composite pipes for offshore applications: Insights from compressive and flexural testing. *Engineering Failure Analysis*, *179*, 109775.

Okolie, O., Latto, J., Faisal, N., Jamieson, H., Mukherji, A., & Njuguna, J. (2023a). Advances in structural analysis and process monitoring of thermoplastic composite pipes. *Heliyon*, *9*(7), e17918.

Okolie, O., Latto, J., Faisal, N., Jamieson, H., Mukherji, A., & Njuguna, J. (2023b). Manufacturing Defects in Thermoplastic Composite Pipes and Their Effect on the in-situ Performance of Thermoplastic Composite Pipes in Oil and Gas Applications. *Applied Composite Materials*, *30*(1), 231–306.

Onyibo, E. C., Gazioglu, A., Abulibdeh, M., Osman, O. M., Huwail, T. Bin, Alkhatib, M., Aburemeis, A., Razavi, S., Sahmani, S., & Safaei, B. (2025). Optimization analysis of stiffness and natural frequency of unidirectional and randomly oriented short fiber-reinforced composite materials. *Acta Mechanica*, *236*(3), 1935–1953.

Packard, H. (1997). *The fundamentals of modal testing*. application note 243-3.

Panda, A. K., & Modak, S. V. (2023). A two-stage approach to stochastic finite element model updating using FRF data. *Journal of Sound and Vibration*, *553*, 117670.

Pang, S., Shang, W., Dai, S., Deng, J., Zhang, F., Zhang, B., & Cong, S. (2024). Stiffness Optimization of Cable-Driven Humanoid Manipulators. *IEEE/ASME Transactions on Mechatronics*, *29*(6), 4168–4178.

Peeters, B., Van der Auweraer, H., Guillaume, P., & Leuridan, J. (2004). The PolyMAX Frequency-Domain Method: A New Standard for Modal Parameter Estimation? *Shock and Vibration*, *11*(3–4), 395–409.

Pei, X.-Y., Hou, Y., Huang, H.-B., & Zheng, J.-X. (2025). A Multi-Objective Sensor Placement Method Considering Modal Identification Uncertainty and Damage Detection Sensitivity. *Buildings*, *15*(5), 821.

Pimenov, D. Yu., Kumar Gupta, M., da Silva, L. R. R., Kiran, M., Khanna, N., & Krolczyk, G. M. (2022). Application of measurement systems in tool condition monitoring of Milling: A review of measurement science approach. *Measurement*, *199*, 111503.

Polilov, A. N., Arutyunova, A. S., & Tatus', N. A. (2021). Effect of Stress Concentration near Grips on the Tensile Strength of Composites. *Inorganic Materials*, *57*(15), 1555–1564.

Pradhan, S., & Modak, S. V. (2018). A two-stage approach to updating of mass, stiffness and damping matrices. *International Journal of Mechanical Sciences*, *140*, 133–150.

Ramli, M. I., Nuawi, M. Z., Abdullah, S., Rasani, M. R. M., Salleh, M. S., & Basar, M. F. (2017). The study of EMA effect on modal identification: a review. *Journal of Mechanical Engineering and Technology (JMET)*, *9*(1), 103–121.

Raza, A., Mieloszyk, M., Rimašauskienė, R., Jūrėnas, V., Maqsood, N., Rimašauskas, M., & Kuncius, T. (2025). Dynamic Properties and Vibration Control of Additively Manufactured Carbon and Glass Fiber Reinforced Polymer Composites Using MFC: A Numerical Study with Experimental Validation. *Journal of Manufacturing and Materials Processing*, *9*(7), 235.

Ren, J., & Cao, Q. (2021). Assignment of Natural Frequencies and Mode Shapes Based on FRFs. *Aerospace*, *8*(9), 262.

Ribeiro, D., Bragança, C., Brehm, M., Zabel, V., & Calçada, R. (2022). A Novel Strategy for Automatic Mode Pairing on the Model Updating of Railway Systems with Nonproportional Damping. *Applied Sciences*, *13*(1), 350.

Sanei, S. H. R., & Fertig, R. S. (2015). Uncorrelated volume element for stochastic modeling of microstructures based on local fiber volume fraction variation. *Composites Science and Technology*, *117*, 191–198.

Sanjeevi, N. S. S., & Vashista, V. (2023). Stiffness Modulation of a Cable-Driven Serial-Chain Manipulator Via Cable Routing Alteration. *Journal of Mechanisms and Robotics*, *15*(2).

Sayahkarajy, M. (2018). Mode shape analysis, modal linearization, and control of an elastic two-link manipulator based on the normal modes. *Applied Mathematical Modelling*, *59*, 546–570.

Schneider, S., Mallareddy, T. T., Alarcón, D. J., Kamenzky, R., & Blaschke, P. (2018). Experimental Modal Analysis of Structures with Conventional Versus Contact-Free Suspension. *Special Topics in Structural Dynamics, Volume 5: Proceedings of the 36th IMAC, A Conference and Exposition on Structural Dynamics 2018*, 149–156.

Schoukens, J., Swevers, J., Pintelon, R., & Van der Auweraer, H. (2004). Excitation design for FRF measurements in the presence of non-linear distortions. *Mechanical Systems and Signal Processing*, *18*(4), 727–738.

Sekulic, D., & Dedović, V. (2011). The Effect of Stiffness and Damping of the Suspension System Elements on the Optimisation of the Vibrational Behaviour of a Bus. *INTERNATIONAL JOURNAL FOR TRAFFIC AND TRANSPORT ENGINEERING (IJTTE)*, *1*.

Sevkat, E., Liaw, B., Delale, F., & Raju, B. B. (2010). Effect of repeated impacts on the response of plain-woven hybrid composites. *Composites Part B: Engineering*, *41*(5), 403–413.

Shao, H., Zuo, Y., & Jiang, Z. (2022). Dynamic Finite Element Model Updating Based on Correlated Mode Auto-Pairing and Adaptive Evolution Screening. *Applied Sciences*, *12*(6), 3175.

Sharma, J. K. (2019). *Theoretical and Experimental Modal Analysis of Beam* (pp. 177–186).

Sinha, U., Das, S., & Chakraborty, S. (2024). Enhancing damping estimation accuracy of exponential windowed responses of a GFRP plate through Finite Element Model Updating approach. *Ocean Engineering*, *303*, 117710.

Song, P., Trivedi, A., & Siviour, C. R. (2023). Tensile testing of polymers: Integration of digital image correlation, infrared thermography and finite element modelling. *Journal of the Mechanics and Physics of Solids*, *171*, 105161.

Sudin, M. A., Mohd Kahar, M. S. A., Kyprianou, A., Wan Iskandar Mirza, W. I. I., Yunus, M. A., Febrina, R., Mutra, R. R., & Abdul Rani, M. N. (2025). Predicting vibration characteristics of a bolted pipe assembly with complex boundary and interface constraints via the frequency based substructuring method. *Journal of Mechanical Engineering (JMechE)*, *22*(3), 76–94.

Sun, Z., Mahmoodian, M., Sidiq, A., Jayasinghe, S., Shahrivar, F., & Setunge, S. (2025). Optimal Sensor Placement for Structural Health Monitoring: A Comprehensive Review. *Journal of Sensor and Actuator Networks*, *14*(2), 22.

Tamizifar, M., Mosayebi, M., & Ziaei-Rad, S. (2022). Optimal sensor placement and model updating applied to the operational modal analysis of a nonuniform wind turbine tower. *Mechanical Sciences*, *13*(1), 331–340.

Tang, Z. (2025). Vibration Analysis and Control Technology in Mechanical Engineering. *Theoretical and Natural Science*, *142*(1), 77–82.

Tian, Q., Yao, K., & Cao, S. (2024). Research on Quantification of Structural Natural Frequency Uncertainty and Finite Element Model Updating Based on Gaussian Processes. *Buildings*, *14*(6), 1857.

Topaloglu, N., & Karadag, C. V. (2022). A novel amplitude-FRF based SDOF resonator parameter extraction method. *Journal of Sound and Vibration*, *517*, 116551.

Treviso, A., Van Genechten, B., Mundo, D., & Tournour, M. (2015). Damping in composite materials: Properties and models. *Composites Part B: Engineering*, *78*, 144–152.

Úradníček, J., Musil, M., Gašparovič, Ľ., Páleník, M., & Bachratý, M. (2025). Enhancing reliability in estimating modal parameters for automotive disk Brakes: A comprehensive approach using the Eigensystem Realization algorithm and additional criteria. *Mechanical Systems and Signal Processing*, *224*, 112069.

Varahram, S., Jalali, P., Sadeghi, M. H., & Lotfan, S. (2019). Experimental Study on the Effect of Excitation Type on the Output-Only Modal Analysis Results. *Transactions of FAMENA*, *43*(3), 37–52.

Wang, C., Xu, Z., & Liu, X. (2022). Structural Dynamics and Vibration. *Journal of Physics: Conference Series*, *2386*(1), 012096.

Wang, Y., Ma, Y., & Hong, J. (2022). Study on dynamic stiffness of supporting structure and its influence on vibration of rotors. *Chinese Journal of Aeronautics*, *35*(11), 252–263.

Waterbury, M. C., & Drzal, L. T. (1989). Determination of Fiber Volume Fractions by Optical Numeric Volume Fraction Analysis. *Journal of Reinforced Plastics and Composites*, *8*(6), 627–636.

Wilk-Jakubowski, J. L., Pawlik, L., Frej, D., & Wilk-Jakubowski, G. (2025). The Evolution of Machine Learning in Vibration and Acoustics: A Decade of Innovation (2015–2024). *Applied Sciences*, *15*(12), 6549.

Will, D. T., & Zhu, W. D. (2024). Experimental Modal Analysis and Operational Deflection Shape Analysis of a Cantilever Plate in a Wind Tunnel with Finite Element Model Verification. *Experimental Techniques*, *48*(4), 623–642.

Xie, W., & Hua, Y. (2024). Structural Vibration Comfort: A Review of Recent Developments. *Buildings*, *14*(6), 1592.

Xu, L., & Lu, T. (2021). Influence of track flexibility and spatial coherence of track irregularity on vehicle-slab track interaction: frequency-domain analysis. *International Journal of Rail Transportation*, *9*(4), 342–367.

Yaacob, R. M., Abdullah, N. A. Z., Zikri, J. M., & Mohd Sani, M. S. (2025). Effect of vibration analysis towards dynamic properties in dissimilar joining materials: A review. *Journal of Mechanical Engineering and Sciences*, 10998–11026.

Yarar, E., Ertürk, A. T., Açıkgöz, Ç., & Karabay, S. (2023). Experimental and numerical vibration analysis of surface mechanical attrition treatment. *Journal of Vibration and Control*, *29*(23–24), 5737–5749.

Yazdi, M., Zarei, E., Adumene, S., & Beheshti, A. (2024). Navigating the Power of Artificial Intelligence in Risk Management: A Comparative Analysis. *Safety*, *10*(2), 42.

Yildiz, İ. (2025). Determination of Young's modulus for complex geometries using an acoustic resonance and finite element analysis. *Nondestructive Testing and Evaluation*, 1–17.

Yilmaz, Z., Okur, F. Y., Günaydin, M., & Altunişik, A. C. (2023). Enhanced Modal Participation Ratio-Based Structural Damage Identification: A New Filtering Approach Using Modal Assurance Criteria. *Buildings*, *13*(10), 2467.

You, Y.-S., Song, K.-Y., & Sun, M.-Y. (2022). Variable Natural Frequency Damper for Minimizing Response of Offshore Wind Turbine: Principle Verification through Analysis of Controllable Natural Frequencies. *Journal of Marine Science and Engineering*, *10*(7), 983.

Yu, M., Zhao, L., Chen, S., Han, X., Jia, C., Xia, Y., Wang, X., Wang, Y., Yang, P., Lu, D., & Jiang, Z. (2023). Monolithically integrated triaxial high-performance micro accelerometers with position-independent pure axial stressed piezoresistive beams. *Microsystems & Nanoengineering*, *9*, 9.

Zahari, S. N., & Sani, M. S. M. (2017). Investigation on Impact Hammer Testing with Different Types of Hammer Tip for Welded Thin Plate. *Advanced Science Letters*, *23*(11), 11325–11329.

Zareian, F., & Medina, R. A. (2010). A practical method for proper modeling of structural damping in inelastic plane structural systems. *Computers & Structures*, *88*(1–2), 45–53.

Zeng, X., Han, B., Kuang, Z., Ding, H., Wang, K., Du, C., Wu, W., Li, H., & Wang, J. (2025). Design and Experimentation of Variable-Density Damping Materials Based on Topology Optimization. *Processes*, *13*(7), 2276.

Zhao, H., Lv, J., Wang, Z., Gao, T., & Xiong, W. (2023). Finite Element Model Updating Using Resonance–Antiresonant Frequencies with Radial Basis Function

Neural Network. *Applied Sciences*, *13*(12), 6928.

Zhu, T., Zang, C., & Zhang, G. (2020). Noise Reduction for Modal Parameter Identification of the Measured FRFs Using the Modal Peak-Based Hankel-SVD Method. *Shock and Vibration*, *2020*, 1–21.

Zmarzły, P., Wrzochal, M., & Adamczak, S. (2025). Evaluation of the Variability of Vibration Measurement Results in Rolling Bearing Quality Control. *Applied Sciences*, *15*(2), 904.

Żółtowski, M., & Napieraj, K. (2017). Experimental modal analysis in research. *Budownictwo i Architektura*, *16*(3), 005–012.

Zrayka, A. K., & Mucchi, E. (2019). A comparison among modal parameter extraction methods. *SN Applied Sciences*, *1*(7), 781.

APPENDICES

APPENDIX 1

Tensile Testing Reports for Steel Dog-Bone Specimens

SAMPLE 1

POLITEKNIK MALAYSIA
SULTAN SALAHUDDIN ABDUL AZIZ SHAH

POLITEKNIK SHAH ALAM TENSILE TESTING

FATIN

Sample	fatin-1	TestDate	2026-01-14
Size(mm)	12*10	Area(mm^2)	120.0
Gauge Lenght(mm)	50.00	Elongation(mm)	27.708
Elongation(%)	55.42	Force max(kN)	58.7
Tensile Strenght (MPa)	489	Coil No/Packet No	
Type	Flat	Tensile Ratio	1.6
Su(mm^2)		Z(%)	
FeH(kN)	/	ReH(MPa)	
FeL(kN)	36.8	ReL(MPa)	306
Fp(kN)	36.8	Rp(MPa)	306
Ft(kN)	1.1	Rt(MPa)	9
E(GPa)	4		

comment:

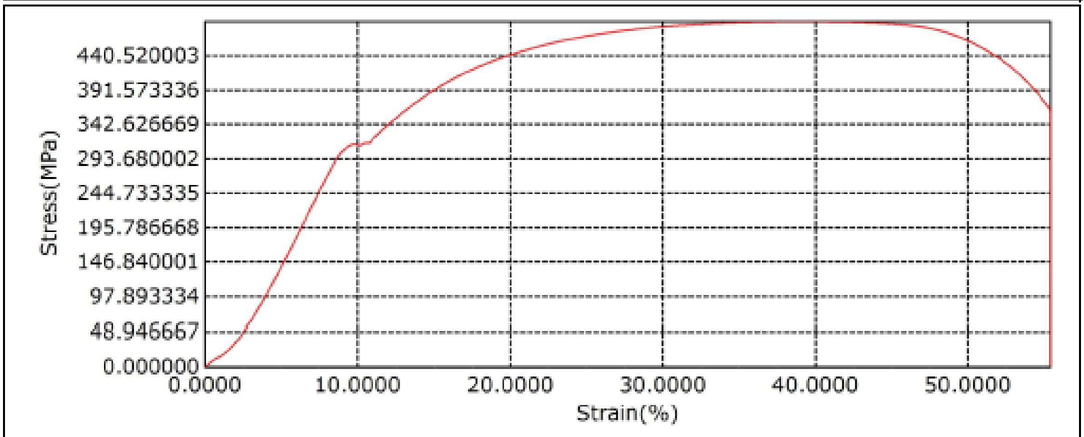

assessor: ______ ratifier: ______ test person: ______

SAMPLE 2

POLITEKNIK SHAH ALAM TENSILE TESTING

FATIN

Sample	fatin-2	TestDate	2026-01-14
Size(mm)	12*10	Area(mm^2)	120.0
Gauge Lenght(mm)	60.00	Elongation(mm)	28.937
Elongation(%)	48.23	Force max(kN)	59.7
Tensile Strenght (MPa)	497	Coil No/Packet No	
Type	Flat	Tensile Ratio	1.6
Su(mm^2)		Z(%)	
FeH(kN)	/	ReH(MPa)	
FeL(kN)	37.3	ReL(MPa)	311
Fp(kN)	37.3	Rp(MPa)	311
Ft(kN)	1.3	Rt(MPa)	11
E(GPa)	4		

comment:	

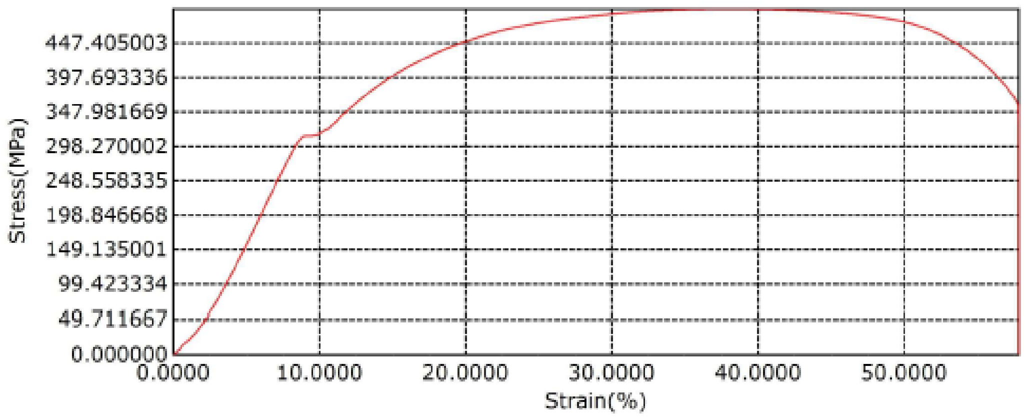

assessor: ____________ ratifier: ____________ test person: ____________

SAMPLE 3

POLITEKNIK SHAH ALAM TENSILE TESTING

FATIN

Sample	fatin-3	TestDate	2026-01-14
Size(mm)	12*10	Area(mm^2)	120.0
Gauge Lenght(mm)	60.00	Elongation(mm)	27.726
Elongation(%)	46.21	Force max(kN)	59.9
Tensile Strenght (MPa)	499	Coil No/Packet No	
Type	Flat	Tensile Ratio	1.6
Su(mm^2)		Z(%)	
FeH(kN)	38.9	ReH(MPa)	324
FeL(kN)	38.1	ReL(MPa)	317
Fp(kN)	37.9	Rp(MPa)	316
Ft(kN)	1.2	Rt(MPa)	10
E(GPa)	5		

comment:	

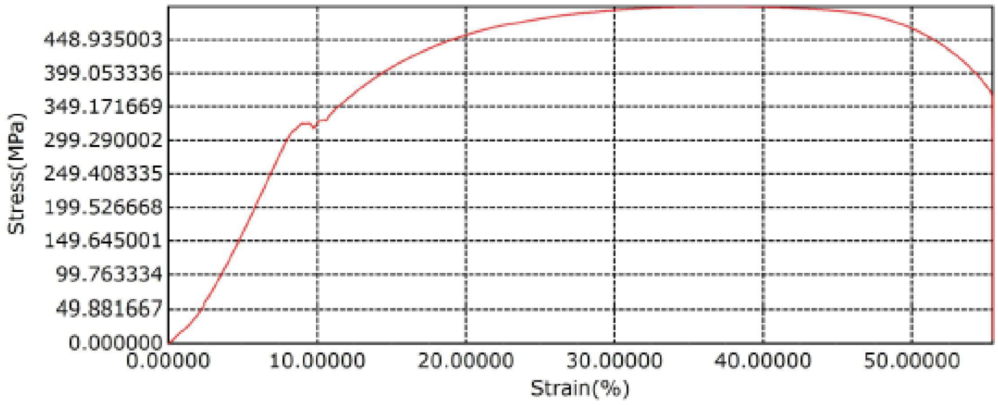

assessor: ______________ ratifier: ______________ test person: ______________

AUTHOR'S PROFILE

Nurul Fatin Hamizah binti Ah Siak @ Mohd Helmi obtained a Diploma in Mechanical Engineering from Universiti Teknologi MARA (UiTM) Pasir Gudang and a Bachelor of Mechanical Engineering (Hons.) from UiTM Shah Alam. She is currently pursuing a Master of Science in Mechanical Engineering at UiTM Shah Alam. Her research interests include structural dynamics, experimental modal analysis, finite element (FE) modelling, and FE model updating, with a focus on composite and bio-composite materials. Her Master's research centres on improving damping representation in FE models through correlation with experimental modal analysis data using tools such as MSC NASTRAN, PATRAN, LMS SCADAS, and FEMTools.

LIST OF PUBLICATION:

Ah Siak @ Mohd Helmi, N. F. H., Yunus, M. A., Kyprianou, A., Van Der Auweraer, H., Mohd Kahar, M. S. A., & Abdul Rani, M. N. (2025). Accurate prediction of frequency response functions of tobacco composite panel. *Journal of Physics: Conference Series*, *3156*, Article 012010.

Abdul Jami, M., Mohd Kahar, M., Ah Siak, N., Mohd Zin, M. S., Yunus, M., & Abdul Rani, M. N. (2025). Identification of the modal parameters of a golf club. *Journal of Acoustics and Vibration Research*, *3*(1), 1–13.

Ismayatim, M., Mohd Kahar, M., Ah Siak, N., Yunus, M., & Abdul Rani, M. N. (2025). Investigation of the modal parameters of a cricket bat via simulation and experimental modal analysis. *Journal of Acoustics and Vibration Research*, *3*(1), 36–49.

Abdul Rani, M. N., Sudin, M., Mohd Helmi, N., Yunus, M., Kyprianou, A., Mutra, R., & Wan Iskandar, I. W. I. (2024). Predicting frequency response function of a bolted flanged pipe assembly using frequency based substructuring. *Journal of Acoustics and Vibration Research*, *2*(1), 62–71.

Mohd Kahar, M. S. A., Ah Siak, N. F. H., Yunus, M. A., Mohd Sani, M. S., Wan Iskandar Mirza, W. I. I., Rahim, M. A., & Abdul Rani, M. N. (2026). Identification of suitable excitation nodes for assembled structures using modal participation factors. *Journal of Acoustics and Vibration Research*, *4*(1), 32–41.

Sari, N. H., Yunus, M. A., Abdul Majid, M. L., Mohd Sani, M. S., Ah Siak, N. F. H., & Ab Rahim, M. (2026). Structural material identification of tobacco natural fibre composite panel (TNFCP) using stochastic inverse method. *Journal of Mechanical Engineering*, *23*(2), 151–170.